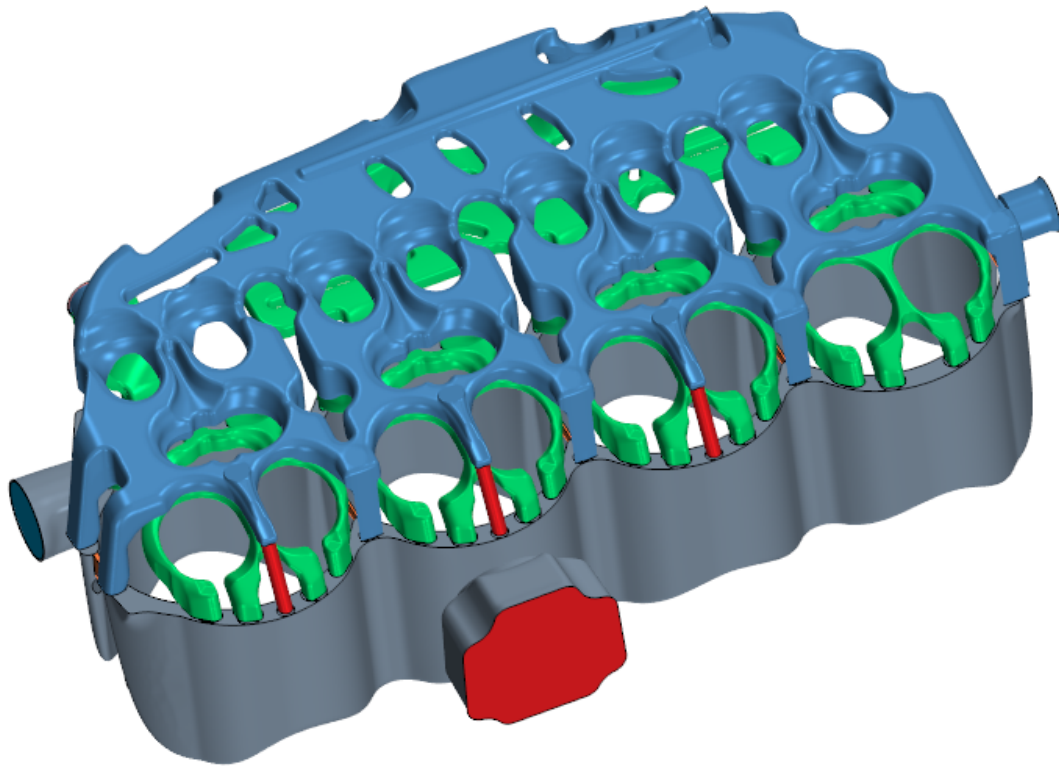




CHALMERS



Internal Combustion Engine Coolant Jacket design guidelines study with 3D CHT-CFD

Master's thesis in Applied Mechanics

ANDREAS JOHANSSON

MASTER'S THESIS IN APPLIED MECHANICS

Internal Combustion Engine Coolant Jacket design guidelines study with 3D
CHT-CFD

ANDREAS JOHANSSON

Department of Mechanics and Maritime Sciences
Division of Fluid Dynamics
CHALMERS UNIVERSITY OF TECHNOLOGY
Göteborg, Sweden 2019

Internal Combustion Engine Coolant Jacket design guidelines study with 3D CHT-CFD
ANDREAS JOHANSSON

© ANDREAS JOHANSSON, 2019

Master's thesis 2019:53
Department of Mechanics and Maritime Sciences
Division of Fluid Dynamics
Chalmers University of Technology
SE-412 96 Göteborg
Sweden
Telephone: +46 (0)31-772 1000

Cover:
Geometry of coolant jacket on which parameter study has been performed

Chalmers Reproservice
Göteborg, Sweden 2019

Internal Combustion Engine Coolant Jacket design guidelines study with 3D CHT-CFD
Master's thesis in Applied Mechanics
ANDREAS JOHANSSON
Department of Mechanics and Maritime Sciences
Division of Fluid Dynamics
Chalmers University of Technology

ABSTRACT

High thermal loads lead to high demands on the engine cooling system. When analysing the heat transfer within the engine, from the combustion/exhaust gases to the coolant, CFD and FE has historically been performed separately for the coolant and solid regions. When the heat loads become more complex, the coolant jacket design does as well. Thus it is important to analyse how the coolant and solid interact with changes to the coolant jacket design. By using CHT, the temperature field within both the coolant and solid regions can be simulated within a common model.

In this master thesis, a parameter sensitivity analysis has been performed on a cylinder head of a SI engine using a 3D-CHT-CFD model. The analysis investigate how coolant mass flow, coolant pressure/saturation temperature, thermal conductivity, coolant jacket displacement and surface topology affect the heat transfer within the cylinder head. Temperature fields on both the coolant jacket walls and the gas/solid interfaces are analysed, as well as the wall boiling heat flux calculated using a correlation proposed by W.M. Rohsenow [1]. The analysis has also compared local static pressure dependent saturation temperatures of the coolant with constant saturation temperature.

For the geometrical parameters, further analysis is needed to draw conclusions on the effect of structure durability as well as heat transfer and boiling.

Keywords: Engine cooling, Conjugate heat transfer, wall boiling, coolant jacket, IEM

PREFACE

This master's thesis has been performed during the spring of 2019 by Andreas Johansson as a part of the master's program Applied Mechanics at Chalmers University of Technology. The thesis was performed at Volvo Cars, who provided the CAD geometries as well as thermal boundary conditions. The project was supervised by Mirko Bovo at Volvo Cars and examined by Lars Davidson at the Division of Mechanics and Maritime Sciences at Chalmers University of Technology.

ACKNOWLEDGEMENTS

I would like to thank my supervisor at Volvo Cars, Mirko Bovo for his patience and support during this project. Mirko has helped me with his great expertise regarding heat transfer within engines, both on a system level and local phenomenons. I would also like to thank Oscar Bergman for his support regarding geometry preparation as well as tips and tricks when using StarCCM+.

From Chalmers University of Technology I would like to thank Lars Davidson for being my examiner. The knowledge of how turbulent flows affect heat transfer gained through his courses has definitely helped me during this thesis.

Finally, I would like to thank the entire engine CAE group at Volvo Cars for making me feel welcome during these months.

CONTENTS

Abstract	i
Preface	iii
Acknowledgements	iii
Contents	v
Nomenclature	vii
1 Introduction	1
1.1 Aim	1
1.2 Limitations	1
1.3 Specification of issue under investigation	2
2 Theory	3
2.1 Thermodynamics of SI engines	3
2.1.1 Integrated exhaust manifold	4
2.2 Engine materials	4
2.2.1 Material limitations	4
2.3 Engine cooling system	5
2.3.1 Heat transfer	6
2.3.2 Boiling in engine coolant jackets	7
2.4 Modelling heat transfer in engines	9
2.4.1 Governing equations	9
2.4.2 CFD	9
2.4.2.1 Turbulence	10
2.4.2.2 Conjugate heat transfer	11
2.4.2.3 Modelling boiling	12
3 Method	13
3.1 Geometry	13
3.2 Coolant properties	14
3.3 Pre processing	14
3.3.1 Mesh	15
3.4 Simulation setup	15
3.4.1 Reference simulation	16
3.4.2 Non geometrical parameters	16
3.4.3 Geometrical changes	17
4 Results and discussion	21
4.1 Reference case	21
4.1.1 Flow field	21
4.1.2 Temperature	21
4.1.2.1 Gas side	21
4.1.2.2 Coolant jacket	22
4.1.3 Heat flux	22
4.1.3.1 Wall boiling heat flux	23
4.2 Non geometrical parameters	24
4.2.1 Mass flow rate	24
4.2.1.1 Coolant jacket	24
4.2.1.2 Gas side	27
4.2.2 Mass flow distribution	29
4.2.3 Pressure dependent saturation temperature	32

4.2.3.1	Constant vs pressure dependent saturation temperature	32
4.2.3.2	Different outlet pressures	34
4.2.4	Thermal conductivity	36
4.3	Geometrical changes	37
4.3.1	Displacement	37
4.3.2	Surface topology modification	38
5	Conclusions	41
5.1	Recommendations	41
6	Future work	43
	References	45
A	Appendix	47
A.1	Reference simulation	47
A.2	Mass flow rate	54
A.3	Mass flow distribution	65
A.4	Constant vs pressure dependent saturation temperature	75
A.5	Outlet pressure	84
A.6	Thermal conductivity	95
A.7	Displacement	100
A.8	Surface modification	104

Nomenclature

Variables and constants

ΔT_{sat}	Wall superheat [K]
δ_{ij}	Kronecker delta [-]
\dot{m}	Mass flow rate
η_{th}	Thermal efficiency [-]
\mathbf{n}	Normal vector [-]
μ	Dynamic viscosity [kg/(m/s)]
μ_t	Turbulent viscosity [kg/(m/s)]
ρ	Density [kg/m ³]
σ	Stress tensor [N/m ²], surface tension [N/m]
σ_k	Equation constant in Eq. (2.14)
σ_ε	Equation constant in Eq. (2.15)
τ	Viscous stress tensor [N/m ²]
ε	Dissipation [m ² /s ³]
A	Area [m ²]
c_p	Specific heat capacity at constant pressure [J/(kgK)]
C_μ	Equation constant in Eq. (2.16)
$C_{\varepsilon 1}, C_{\varepsilon 2}$	Equation constants in Eq. (2.15)
C_{qw}	Equation constant in Eq. (2.17)
f	Volume/body forces [m/s ²]
f_2	Damping function in Eq. (2.15)
f_μ	Damping function in Eq. (2.16)
h	Heat transfer coefficient [W/(m ² K)]
h_{lat}	Latent heat (Energy absorbed/released during phase change) [J/kg]
k	Thermal conductivity [W/(mK)], turbulent kinetic energy [m ² /s ²]
p	Pressure [Pa]
P_k	Production term in Eq. (2.14)
P_ε	Production term in Eq. (2.15)
Q	Thermal energy per second [W]
q, \mathbf{q}	Heat flux [W/m ²]
S_ε	User defined source term in Eq. (2.15)
S_k	User defined source term in Eq. (2.14)
T	Temperature [K]
T_f	Characteristic fluid temperature [K]
t_t	Turbulent time scale [s]
T_w	Wall temperature (fluid/solid interface) [K]

T_{sat}	Saturation/boiling temperature [K]
u	Internal energy [J/kg]
v	Velocity [m/s]
W	Mechanical power [W]

Subscripts

b	Boiling
cj	Coolant jacket
env	Environment (ambient air)
$fric$	Friction
gas	Combustion chamber and/or exhaust gas
l	Liquid
$lubr$	Lubrication oil
ref	Reference value
v	Vapour

Other Symbols

$(-)'$	Fluctuating
$\overline{(-)}$	Time averaged

Acronyms

CAD	Computer Aided Design
CFD	Computational Fluid Dynamics
CHT	Conjugate Heat Transfer
CO ₂	Carbon dioxide
DNS	Direct Numerical Simulation
FE	Finite Element
FVM	Finite Volume Method
HCF	High Cycle Fatigue
HVAC	Heating, Ventilation and Air Conditioning
ICE	Internal Combustion Engine
IEM	Integrated Exhaust Manifold
LCF	Low Cycle Fatigue
LES	Large Eddy Simulation
RANS	Reynolds-Averaged Navier-Stokes
SI	Spark Ignition
1D	One-Dimensional
3D	Three-Dimensional

1 Introduction

The car is, and has been for decades, the dominant mode of transport in many parts of the world. By far the most common propulsion mechanism in the automotive industry is the internal combustion engine (ICE) which use fossil fuel (petrol or diesel) as its energy source. A problem with ICEs is that the exhaust gases consist in large part of carbon dioxide (CO₂), which contributes to global warming. Due to the threat of global warming, the automotive industry is pressured, both by regulation and customer demand, to decrease the emissions of CO₂ from their cars [2, 3]. This has led to the development of new cars using different sources of energy including electricity, hydrogen, ethanol and different kinds of hybrid solutions in order to reduce the CO₂ emissions [4, 5].

New energy sources are not the only way the manufacturers reduce the emissions from their car fleets. They also focus on incremental development of their engines to consume less fuel and emit less CO₂ [2, 6]. One problem developers have is to maintain the power output from the engines while reducing CO₂ emissions in order to meet customer demands. Decreasing emissions while maintaining the power output requires an increased thermal efficiency of the engine since thermal efficiency can be defined as the

$$\eta_{th} = \frac{W_{out}}{Q_{in}} \quad (1.1)$$

where η_{th} is the thermal efficiency, W_{out} is the work output in the form of mechanical energy and Q_{in} is the thermal energy input, which in the case of an engine is the chemical energy of the fuel. The thermal efficiency of combustion increases with higher gas temperatures. Therefore a higher thermal efficiency in the engine often mean higher combustion temperatures and thus higher thermal loads on the engine solid [7]. This means that a higher level of cooling of the cylinder block and head is needed.

To analyse the structural durability of the engine, Finite Element (FE) analyses are performed on the engine. To take the effects of the thermal loads into account, the FE analyses require the temperature field of the engine. The temperature fields of the coolant and the solid has historically been calculated through separate independent Computational Fluid Dynamics (CFD) and FE simulations respectively. Furthermore, rough approximations were used for boundaries on the gas/solid interface.

With higher thermal loads comes the need for more effective and complex engine cooling and the simulation models need to become more sophisticated. Since the coolant jacket, engine solids and combustion/exhaust gases all affect each other thermally, the model simulating this system need to take this into account.

Conjugate heat transfer (CHT) is a method for modelling the temperature distribution and heat transfer between a solid and a fluid. Recently, a 3D-CHT-CFD model simulating the temperature and heat transfer between the engine solid and the coolant flow has been adopted at Volvo Cars. The 3D-CHT-CFD model is looped with 3D in-cylinder and exhaust gas CFD models enabling high resolution mapping of the thermal load on the gas/solid interfaces.

This model opens up new possibilities for analysing how different cooling jacket geometries and flow properties affect the temperature and heat flow of the solid material, exhaust gases etc.

1.1 Aim

The aim of this master thesis is to conduct a parametric sensitivity study on a coolant jacket for a spark ignition (SI) engine with an integrated exhaust manifold (IEM) using the 3D-CFD software StarCCM+ in order to produce design guidelines for the future development of coolant jackets. This includes changes in both non-geometrical parameters, such as coolant pressure, mass flow, cylinder head material, as well as geometrical changes to the coolant jacket.

1.2 Limitations

The project is limited by the following:

- The cylinder head and coolant jacket are only analysed thermally, no consideration to mechanical effects are taken.
- All analyses are performed using steady state simulations.

- The design guide is limited to the result of a parameter study where design changes to an existing coolant jacket will be analysed. The parameters include both non-geometrical changes to the coolant flow and solid materials and geometrical changes. Optimisation is not included in this study.
- The geometrical changes to the coolant jacket are limited to minor global displacement and small local surface topology change. The changes do not significantly alter the design of the coolant jacket.
- No geometrical changes to the inlet and outlets of the coolant jacket are included.
- The study focus on SI engines (petrol) but most conclusions about the cooling performance should be applicable for other combustion engines as well.

1.3 Specification of issue under investigation

In order to fulfil the aim of this master thesis, the sensitivity analysis addresses the following questions:

- How is
 - the coolant flow distribution, especially variations between cylinders
 - heat flux (boiling and convection)
 - maximum solid temperature/gradient
 - coolant-solid interface temperature

affected by changes in

- coolant mass flow
- coolant pressure
- cylinder head material (thermal conductivity of cylinder head)
- minor global displacement of coolant jacket
- local surface topology change
- saturation temperature

2 Theory

2.1 Thermodynamics of SI engines

In a turbocharged direct injection SI engine the thermodynamic cycle consists of four strokes, graphically illustrated in Figure 2.1 in the following order: intake, compression, power and exhaust.

During the *intake* stroke (Figure 2.1a), pressurised air enters into the cylinder through the intake valve. The fuel is injected into the combustion chamber with high pressure through a separate inlet. The air/fuel ratio and the mass flow of the mixture has a direct influence on the power output and the thermal load on the engine as well as the composition of the exhaust gases [8].

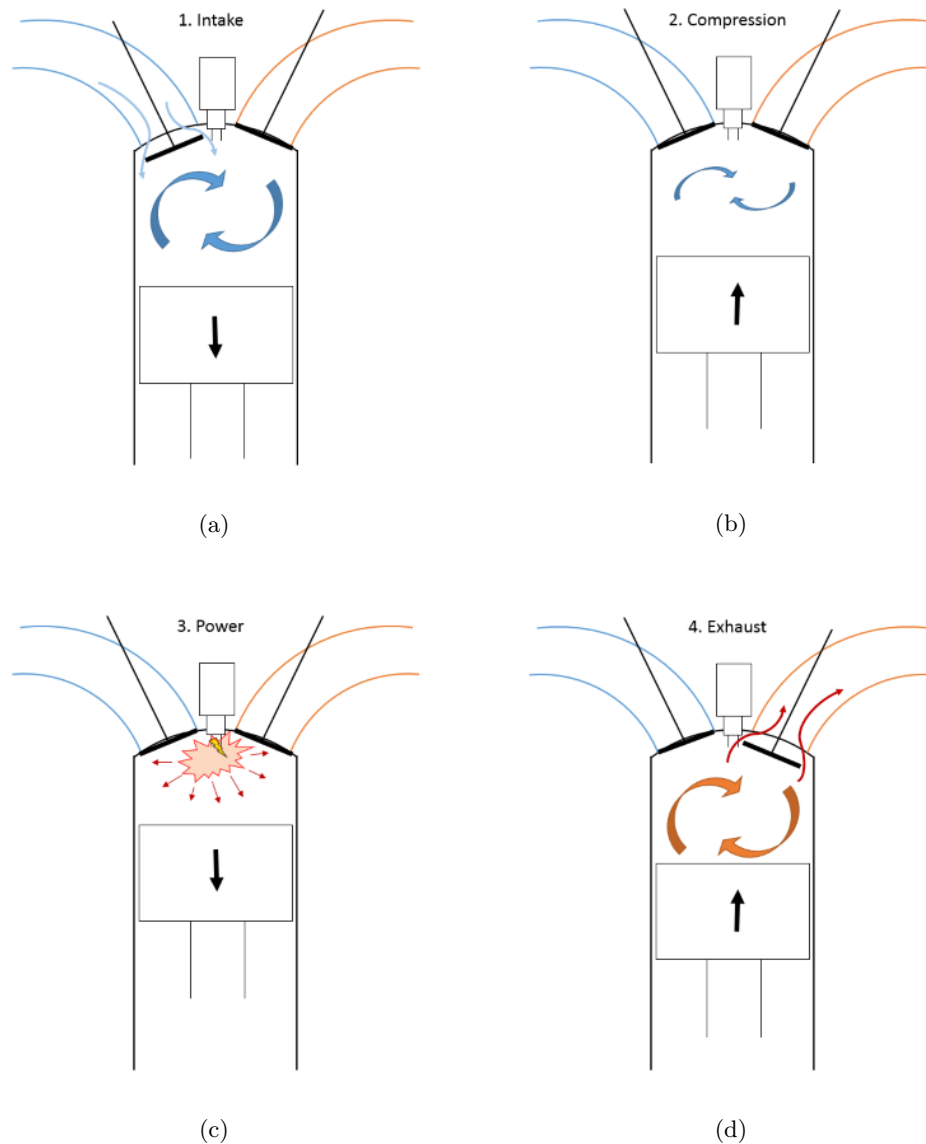


Figure 2.1: A simplified view of the combustion cycle of a four-stroke SI engine

Following the intake comes the *compression* stroke (Figure 2.1b) where the mixture is compressed inside the cylinder as the piston moves upward towards the top of the cylinder. This stage increases the pressure and temperature in the combustion chamber [8].

At an appropriate time at the end of the compression stroke, right before the piston reaches its highest point,

the air/fuel mixture is locally ignited by a spark plug and the flame then propagates through the combustion chamber. The combustion creates a large increase in pressure and temperature in the combustion chamber as the chemical energy of the fuel is transformed into heat inside. After combustion, the pressure inside the combustion chamber reach over 50 bar and the temperature reaches up to 2500K. The high pressure gas pushes the piston down in order to expand and this expansion is called the *power* stroke (Figure 2.1c) [8].

After the power stroke, the burned gas is pushed out of the combustion through the exhaust ports during the *exhaust* stroke (Figure 2.1d) before the intake of the next cycle begins. After leaving the combustion chambers, the exhaust gases flow through the exhaust manifold leading to a turbine. The turbine drives a compressor that pressurises the intake air upstream the intake valve. The concept with an exhaust gas turbine driving a compressor pressurising the intake air is called turbocharging [8].

The increased pressure and temperature during the compression and power strokes puts a large strain on the engine solid parts, both mechanically and thermally. Also, the ignition causes a pressure wave through the combustion chamber which is faster than the flame front. This pressure wave can lead to uncontrolled spontaneous combustion on the heated walls in the combustion chamber independent of the controlled flame. This phenomenon is called knocking, it reduces the performance of the engine and should therefore be avoided. There are several ways of reducing the risk of knocking including optimising ignition timing or fuel/air ratio but also cooling the combustion chamber walls to reduce the risk of spontaneous combustion at the walls. To maximise the power of the engine the ignition timing is very important which is why the combustion needs to be controlled and knocking is avoided [8].

To increase the power output, one can either increase the efficiency or increase the energy input, in this case the mass flow of the fuel/air mixture. Increased mass flow of the fuel/air mixture leads to higher temperatures and increased thermal loads on the engine. At high loads, the exhaust gas temperatures can be so high that it damages the turbine. To mitigate this, a higher fuel to air ratio can be used, where the extra fuel cools the exhaust gases. This approach however reduces the efficiency and leads to higher emissions. Another way to cool the exhaust gases before the turbine is to cool the exhaust manifold using the coolant jacket.

2.1.1 Integrated exhaust manifold

In recent engine designs at Volvo Cars, the exhaust manifold has been developed to fit inside the cylinder head. This new exhaust manifold is called integrated exhaust manifold (IEM). Integrating the exhaust manifold reduces the engine weight and cost, which is a goal for engine developers. It also enables cooling of the exhaust gases in order to protect the turbine [9, 10].

However, due to the high temperatures in the exhaust gases, this results in higher thermal loads in the cylinder head compared to a conventional exhaust manifold. This puts higher demand on the cooling in the cylinder head and leads to more complex coolant jacket designs [10]. It is therefore of great interest to investigate how different parameters affect the performance of the cooling jacket for an engine with IEM in order to develop a good design of future coolant jackets.

2.2 Engine materials

The cylinder block and cylinder head are usually produced in either cast iron or an aluminium alloy. Since aluminium is lighter than iron, and weight reduction is important for car manufacturers, aluminium alloys have become the most common material for building car engines. In heavy duty vehicles where power output is more important than engine weight, cast iron is more common since it can withstand higher temperatures than aluminium [8].

Because of the high temperatures in the combustion chambers and the relatively low melting point of aluminium, the combustion chamber walls need to be protected. They are therefore covered by a liner (metal cylinder) made from iron or steel in order to withstand the thermal loads [8].

2.2.1 Material limitations

Metal density is temperature dependent, therefore the metal will expand with increased temperature. Since temperature gradients are present in the solid parts, the expansion will not be homogeneous and this leads to thermal stresses in the structure [11, 12]. Cyclic stresses in a material will lead to fatigue and ultimately mechanical failures such as cracks. The engine is subjected to two kinds of fatigue, high cycle fatigue (HCF) and low cycle fatigue (LCF). HCF is linked to high frequency vibrations in the structure causing stress in the

material, rotating parts and varying pressure through the combustion cycle are phenomenon that lead to HCF. LCF is when high amplitude, low frequency stresses gradually weaken the material. One cause of LCF is the thermal stresses in the material due to the uneven material expansion caused by the temperature gradients induced warm up and cool down of the engine.

Different materials react differently to load variations, for example the coefficient of thermal expansion and fatigue limits will be different depending on the material. When the temperature increase, the coefficient of thermal expansion will increase as well, in particular for materials with a low melting point. This means that at higher temperatures, $\frac{\partial \sigma}{\partial T}$ will be larger than at low temperatures [13].

To prolong the life of a structure, either the stresses need to be reduced or the material toughness (fracture toughness, fatigue limit etc.) need to be increased [13]. In this regard, only the thermal stresses are of interest for this project. To reduce the thermal stresses, the material temperature needs to decrease. Therefore a cooling system is needed to transport heat away from the engine and thus reduce the metal temperature.

2.3 Engine cooling system

The largest heat source on the engine solid is the heat transferred from the high temperature combustion/exhaust gases on the gas/solid interface. Another source of heat is the friction between solid components e.g. between piston and liner. To reduce the friction, oil is used as a lubricant between the moving parts. The oil is also used to cool the piston.

Most of the generated heat in the engine is removed by a coolant jacket which surrounds the combustion chamber walls, the intake and exhaust ports. The coolant jacket surrounds and cools the exhaust gases within the cylinder head. Some heat is also rejected directly out to the ambient air [8].

In fatigue analyses, the time history of the stress and strain is of interest but this parameter study will be limited to analysing a steady state solution at a fixed thermal load which corresponds to the rated power of the engine. Because of the high thermal inertia of the solid and the short time scale of the combustion process, when analysing the thermal load on the solid, cycle averaged temperatures can be used without significant losses in model accuracy. The heat transfer through the engine can be summarised as a thermal balance equation

$$Q_{gas} + Q_{fric} = Q_{coolant} + Q_{env} + Q_{lubr} \quad (2.1)$$

with the heat sources on the left side and heat sinks on the right side where Q is the heat transferred.

The coolant jacket in the cylinder head is produced using a sand core during the casting of the cylinder head [8]. Following the casting process, the sand core is removed and the coolant jacket is finished by drilling a number of channels connecting different parts of the coolant jacket. After the cylinder head has been completed, it is hard to evaluate the quality of the coolant jacket, e.g. if a small channel is blocked or if there is a small displacement of the coolant jacket. Therefore it is important to know what effect the production variance will have on the cooling performance.

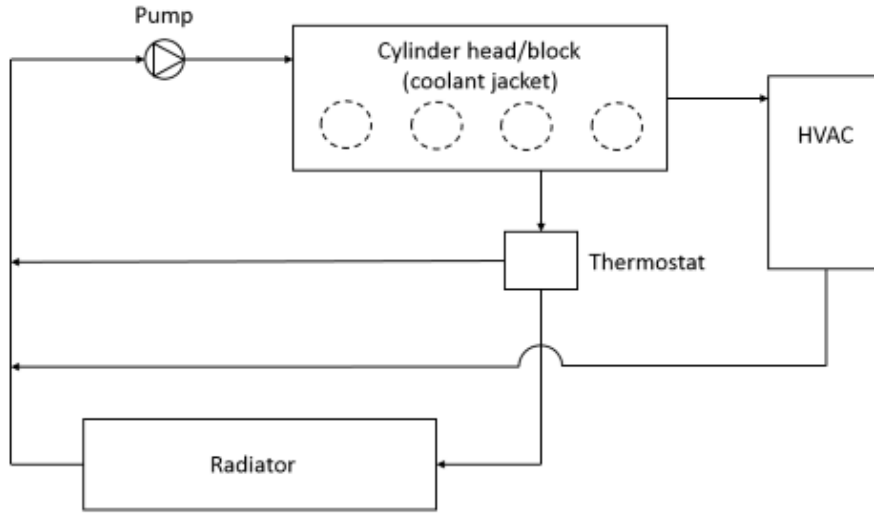


Figure 2.2: A simplified schematic view of a typical coolant circuit

A schematic view of a simplified coolant circuit can be seen in Figure 2.2. The coolant is driven by a pump into the coolant jacket in the cylinder head/block. The coolant jacket has two outlets, one main outlet which leads to a thermostat, and a smaller outlet that leads to the *heat ventilation air condition* (HVAC) after which the coolant returns to the primary circuit. A more detailed description of the geometry and flow through the coolant jacket is found in Section 3.1. When the coolant has not yet reached working temperature (around 90°C) the thermostat remains closed and leads the flow directly back to the pump. This allows the engine to quickly reach working temperature which will lead to a more efficient combustion process, as explained in Section 2.1. When the coolant reaches working temperature, the thermostat gradually opens a path to a radiator which cools the coolant. After being cooled in the radiator, the coolant returns to the pump [8]. After the engine has warmed up, the cooling system keeps the engine in a thermal equilibrium.

2.3.1 Heat transfer

Heat is the flow of thermal energy. There are three basic modes of heat transfer. These are conduction, convection and radiation. Figure 2.3 shows a schematic view of how the temperature propagates through the engine.

The heat is transferred throughout the engine solid via conduction from the high temperature regions on the gas side to the lower temperature regions on the solid/coolant and solid/ambient interfaces. In the fluid regions (gas, coolant and ambient air) the heat transfer is driven by forced convection. Conduction is present in the fluids as well but in a moving fluid, convection is the dominant mode of heat transfer. Radiation does occur within the engine between different bodies but is not considered in this study as it is assumed to be small compared to convection and conduction.

In all continua with a temperature difference, conduction is present. Conduction is the heat transfer from a region or body with a high temperature to one with a lower temperature that is driven by molecular interactions. Temperature is a measure of the kinetic energy of vibrating molecules and the average kinetic energy of the molecules are higher in high temperature regions than in low temperature regions. The molecules vibrate randomly and collide with other molecules thus exchanging momentum with each other. The collisions between high and low energy molecules lead to a continuous energy transfer from high to low temperature regions. Convection is well described by Fourier's law

$$\mathbf{q} = -k\nabla T \quad (2.2)$$

where k is the thermal conductivity and T is the temperature. The thermal conductivity is a material parameter which depends on the material temperature. Looking at Equation (2.2) it can be noted that the heat flux is a flow of thermal energy in the direction of the temperature gradient [14].

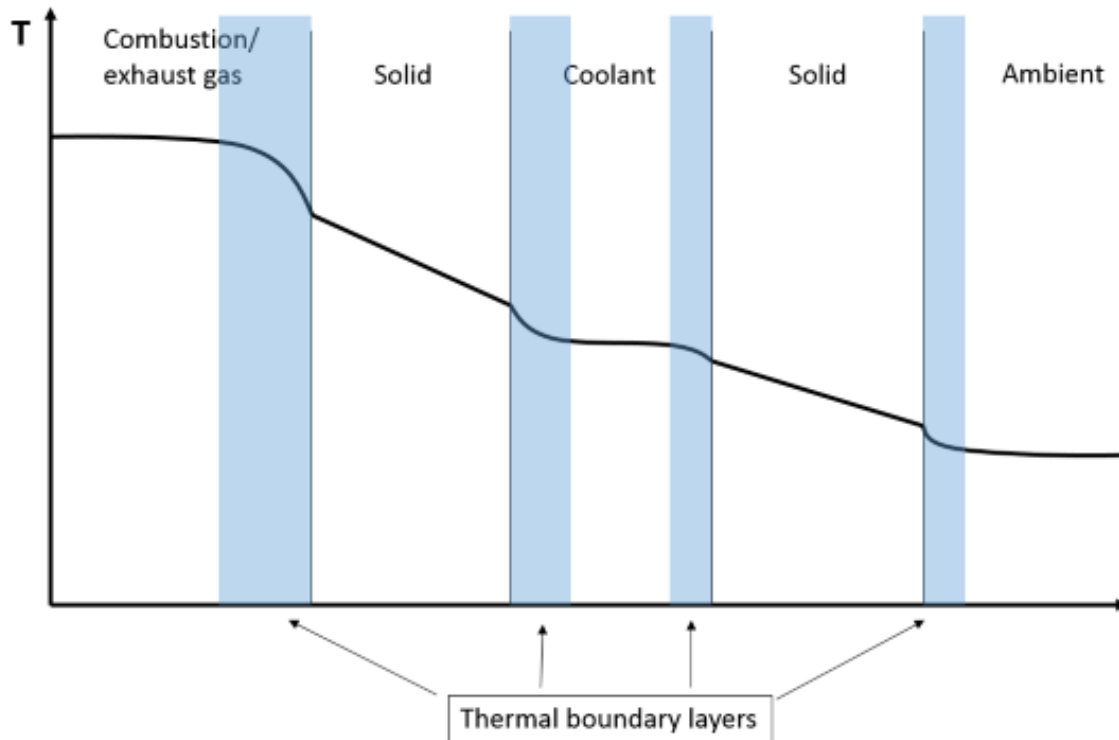


Figure 2.3: A schematic view of the temperature throughout the engine

Convection relates to the heat transfer between a solid surface and a moving fluid or the transportation of internal energy due to fluid motion. In Figure 2.3 it is the convection that produces the thermal boundary layer in the fluid regions. Convection can be divided into two categories: natural convection, when the fluid motion is driven by density variations in the fluid, and forced convection, when the flow is induced by an external source. The convective heat flux between a solid surface and the fluid can be described by Newtons law of cooling

$$\mathbf{q} = h(T_w - T_f)\mathbf{n} \quad (2.3)$$

where h is the heat transfer coefficient, T_w is the temperature at the wall and T_f is a characteristic fluid temperature e.g. the bulk temperature of the fluid and \mathbf{n} is a wall normal unit vector. The heat transfer coefficient, h , depends on the geometry, physical properties of the solid and fluid as well as flow characteristics, e.g. velocity and turbulence. Because h is dependent on several different variables it is difficult to solve convection problems analytically and numerical models are needed [14].

Radiation refers to the heat transferred via electromagnetic waves. Unlike conduction and convection which requires a medium for the heat transfer, thermal radiation is also possible through a vacuum [14]. While some radiation is present in the engine, in particular emitted by the gas in the combustion chambers, radiation is generally neglected when doing thermal analyses of the engine.

2.3.2 Boiling in engine coolant jackets

Within most of the coolant jacket, the heat transfer is driven by forced convection. In areas with higher thermal load, the wall temperature, T_w increases and in some regions it exceeds the saturation temperature of the coolant, T_{sat} . The saturation temperature of a fluid is dependent on the static pressure of the fluid. To explain what happens when the wall temperature is higher than the fluids saturation temperature the term wall superheat is used and it is defined as [15]

$$\Delta T_{sat} = T_w - T_{sat} \quad (2.4)$$

Since the heat transfer within the coolant jacket is driven by forced convection, the boiling in the coolant jacket is called flow boiling. In the case of natural convection, the boiling is called pool boiling. As a reference Figure 2.4, which shows the boiling curve for pool boiling water at atmospheric pressure, is used to explain how the wall heat flux is affected by the wall superheat. Even if T_w is higher than T_{sat} , the heat transfer is still only governed by convection. When the wall superheat reaches a certain limit, point B in Figure 2.4, the fluid in small isolated cavities on the solid surface starts to evaporate forming vapour bubbles. This is called nucleate boiling. When the bulk temperature is lower than the saturation temperature (which is the case in a coolant jacket) the bubbles condense after departing from the wall. This phenomenon is called sub-cooled nucleate boiling [15, 16].

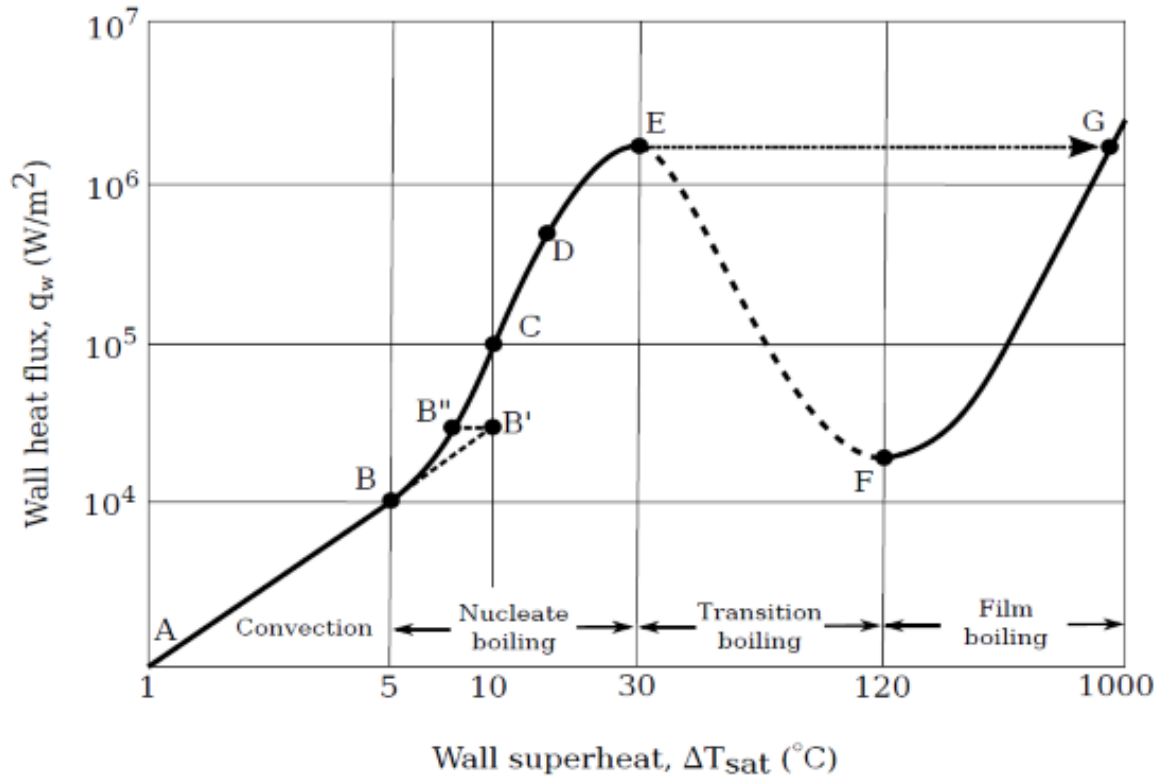


Figure 2.4: Pool boiling curve for water in atmospheric pressure showing the wall heat flux as a function of wall superheat [17]

During the phase change from liquid to vapour, the coolant absorbs heat without a temperature increase. When the bubbles then condense, this heat is transferred to the surrounding fluid. Furthermore, when the bubbles leave the wall, coolant with lower temperature flows in from the bulk to where the bubble was. Both these phenomena lead to a significantly increased heat transfer between the solid surface and the coolant compared to only convection [15]. This effect can be seen in Figure 2.4 as B' represents heat transfer with pure convection while B'' represents heat transfer with sub-cooled nucleate boiling for which the same heat flux is obtained for a lower ΔT_{sat} .

As the wall superheat increases, more bubbles form on the wall and the bubbles also grow larger. This magnifies the boiling effect on the heat flux. However, if T_{sat} increases even more the near wall region becomes so packed with vapour bubbles that the additional heat flux due to boiling decreases. This is because the bubbles block the bulk fluid from reaching the wall. If T_{sat} increases even further, the isolating effect from the vapour bubbles lead to the wall heat flux reaching a critical point, E after which the heat transfer decreases with increased wall superheat [15]. At this point the coolant jacket loses its functionality and the engine will break due to thermal overload. Therefore when designing a coolant jacket, T_{sat} need to be kept safely below this critical point to ensure that the cooling system is reliable.

2.4 Modelling heat transfer in engines

Within the engine, there are multiple different solid components with different materials and different fluids. As mentioned in Section 2.2 the cylinder head and block are cast in aluminium alloys but there are parts within the engine from other materials as well, including iron liners on the combustion chamber walls. There are also the fluid regions which consists of the combustion/exhaust gases and the coolant/oil liquids. As mentioned the coolant can also exist as a vapour. The different materials and phases lead to a complex thermo-fluid dynamic model which should both be accurate and still be fast enough to be a reasonable tool in engine development.

2.4.1 Governing equations

In continuum mechanics (both solid and fluid mechanics) mass, momentum and energy always have to be conserved. To ensure this is the case, the continuity (2.5), momentum (2.6) and energy (2.7) equations must be fulfilled.

$$\frac{\partial \rho}{\partial t} + \frac{\partial(\rho v_j)}{\partial x_j} = 0 \quad (2.5)$$

$$\frac{\partial(\rho v_i)}{\partial t} + \frac{\partial(\rho v_i v_j)}{\partial x_j} = \frac{\partial \sigma_{ij}}{\partial x_j} + \rho f_i \quad (2.6)$$

$$\frac{\partial(\rho u)}{\partial t} + \frac{\partial(\rho u v_j)}{\partial x_j} = \sigma_{ij} \frac{\partial v_i}{\partial x_j} - \frac{\partial q_i}{\partial x_i} \quad (2.7)$$

Here ρ is the density, v the velocity, σ the stress tensor representing surface forces, f represents the volume forces acting on an element (e.g. bouyancy), u is the internal energy and q is the heat flux. In Equation (2.7) radiation is neglected as radiation is not considered in this project. The stress tensor is built up by the pressure as well as viscous stresses

$$\sigma_{ij} = -p\delta_{ij} + \tau_{ij} \quad (2.8)$$

where p is the pressure, δ_{ij} is the Kronecker delta and τ_{ij} is the viscous stress tensor. Furthermore, for Newtonian fluids the viscous stress tensor can be defined as

$$\tau_{ij} = \mu \left(\frac{\partial v_i}{\partial x_j} + \frac{\partial v_j}{\partial x_i} \right) - \frac{2}{3} \mu \frac{\partial v_k}{\partial x_k} \delta_{ij} \quad (2.9)$$

with μ being the dynamic viscosity of the fluid. Including this definition of the stress tensor into the momentum equations form the Navier-Stokes equations.

$$\frac{\partial(\rho v_i)}{\partial t} + \frac{\partial(\rho v_i v_j)}{\partial x_j} = -\frac{\partial p}{\partial x_i} + \frac{\partial}{\partial x_j} \left(\mu \left(\frac{\partial v_i}{\partial x_j} + \frac{\partial v_j}{\partial x_i} \right) - \frac{2}{3} \mu \frac{\partial v_k}{\partial x_k} \delta_{ij} \right) + \rho f_i \quad (2.10)$$

The continuity equation controls that mass is conserved as the medium flows through a control volume, the momentum equation is a field representation of Newtons second law of motion and the energy equation conserves the first law of thermodynamics which states that energy cannot be created or destroyed, only transformed [18].

2.4.2 CFD

Computational fluid dynamics (CFD) is a computer based tool for analysis of systems including fluid flow and heat transfer. Most CFD codes use the Finite Volume Method (FVM) where the computational domain is divided into small cells (control volumes). Together the cells form a computational mesh of the domain. In the FVM the governing equations are solved in three steps.

1. The governing equations are integrated over all control volumes in the domain
2. The integral forms of the governing equations are then discretised over the control volumes, converting them into a system of algebraic equations
3. The equation system is then solved with an iterative approach [19].

In this project, the heat transfer in the engine is analysed assuming the flow and heat transfer is steady state which means that all time dependent terms are neglected.

2.4.2.1 Turbulence

The fluid flow, both on the gas side and in the coolant jacket is turbulent which means that inertial forces in the fluid are comparable to, or larger than, the viscous forces. Turbulent flow is highly irregular with fluctuations of different magnitude and duration. This makes turbulent flow difficult to predict. Turbulent flows are also highly diffusive compared to laminar flow. This increases the heat transfer in channel flows [18].

When analysing turbulent flow, the velocity is, in each point in space, divided into a fluctuating (v'_i) and a mean (time averaged, \bar{v}_i) part.

$$v_i = \bar{v}_i + v'_i \quad (2.11)$$

The fluctuations are a result of the flow consisting of turbulent eddies associated to different time and length scales. Large eddies extract kinetic energy from the mean flow and then the kinetic energy is transferred to smaller and smaller eddies until the energy dissipates and is transformed into heat by viscous forces (friction). The energy transfer from large to small eddies is called the cascade process [18, 20].

Three common ways of analysing turbulence using CFD are described below with decreasing computational cost but also decreased amount of resolved scales. In Direct Numerical Simulation (DNS), the cells and time steps are both small enough for resolving the turbulent eddies of the smallest scales. While this results in very high accuracy in the simulations since all velocity fluctuations are resolved without modelling, the demand for small cells and time steps makes DNS computationally expensive and is therefore used mostly for research purposes [20].

Another method is the Large Eddy Simulation (LES) where the cells are small enough to resolve the larger turbulent scales while the smaller scales are modelled. The scales that are too small to be resolved are called sub grid scales (SGS) and the turbulence inside the cells is modelled using a SGS model. LES is not as computationally expensive as DNS but still, the large amount of cells needed to resolve some of the turbulent scales leads to high computational cost [20].

The third method for analysing turbulent problems is to model all of the turbulence. Naturally this means that the cells can be larger and the computational cost for this method is lower than for DNS and LES. The fact that all of the turbulence is modelled also means that the flow can be solved with a steady state solver, in contrast to both DNS and LES which require a transient solver. Generally this method is based on the Reynolds-Averaged Navier-Stokes (RANS) equations which are obtained by dividing the velocity and pressure in The Navier-Stokes equations (Equation (2.10)) according to Equation (2.11) and then time averaging the entire Equation (2.10). Since the equation is averaged over time, the transient term in Equation (2.10) disappears in (2.12).

$$\frac{\partial}{\partial x_j}(\rho \bar{v}_i \bar{v}_j) = -\frac{\partial \bar{p}}{\partial x_i} + \frac{\partial}{\partial x_j}(\tau_{ij} + \overline{\rho v'_i v'_j}) + \rho f_i \quad (2.12)$$

The $\overline{v'_i v'_j}$ term is called the Reynolds stress tensor as it is a stress tensor due to turbulence that appears as a result of the time averaging (also called Reynolds averaging). This turbulent stress is unknown and needs to be modelled. This can be done either by the use of Reynolds stress models or an eddy viscosity model where the Reynolds stress is assumed to be proportional to a turbulent viscosity, μ_t , the same way the viscous stress is proportional to the dynamic viscosity. The difference is that the dynamic viscosity, μ , is a physical parameter dependent on the fluid while the turbulent viscosity, μ_t , depends on the flow and can therefore vary in space (and time in unsteady flows) [18].

Most eddy viscosity models are based on the Boussinesq approximation which approximates the Reynolds stress according to

$$\overline{v'_i v'_j} = -\nu_t \left(\frac{\partial \bar{v}_i}{\partial x_j} + \frac{\partial \bar{v}_j}{\partial x_i} \right) + \frac{1}{3} \delta_{ij} \overline{v'_k v'_k} \quad (2.13)$$

where $\overline{v'_k v'_k}/2 = k$ is called turbulent kinetic energy and $\nu_t = \mu_t/\rho$.

One of the most widely used eddy viscosity models is the $k - \varepsilon$ model [20, 21] where the turbulent viscosity is derived from modelled transport equations for the turbulent kinetic energy, k , and the dissipation, ε .

$$\frac{\partial}{\partial x_j}(\rho k \bar{v}_j) = \frac{\partial}{\partial x_j} \left[\left(\mu + \frac{\mu_t}{\sigma_k} \right) \frac{\partial k}{\partial x_j} \right] + P_k - \rho \varepsilon + S_k \quad (2.14)$$

$$\frac{\partial}{\partial x_j}(\rho \varepsilon \bar{v}_j) = \frac{\partial}{\partial x_j} \left[\left(\mu + \frac{\mu_t}{\sigma_\varepsilon} \right) \frac{\partial \varepsilon}{\partial x_j} \right] + \frac{\varepsilon}{k} C_{\varepsilon 1} P_\varepsilon - C_{\varepsilon 2} f_2 \rho \frac{\varepsilon^2}{k} + S_\varepsilon \quad (2.15)$$

where σ_k , σ_ε , $C_{\varepsilon 1}$ and $C_{\varepsilon 2}$ are constants, S_k and S_ε are user defined source terms and P_k and P_ε are production terms including turbulent production and buoyancy [21]. The turbulent viscosity is calculated as a function of the turbulent kinetic energy and the dissipation

$$\mu_t = \rho C_\mu f_\mu k t_t \quad (2.16)$$

where C_μ is a model constant, f_μ is a damping function and t_t is a turbulent time scale.

Turbulence is affected by the presence of walls. The inner part of the turbulent boundary layer is often divided into three regions, the viscous sublayer which is the closest to the wall, a buffer region and the log-law region. In the viscous sublayer the inertial forces are negligible compared to the viscous forces. In the log-law region, the turbulent stresses start to be dominated by the inertial forces.

The $k - \varepsilon$ model described above works well in the bulk flow but has problems to solve for the wall effects in the turbulent boundary layer. To mitigate the problem with modelling the boundary effects, the model needs to be modified in this region. In general there are two ways to model the near wall effects, either by using wall functions to calculate k and ε (high Re number models) or by using damping functions when solving the transport equations for k and ε (low Re number models). Since low Re number models solve the transport equations inside the viscous sublayer they require a very fine grid close to the wall. For high Re number models the node closest to the wall can be located in the log-law region and thus the mesh doesn't need to be as fine as for low Re number models [18, 19].

An alternative for the wall models above is two-layer models where the domain is divided into a near wall region and an outer region. In the near wall region a one equation model is used where k is calculated using Equation (2.14) while ε and μ_t are modelled with a wall function depending on wall distance and k [21].

2.4.2.2 Conjugate heat transfer

Conjugate heat transfer (CHT) is an approach for heat transfer modelling between a solid and a fluid where the two regions are thermally coupled and the temperature in the solid and fluid domains are solved for simultaneously using CFD [22]. The CHT approach can be both partitioned, where the energy equation in each domain is solved independently and temperature and heat flux are forced to be continuous on the interface, or monolithic, where a single solver is used on all regions at once [23]. One way to formulate a partitioned, or segregated, CHT solver is to write an energy transport equation for each region, both solid and fluid. This is the approach that is implemented into the CFD software StarCCM+ [21].

In order to avoid interpolation errors, it is advised to construct a conformal mesh at the interface [20]. This means that the boundary nodes of the regions on both sides of the interface coincide at the boundary. In Figure 2.5 a conformal interface between a fluid and a solid region can be seen. In the figure it is clear how the boundary nodes of both regions are located on the same place and thus information can be transferred between the regions over the interface without the need for interpolation.

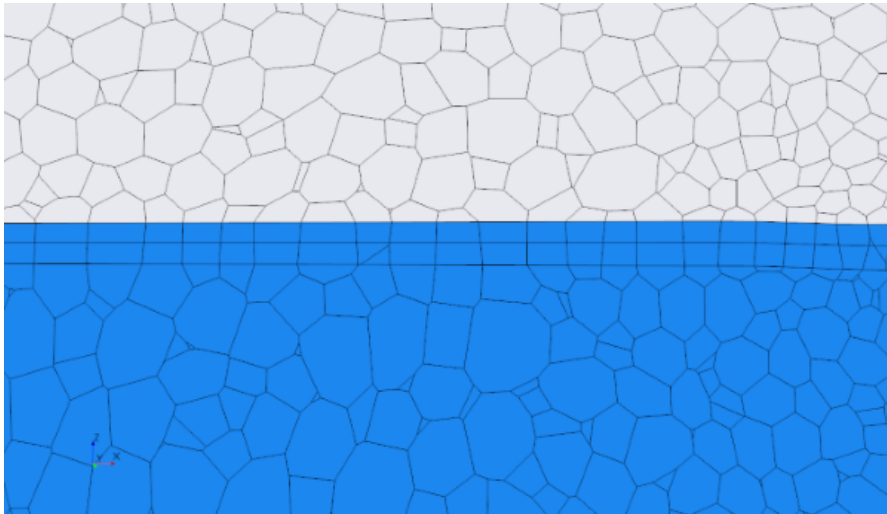


Figure 2.5: *Interface with conformal mesh between the fluid region (blue) and the solid region (grey) and two prism layers on the fluid side of the interface*

2.4.2.3 Modelling boiling

Even though boiling is a two-phase phenomenon (consisting of both liquid and vapour), single-phase boiling models are commonly used since solving multiphase problems is very computationally expensive. When the momentum exchange between the phases is negligible, e.g. nucleate boiling, a single-phase boiling model can be sufficient.

In single-phase boiling models, the phase change from liquid to vapour is ignored while the increased heat transfer between the solid surface and the liquid due to boiling is modelled as a wall boiling heat flux. The drawback of single-phase boiling models is the fact that they can model the heat flux in the nucleate boiling regime but, since no phase change is taken into account in the model, when the boiling becomes more intense and the amount of vapour bubbles increase, the models becomes less accurate [24, 15].

One empirical correlation for calculating the wall boiling heat flux which is widely used [15] was suggested by W.M. Rohsenow in 1951 [1].

$$\frac{c_{p,l}\Delta T_{sat}}{h_{lat}} = C_{qw} \left(\frac{q}{\mu_l h_{lat}} \sqrt{\frac{\sigma}{g(\rho_l - \rho_v)}} \right)^{0.33} \left(\frac{c_{p,l}\mu_l}{k_l} \right)^{1.7} \quad (2.17)$$

where $c_{p,l}$ is the specific heat of the liquid, h_{lat} is the latent heat (energy needed to evaporate the liquid), C_{qw} is a coefficient varying with the liquid-surface combination, μ_l is the dynamic viscosity of the liquid, σ is the surface tension of the liquid-vapour interface, ρ_l and ρ_v is the density for the liquid and vapour respectively and k_l is the thermal conductivity of the liquid. Even though this model is developed for the case of pool boiling, it can also be used for surface boiling in forced convection of a subcooled liquid, e.g. coolant jacket flow [1].

Since a boiling curve similar to Figure 2.4 for flow boiling of the coolant has not been available, a verification of the accuracy of the model has not been performed. However, a logarithmic representation of how the boiling model relates to a typical boiling curve is presented in Figure 2.6. The Rohsenow correlation is reasonable accurate for low to moderate amounts of nucleate boiling but deviates from the boiling curve when approaching the critical heat flux. For the correlation, a critical heat flux is not reached. This means that with this model, unreasonably high heat fluxes can occur outside the nucleate boiling regime.

Note that this is only a schematic representation of how the Rohsenow correlation relates to a typical boiling curve.

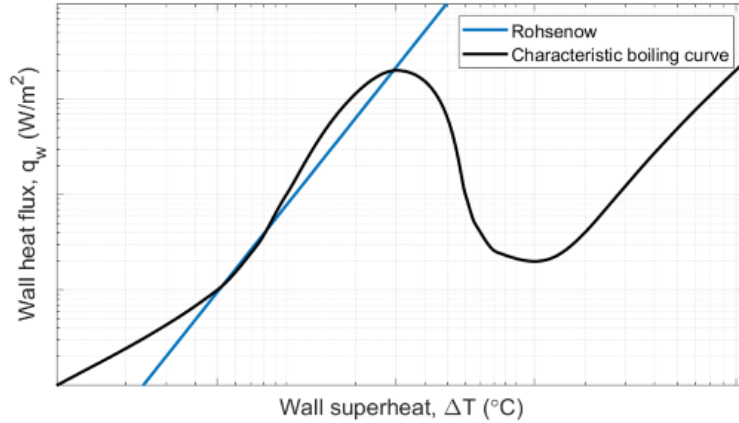


Figure 2.6: Comparison between Rohsenow's boiling heat flux correlation and a typical boiling curve

3 Method

In order to quantify the effect of the parameter changes, and identify the more and less sensitive parameters, a reference simulation is executed against which each parameter change will be compared. The heat transfer in the cylinder head is simulated using a 3D-CHT-CFD model in the CFD software StarCCM+. Changes in the geometry of the coolant jacket is done in a CAD pre-processing tool called ANSA.

3.1 Geometry

The geometry on which the simulations are performed is provided by Volvo Cars. It consists of several solid parts, where the cylinder head of an engine with IEM is the main part. Inlet/exhaust valves, bolts, spark plugs, seat rings and a gasket between the cylinder head and block are other solid parts included in the model. The engine also consists of a fluid part, the coolant jacket.

In order to decrease the meshing and computation time, the cylinder block, pistons and liners are removed from the engine model. The region of the coolant jacket located in the cylinder block is kept in the model in order to model the coolant flow. The removal of the cylinder block solid will lead to the coolant jacket located in the cylinder block not experiencing any wall heat transfer and thus the removal will affect the amount of heat extracted by the coolant. However, this is considered acceptable since this project is a parameter study that will focus on the cooling effects in the cylinder head and not a complete engine thermal analysis. It is assumed that the heat transfer in the cylinder head is not affected significantly by the removal of the cylinder block since the gasket between the cylinder head and block acts as an insulator between the regions. Figure 3.1 shows the computational domain after the cylinder block, pistons and liners are removed.

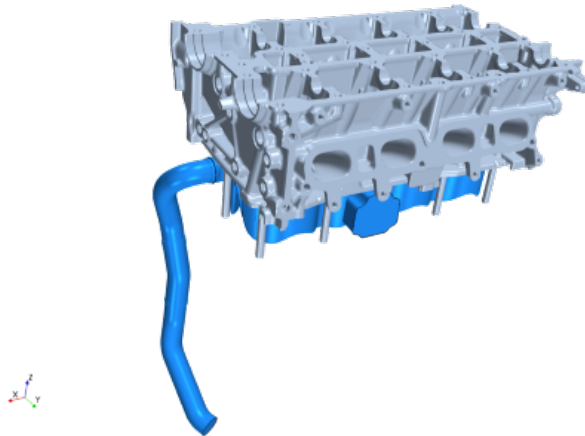


Figure 3.1: *Engine model on which simulations are performed, coolant jacket in blue and solid parts in grey*

Figure 3.2 shows the geometry of the coolant jacket. The grey part of the coolant jacket surrounds the combustion chamber walls and is located in the cylinder block. As mentioned above no heat is transferred from the cylinder block in this region. The coolant jacket inlet and the outlet to the thermostat is located in this part. The green region covers the intake and exhaust valves of the combustion chambers as well as the lower part of the exhaust manifold and the blue region covers the upper side of the IEM. In this region the outlet to the HVAC is located. The red parts are the drilled channels connecting the upper and lower coolant jacket regions.

The coolant flows into the coolant jacket through an inlet pipe connecting to the coolant jacket region located in the cylinder block. The coolant moves through the coolant jacket in the cylinder block and continues up to the cylinder head where it envelops the IEM. From the IEM, the coolant then flows over the combustion chambers and cools the intake and exhaust ports and valves. The coolant then flows down into the cylinder block again and cools the combustion chamber walls on the intake side before exiting the coolant jacket to the thermostat. Some coolant in the upper part of the coolant jacket flows out through the cabin outlet.

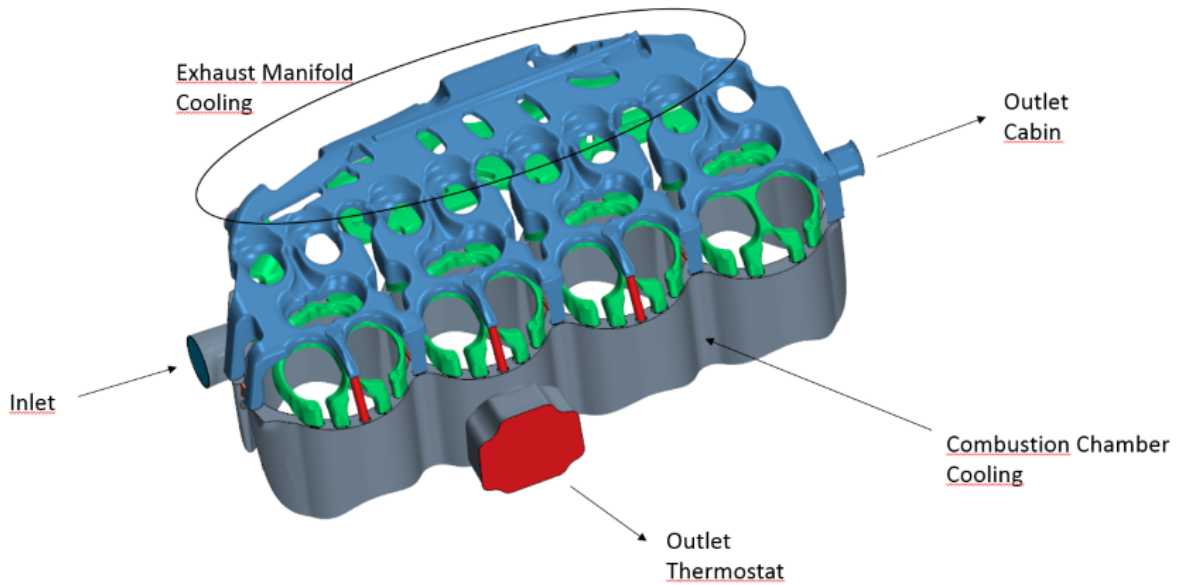


Figure 3.2: Coolant jacket geometry with upper coolant jacket (blue), lower coolant jacket (green) and cylinder block coolant jacket (grey)

Since the change from an external exhaust manifold to an IEM is relatively new, extra focus will be put on the cooling performance of the coolant jacket around the IEM.

3.2 Coolant properties

The coolant flowing in the coolant jacket is a mixture of the anti-freeze liquid Glythermin NF and water. This leads to the liquid freezing at lower temperatures, better protection against corrosion and higher saturation temperatures compared to pure water[25]. In Figure 3.3 the saturation temperature for different Glythermin/water mixtures is shown. The coolant used in this work is a 50-50 mixture between the Glythermin and pure water. This gives the coolant a saturation temperature of 131.5°C at a pressure of 2 bar compared to pure water which has a saturation temperature of 120° at 2 bar.

As mentioned in Section 2.3.2, boiling can lead to increased heat transfer between solid and fluid while excessive boiling cause the vapour to insulate the solid/fluid interface, reducing the boiling heat flux. Thus, while an increased saturation temperature can lead to reduced heat transfer, it also protects against excessive boiling in the coolant jacket.

3.3 Pre processing

The engine model is based on a Catia CAD-model which is imported into ANSA where it is checked for geometrical errors. An initial surface mesh is constructed in ANSA before the geometry is imported into StarCCM+ where the volume mesh of the engine is constructed. The geometry preparation also includes geometrical parameter changes through box morphing. The morphing is performed in ANSA before importing the geometry into StarCCM+.

Each part of the engine is imported into StarCCM+ individually. In order to define the interfaces between the different regions, the coinciding part boundaries need to be merged. This is done through an operation in StarCCM+ called imprinting which creates a common interface and enables the construction of a conformal mesh.

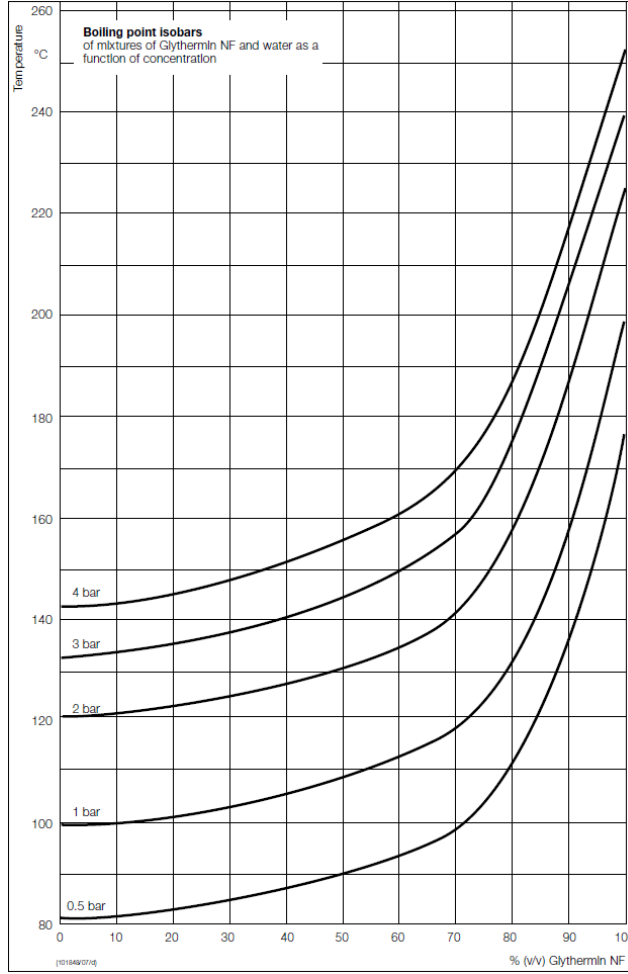


Figure 3.3: Graph of boiling temperature for different pressures and concentrations of Glythermin NF [25]

3.3.1 Mesh

The computational volume mesh is built up of polyhedral cells with a base size of 1 mm and on the fluid/solid interfaces two layers of prism cells are constructed, see Figure 2.5. The prism layers are needed in order to accurately resolve the near wall flow as well as wall heat transfer. The total prism thickness is defined as 0.75 mm and by knowing the width of the prism cells, an appropriate wall treatment can be applied.

This results in a mesh of the cylinder head and coolant jacket of 20.4 million cells with 129 million faces and 110 million vertices. The mesh is based on guidelines for CHT simulations validated at Volvo Cars.

3.4 Simulation setup

The model used for simulating the coolant flow is a 3D steady state model where the realizable $k - \varepsilon$ model is used to model the turbulence. In the near wall region, a two-layer approach is applied.

The sub-cooled nucleate boiling expected in some regions of the coolant jacket is modelled using Rohsenow's correlation (Equation (2.17)) for the wall boiling heat flux. Since Equation (2.17) depends on the wall superheat and is independent on the coolant temperature, heat can theoretically be transferred from the solid surface to the coolant even when the coolant temperature is higher than the temperature at the interface. This can lead to unreasonably high heat fluxes. To prevent this, the heat flux calculated using Equation (2.17) is in StarCCM+ multiplied with the following function

$$\max \left[0, \min \left(\frac{T_w - T}{T_w - T_{sat}}, 1 \right) \right] \quad (3.1)$$

which leads to the boiling heat flux being zero if $T > T_w$. T in this case is the fluid temperature close to the wall. Despite this the wall boiling heat flux can reach levels that are unrealistic since the model is developed for sub-cooled nucleate boiling and does not take the isolating effect of intense boiling into account. Therefore a threshold of the wall boiling heat flux above which the accuracy of the boiling model is questioned is used.

While the continuity and the momentum equations are only solved for in the coolant domain, the energy equation is solved for in both the coolant and solid regions. The difference between the solid and coolant regions is that velocity terms are removed from the energy equation for the solid. The density is constant in the solid but allowed to vary in the coolant.

On the gas/solid interfaces, the gas temperatures (computed in separate CFD models for the in-cylinder combustion and exhaust) are mapped together with a heat transfer coefficient varying over the interface in order to compute a boundary heat flux. The heat flux is calculated according to Equation (2.3) where T_f is the mapped gas temperature, h is the mapped heat transfer coefficient and T_w is the temperature computed in the solid at the interface in each simulation.

3.4.1 Reference simulation

The inlet mass flow rate for the reference case is called \dot{m}_{ref} . In the reference simulation the outlet to the cabin heating (HVAC) system is closed (a wall boundary condition is imposed on the cabin outlet). Therefore, all flow exits through the thermostat outlet on the intake side of the cylinder block.

In the reference simulation the saturation temperature is constant and referred to as, $T_{sat,ref}$. In reality the saturation temperature is dependent on the local static pressure of the coolant but until recently there has not been a function which predict the saturation temperature accurately for the coolant.

The thermostat outlet is a pressure outlet. The outlet pressure is referred to as $P_{out,ref}$. Since the saturation temperature is constant and thus independent of the pressure, the outlet pressure has no effect on the reference simulation. What drives the flow is the pressure drop through the system, not the pressure magnitude.

3.4.2 Non geometrical parameters

With the reference simulation as a starting point, a few different parameters are changed. For each parameter

Mass flow rate

When analysing how the mass flow rate affects the cooling performance of the coolant jacket all boundary conditions except the inlet mass flow is kept identical to the reference simulation. Four different mass flows, aside from the reference, are simulated. These are $0.5\dot{m}_{ref}$, $0.75\dot{m}_{ref}$, $1.5\dot{m}_{ref}$ and $2\dot{m}_{ref}$.

Mass flow distribution

To simulate different distributions of outlet mass flow between the cabin and thermostat outlet the cabin outlets condition is changed from a wall (in the reference simulation) into a mass flow outlet. The coolant jacket performance is analysed for 10, 20 and 30% of the mass flow exiting out to the HVAC system.

Saturation temperature

As mentioned above, the saturation temperature in the reference simulation $T_{sat,ref}$ is independent of the pressure. To see how the saturation temperature affects the heat transfer, the coolant jacket is analysed with a saturation temperature of $T_{sat,ref} + 14\text{K}$ as well.

These two cases are also compared to simulations where the saturation temperature is dependent on the local static pressure. The pressure dependent saturation temperature is derived from the data in Figure 2.4. When comparing the pressure dependent saturation temperature with the constant temperature of $T_{sat,ref}$ and $T_{sat,ref} + 14\text{K}$, the coolant jacket is analysed with the thermostat outlet pressure being $P_{out,low}$ and $P_{out,ref}$. These pressures corresponds to mean saturation temperatures in the coolant jacket of $T_{sat,ref} + 2.2$ and $T_{sat,ref} + 14.8$.

To further analyse the effect of pressure dependent saturation temperature, the coolant jacket is also analysed at thermostat outlet pressures of $P_{out,1}$, $1.33P_{out,1}$, $1.67P_{out,1}$ and $2P_{out,1}$.

Thermal conductivity

The thermal conductivity of the aluminium in the cylinder head affects how easily the heat spreads through the engine. A higher thermal conductivity means a smaller temperature gradient given a certain heat flux, see Equation (2.2), so a change in thermal conductivity should affect the temperature distribution of the engine. To see how big this effect is, the cooling performance is simulated with two different thermal conductivities which are compared to the reference simulation. The thermal conductivities are referred to as k_{ref} , k_{mid} and k_{low} . The thermal conductivities simulated are shown in Figure 3.4 as functions of temperature.

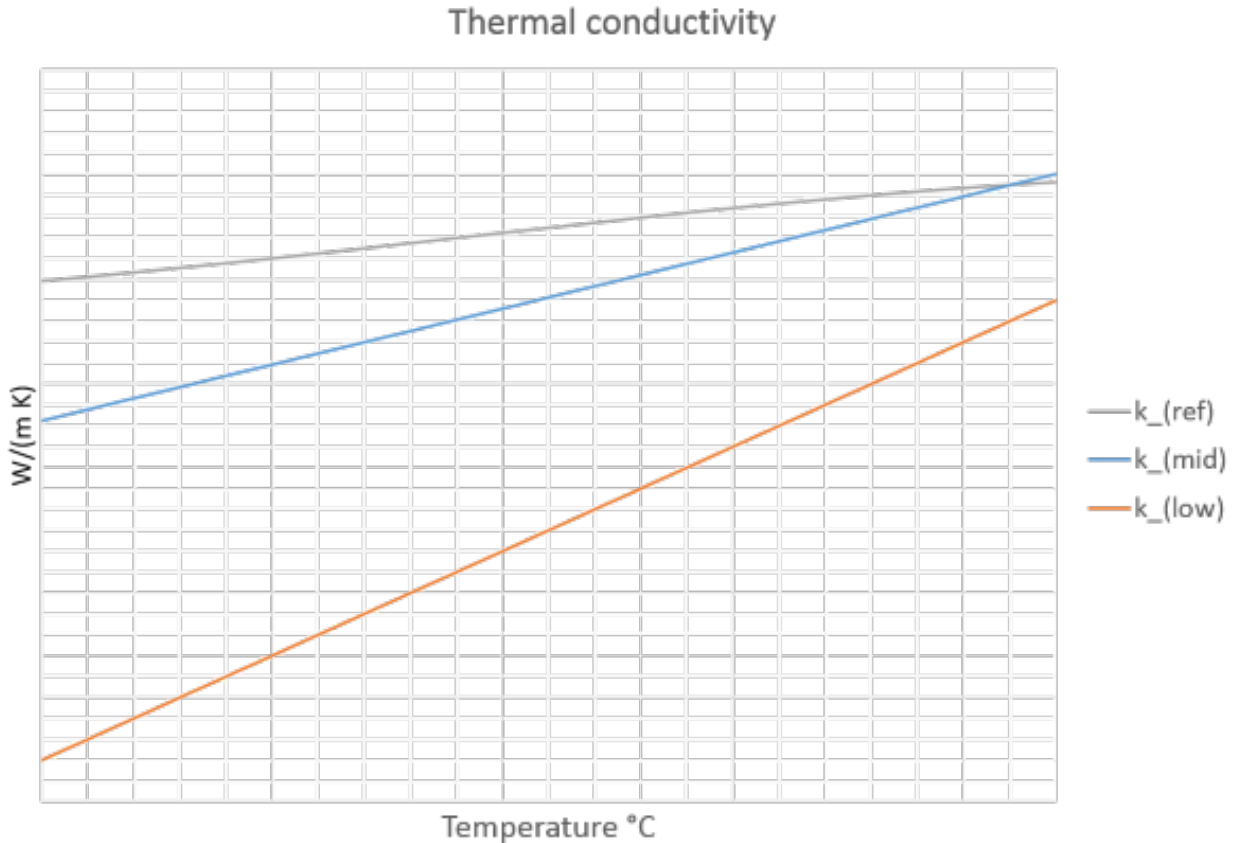


Figure 3.4: *Thermal conductivity for different simulations*

3.4.3 Geometrical changes

The geometry changes done are performed exclusively on the coolant jacket in the cylinder head and all inlets and outlets are unchanged.

Two different geometry changes are performed, one displacement and one surface topology modification.

Displacement

The displacement moves the coolant jacket 1mm in the x-direction. This is to simulate variations during the casting process. A close view of the resulting geometry of the coolant jacket in the cylinder head is seen in Figure 3.5. Since the interfaces between the upper coolant jacket and the gasket and lower coolant jacket are not moved, the channels connecting the different regions are slightly distorted.

The regions that are expected to be the most sensitive to displacement of the coolant jacket are the channels above the combustion chambers. Therefore, focus is put mostly on the temperature field in the cylinder head between the gas side and the coolant around the marked regions in Figure 3.6.



Figure 3.5: *View of coolant jacket displaced 1 mm in x-direction*

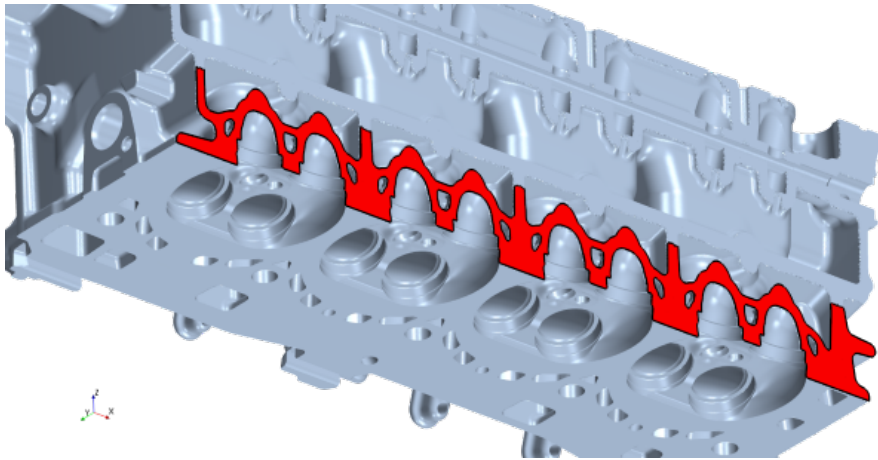


Figure 3.6: *Region where the temperature of the cylinder head is analysed*

Surface topology

In the surface topology change, hills and valleys are created on the area near the exhaust flange of the upper coolant jacket as seen in Figure 3.7. The purpose of the surface topology modification is to see how the wall boiling heat flux in this region is affected.

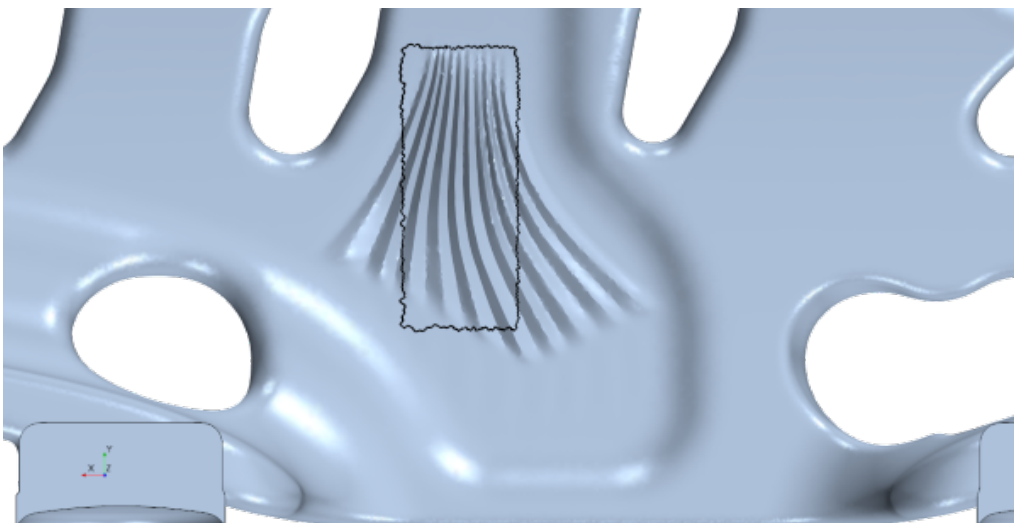


Figure 3.7: *Upper coolant jacket modified surface topology as seen from below*

The surface enclosed by the rectangle is 30% larger than the same surface in the reference simulation. This way the heat transfer to the coolant is spread out on a larger area which should decrease the heat flux and could reduce the boiling heat flux.

4 Results and discussion

The sensitivity analysis produced a large amount of results. In this section the results leading to the main findings of the study are shown. Additional contours of flow fields, temperature and boiling can be found in Appendix A. In some figures, the coolant jacket is called wj (water jacket).

4.1 Reference case

The result of the reference simulation is presented below. It is against these results the parameter changes are compared.

4.1.1 Flow field

The cell relative velocity of the coolant jacket computed in the reference simulation is shown in Figure 4.1. The cell relative velocity is a measure of the velocity a small distance from the wall. This is a good tool to visualise the flow field in the coolant jacket. The coolant jacket above the combustion chamber, see Figure 4.1b, has higher velocities than the region covering the IEM, see Figure 4.1a and 4.1c. The lower velocities in the parts of the coolant jacket covering the IEM mean that the coolant is exposed to high thermal loads for a longer time. This is partly due to the fact that the integration of the exhaust manifold is relatively new and has not been optimised as much as the region above the combustion chamber.

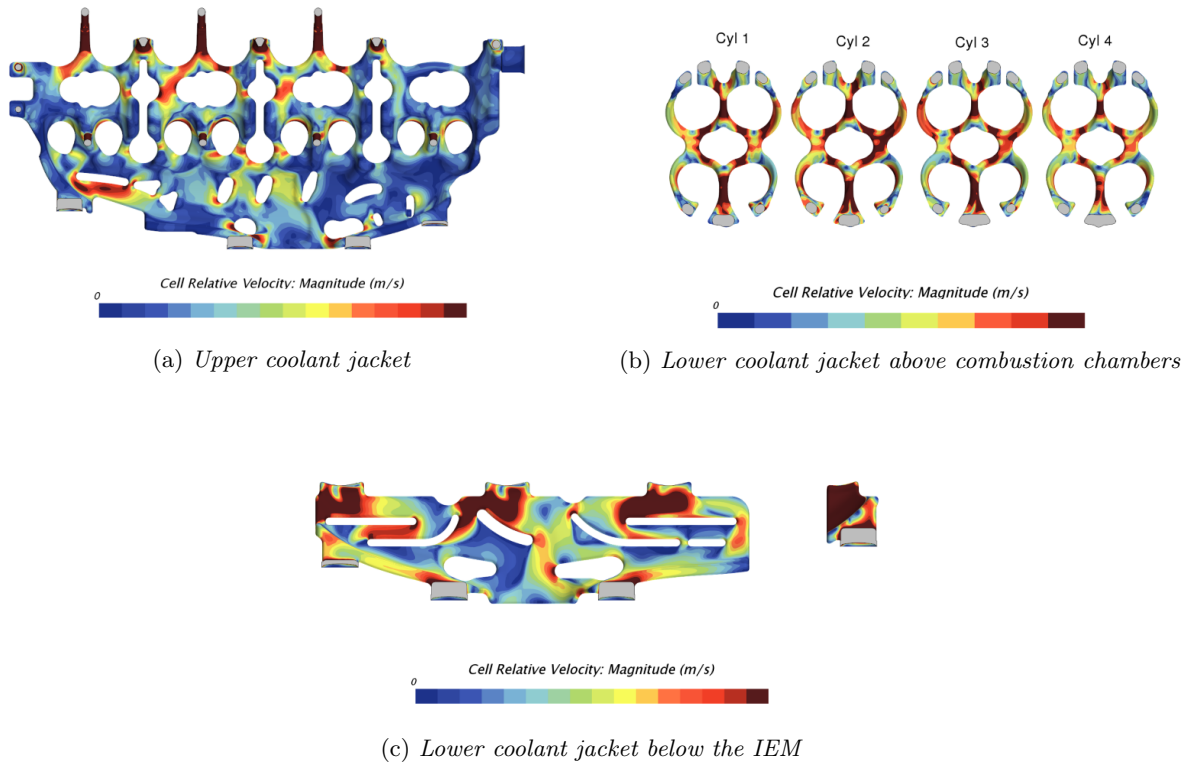


Figure 4.1: Cell relative velocity in the coolant jacket of the reference case

4.1.2 Temperature

4.1.2.1 Gas side

In Figure 4.2 the temperature on the gas/solid interface is shown. These are the regions where the thermal loads, calculated from the in-cylinder/exhaust CFD simulations mentioned in Section 3.4 are applied.

The temperature is especially high in the vicinity of the spark plug and in the IEM where the exhaust ports merge.

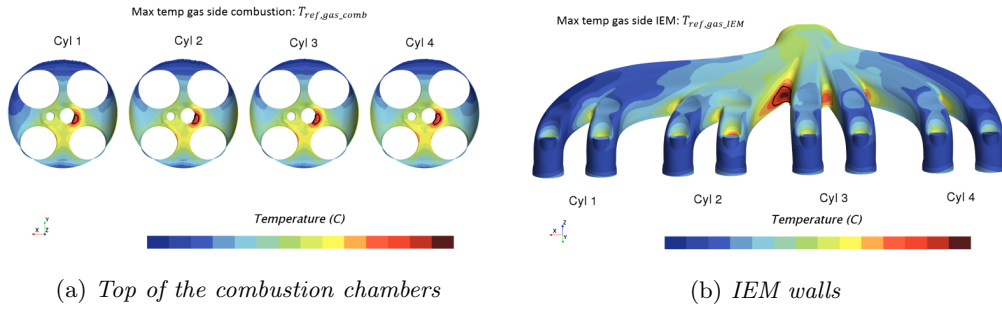


Figure 4.2: Temperature field of the cylinder head walls on the gas side

4.1.2.2 Coolant jacket

In Figure 4.3 contours of the temperature field on the coolant/cylinder head interface is shown. Both Figure 4.3a and 4.3c show high temperatures in the vicinity of the exhaust flange (the lowest regions in the figures). The high thermal load of the exhaust flange and the relatively low coolant velocity in this region, see Figure 4.1a and 4.1c, are contributors to the high temperatures on the coolant jacket walls. It can also be noted that the hotspots in the coolant jacket correspond with the stagnation/recirculation regions which is intuitive as the low velocities in these regions lead to decreased convective heat transfer.

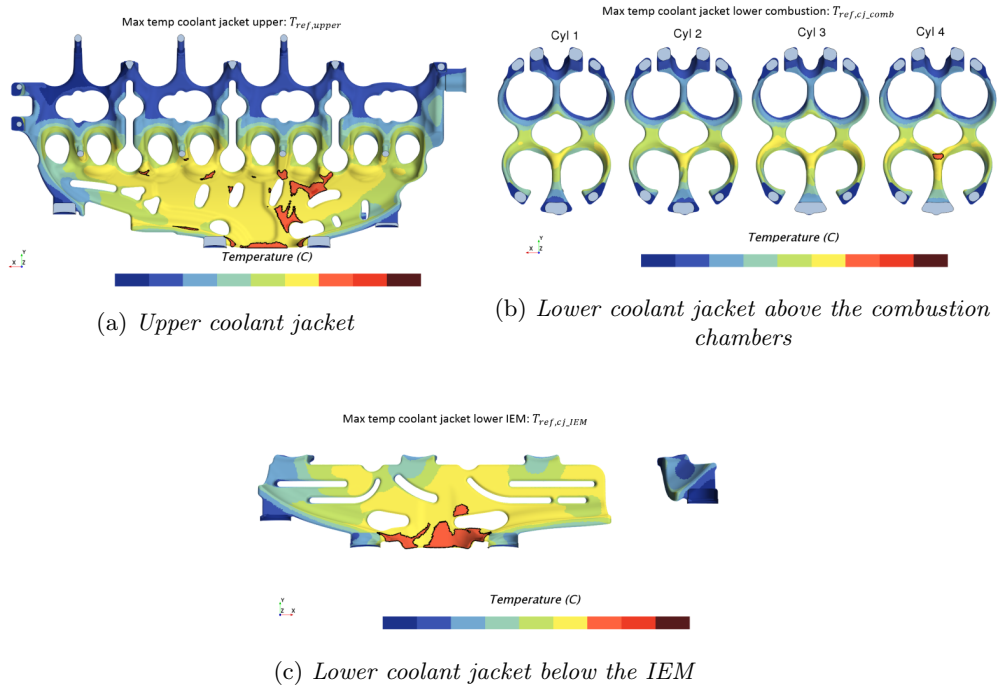


Figure 4.3: Temperature field of the coolant jacket walls

4.1.3 Heat flux

The heat extracted from the solid by the coolant jacket in the cylinder head is shown in Table 4.1. The region where the most heat is extracted by the coolant jacket is the upper part. However, in the region of the lower coolant jacket covering the top of the combustion chambers almost as much heat is extracted. The surface average heat flux is the total heat transferred divided by the area.

	Area of solid/coolant interface	Heat transferred	Surface average heat flux
Upper coolant jacket	$0.57A_{ref}$	$Q_{cj,upper} = 0.41Q_{ref}$	$q_{cj,upper} = 0.71q_{ref}$
Lower above combustion	$0.26A_{ref}$	$Q_{cj,comb} = 0.38Q_{ref}$	$q_{cj,comb} = 1.45q_{ref}$
Lower below IEM	$0.17A_{ref}$	$Q_{cj,IEM} = 0.21Q_{ref}$	$q_{cj,IEM} = 1.27q_{ref}$
Total	A_{ref}	Q_{ref}	q_{ref}

Table 4.1: Heat extracted by coolant jacket in cylinder head

4.1.3.1 Wall boiling heat flux

Figure 4.4 shows contours of the wall boiling heat flux on the coolant jacket walls. The grey areas in the figures show the regions where no boiling is present (the wall temperature is below the saturation temperature). There is a correspondence between the regions with high wall temperatures (see Figure 4.3) and the regions with high wall boiling heat flux and regions with low cell relative velocity (see Figure 4.1).

Since the temperature of the coolant jacket region above the combustion chambers is lower than the IEM covering regions and the saturation temperature is constant in the reference simulation, the wall boiling heat flux is lower in this region as well.

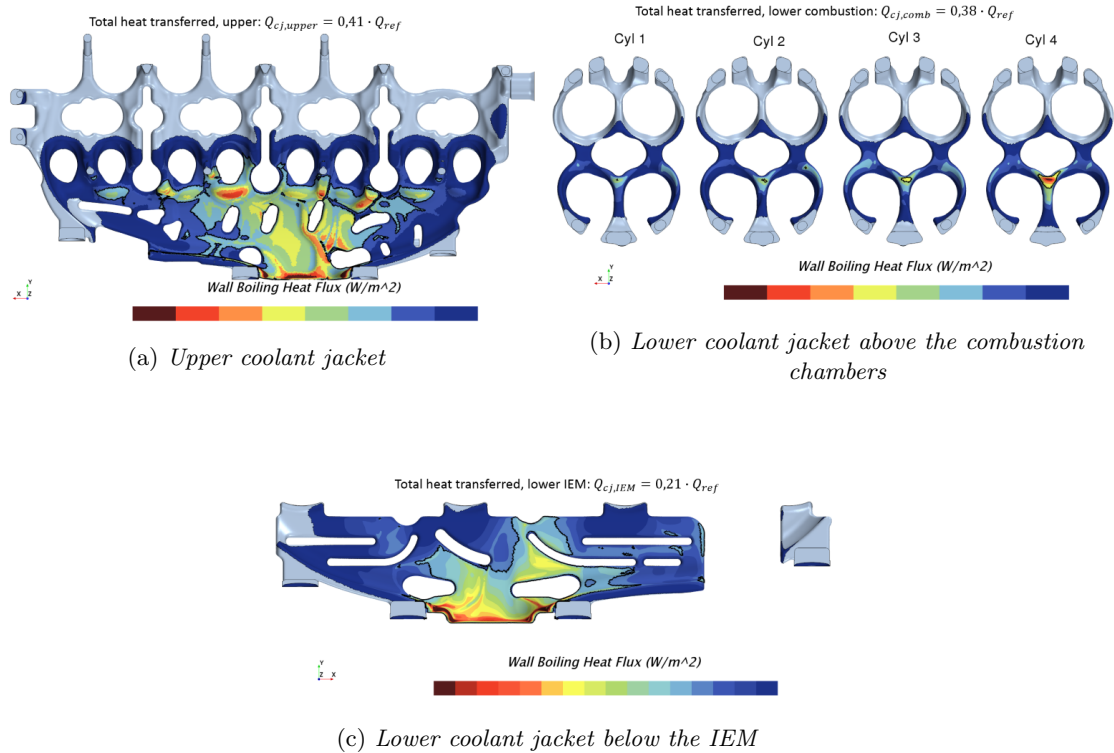


Figure 4.4: Wall boiling heat flux on the coolant jacket walls

Table 4.2 shows how much of the heat transfer in the cylinder head is due to boiling. As indicated above, the boiling contribution to the heat transfer in the coolant jacket region above the combustion chamber is very low. Figure 4.4 and Table 4.2 indicate that both regions covering the IEM has a large proportion of boiling with a high wall boiling heat flux.

	Surface integrated wall boiling heat flux	Surface average wall boiling heat flux
Upper coolant jacket	$Q_{b,cj,upper} = 0.46Q_{cj,upper}$	$0.46q_{cj,upper}$
Lower above combustion	$Q_{b,cj,comb} = 0.03Q_{cj,comb}$	$0.03q_{cj,comb}$
Lower below IEM	$Q_{b,cj,IEM} = 0.35Q_{cj,IEM}$	$0.35q_{cj,IEM}$
Total	$Q_{b,ref} = 0.27Q_{ref}$	$0.27q_{ref}$

Table 4.2: Heat transferred to the coolant jacket from the cylinder head solid due to boiling

4.2 Non geometrical parameters

In this section the results of the sensitivity analysis for the non geometrical parameters are shown for each parameter group, beginning with the mass flow rate.

4.2.1 Mass flow rate

When presenting the results from the analysis of the mass flow rate, the effects on the coolant jacket is presented first, and then the effects on gas side temperatures are shown.

4.2.1.1 Coolant jacket

Figure 4.5 shows the temperature field of the upper coolant jacket for the mass flow rates $0.5\dot{m}_{ref}$, \dot{m}_{ref} and $2\dot{m}_{ref}$. The coolant jacket wall temperature is highly dependent on the mass flow rate. A higher mass flow rate leads to decreased temperature on the coolant jacket walls, which is intuitive. This is because with increased mass flow, convection is increased and the high temperature coolant is removed faster from the cylinder head.

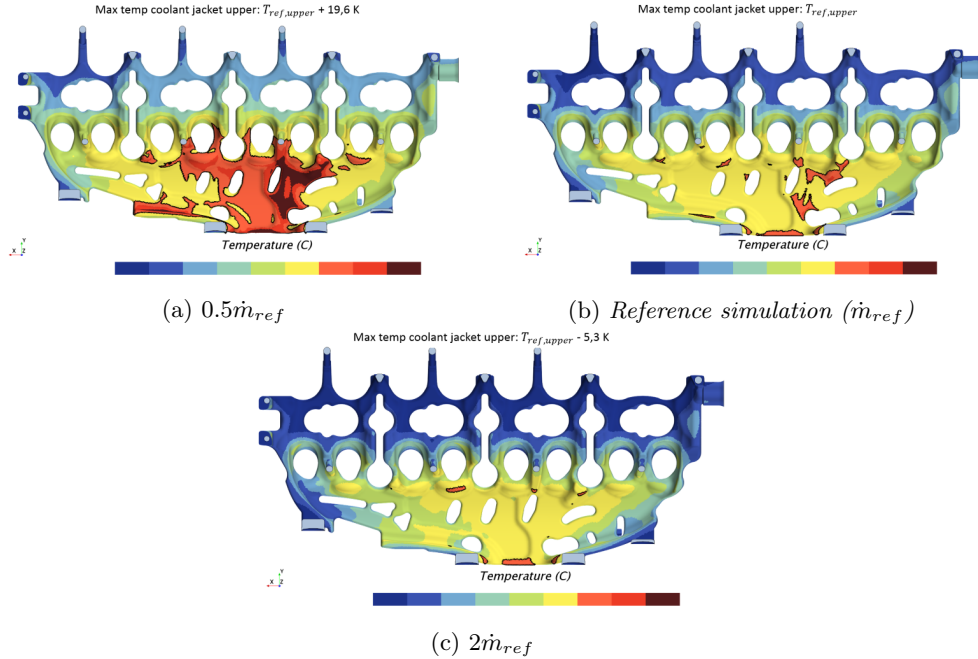


Figure 4.5: Temperature in upper coolant jacket for $0.5\dot{m}_{ref}$, \dot{m}_{ref} and $2\dot{m}_{ref}$

The decrease in temperature with increased mass flow can be seen in the lower coolant jacket as well. Even though the overall temperature decreases with increased mass flow, the change in mass flow may lead to the maximum temperature increasing due to changed flow fields and moved stagnation points. This phenomenon can be seen in Figure 4.7 which shows the maximum temperature on the coolant jacket walls as a function of mass flow rate and in Figure 4.6 where the point of maximum temperature in the lower coolant jacket changes when the mass flow rate is increased from $1.5\dot{m}_{ref}$ to $2\dot{m}_{ref}$.

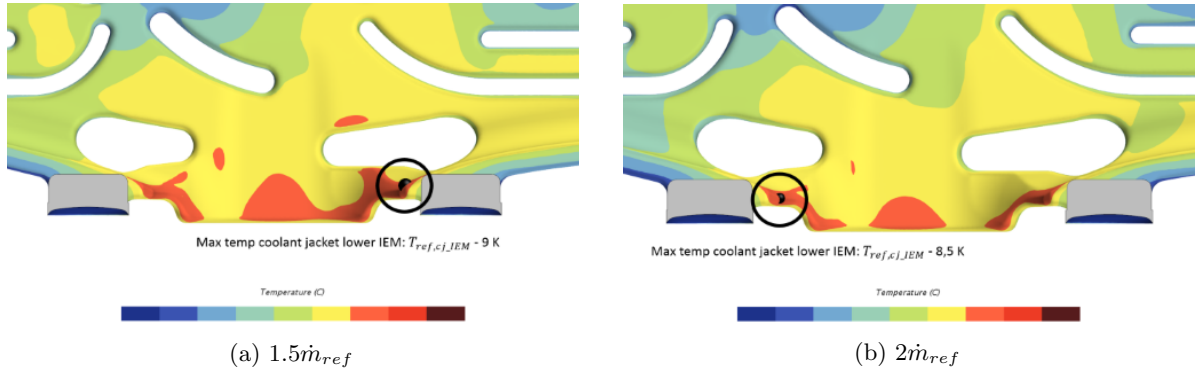


Figure 4.6: Location of the maximum temperature in the coolant jacket below the IEM

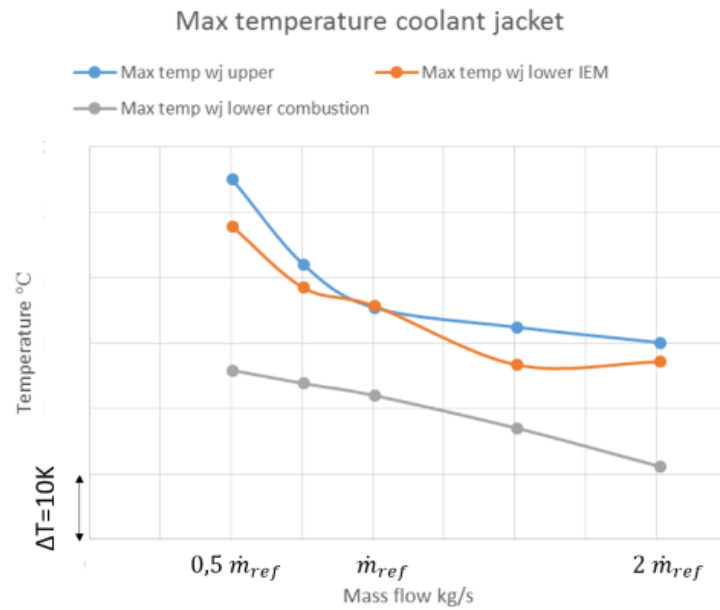
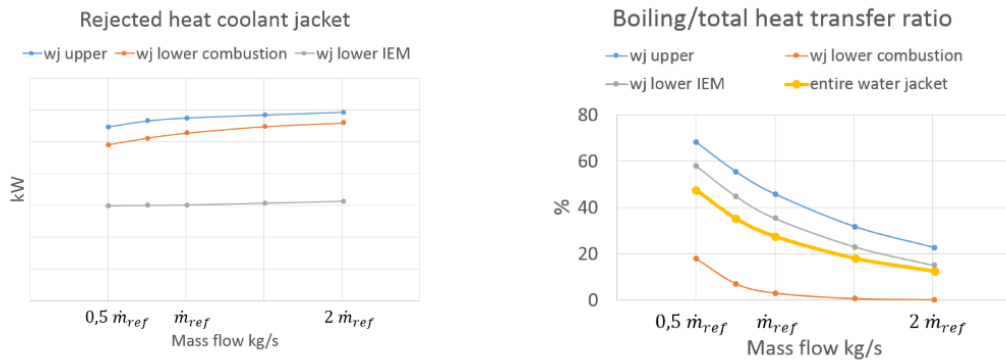


Figure 4.7: Maximum temperature on the coolant jacket wall in each part of coolant jacket. Note: Location of maximum temperature varies

In Figure 4.7 an asymptotic behaviour of the coolant jacket covering the IEM can be seen where the effect of the mass flow change on temperature decreases with increased mass flow. The difference of maximum temperature is larger between $0.5\dot{m}_{ref}$ and $0.75\dot{m}_{ref}$ than between $1.5\dot{m}_{ref}$ and $2\dot{m}_{ref}$. The region of the coolant jacket above the combustion chambers show a more linear behaviour.

In Figure 4.8a the extracted heat from the solid increases slightly with increasing mass flow. Figure 4.8b shows the ratio between the heat transfer due to boiling and the total heat transfer on the coolant jacket walls. The heat transfer due to boiling is lower above the combustion chambers than around the IEM. While the boiling heat transfer is almost negligible above the combustion chambers at mass flows higher than \dot{m}_{ref} the wall boiling heat transfer in the regions surrounding the IEM is still significant and continues to be affected by changes in mass flow rate. The decreasing effect on wall temperature with increasing mass flow correlates with the reduction of wall boiling heat flux in the coolant jacket.



(a) Total heat transferred to the different regions in the coolant jacket

(b) Amount of heat transferred to coolant jacket due to boiling

Figure 4.8: Heat transfer and boiling in relation to mass flow rate

As mentioned above, wall boiling continues to be significant around the IEM for high mass flows and in Figure 4.9 there are regions with very high wall boiling heat flux that are not erased with increased mass flow.

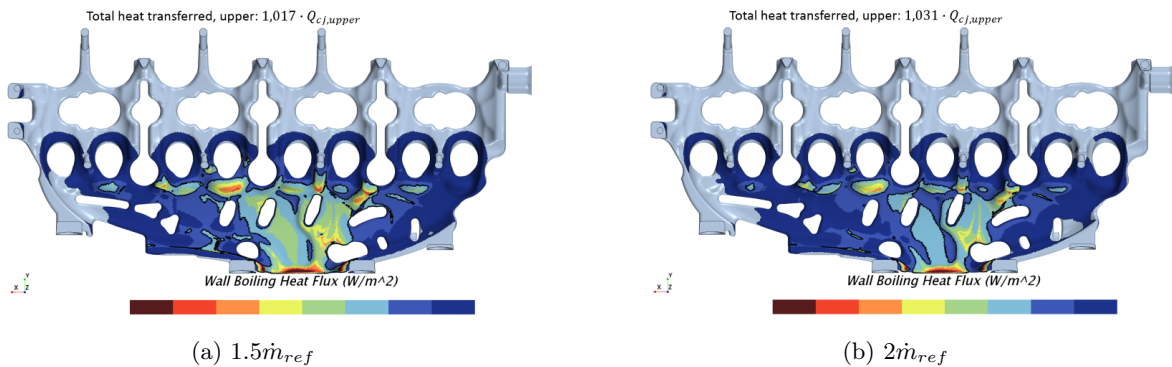


Figure 4.9: Wall boiling heat flux in upper coolant jacket

Looking at Figure 4.10 and comparing it with Figure 4.9 the regions with high wall boiling heat flux mostly match with the regions where the velocity is low.

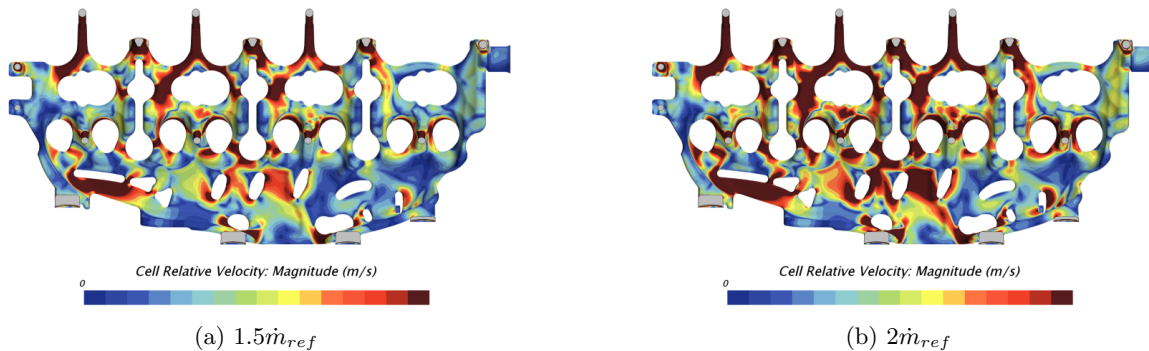


Figure 4.10: Cell relative velocity in the upper coolant jacket

channels from cylinder 2 and 3. In Figure 4.13a the red line shows where the temperature in the cylinder head is plotted in Figure 4.13b. In Figure 4.13c the temperature gradient in the vertical direction along the same line is shown. The temperature gradient in the solid is similar for all mass flows, especially a distance away from the solid/coolant interfaces. On the coolant/solid interfaces, a deviation of the temperature gradient between different mass flow rates can be observed. Lower mass flows indicate an increased temperature gradient on the coolant/solid interface compared to high mass flows. This correlates with the increased wall boiling heat flux for lower coolant mass flows. The increasing temperature gradient at the interfaces indicate that an unreasonably high heat flux is present on the interfaces for low mass flows. This can occur if the wall superheat is close to (or above) the superheat leading to critical heat flux (point *E* in Figure 2.4. The boiling formulation used (Equation (2.17)) loose accuracy for heat fluxes close to and above the critical heat flux.

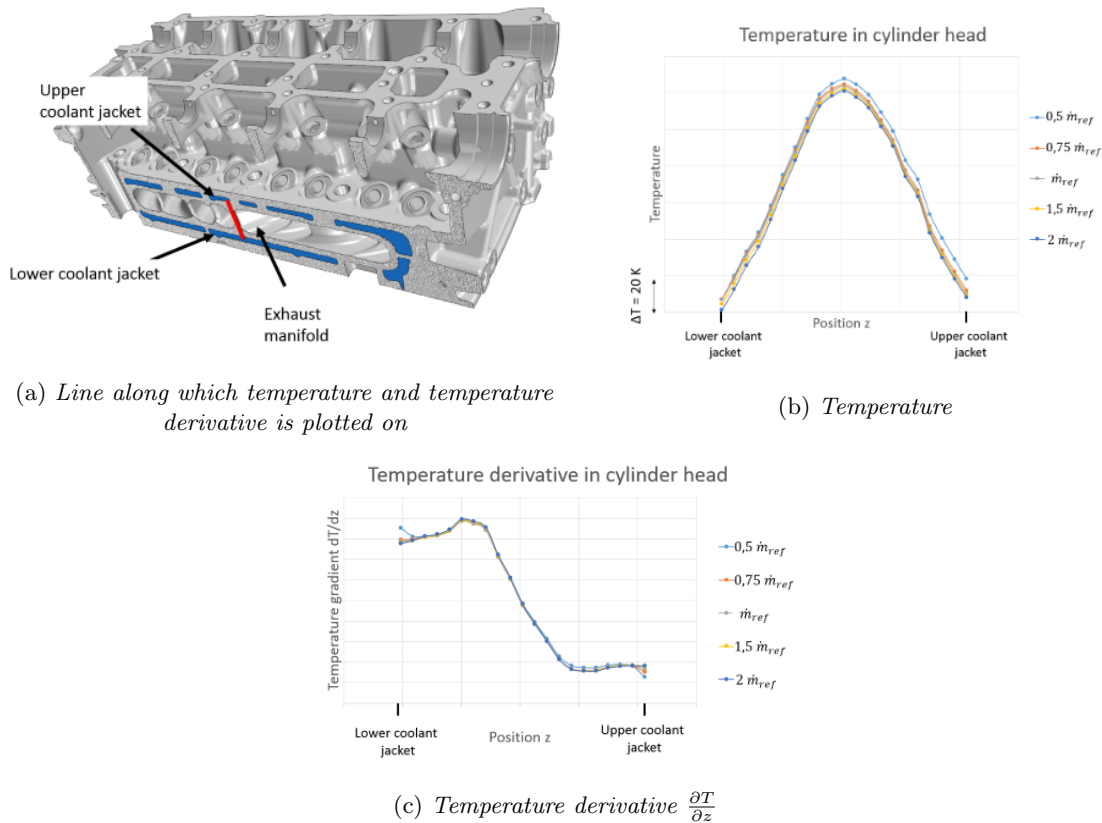


Figure 4.13: Temperature and temperature derivative in the cylinder head for different mass flow rates

The temperature field on the top of the combustion chambers for $0.5\dot{m}_{ref}$ and $2\dot{m}_{ref}$ are shown in Figure 4.14. In general, the temperature is about 20 K lower in the simulation with a mass flow of $2\dot{m}_{ref}$ compared to $0.5\dot{m}_{ref}$.

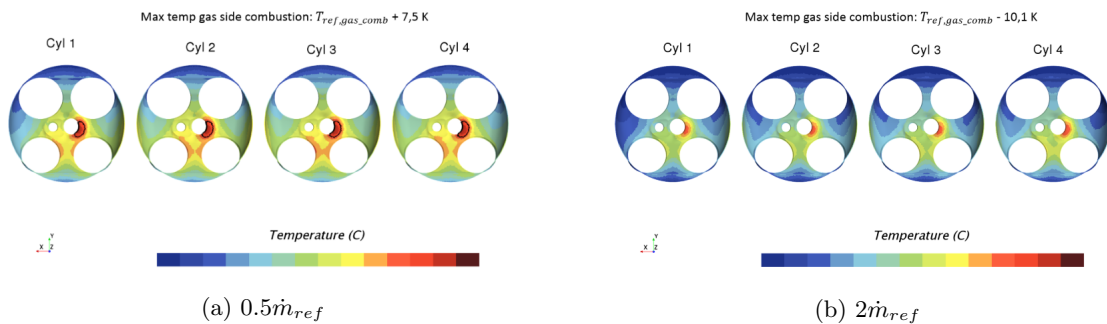


Figure 4.14: Temperature field of the top of the combustion chambers for mass flows of $0.5\dot{m}_{ref}$ and $2\dot{m}_{ref}$

4.2.2 Mass flow distribution

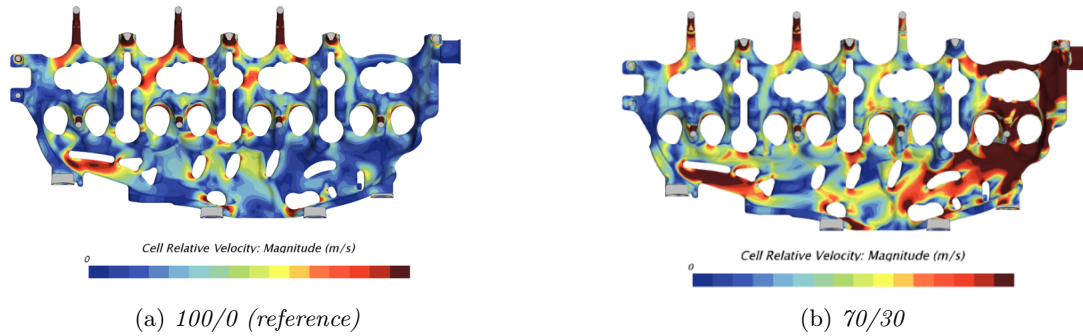


Figure 4.15: *Cell relative velocity in the upper part of the coolant jacket for 100% and 70% of the flow through the thermostat outlet*

Figure 4.15 shows the cell relative velocity in the upper coolant jacket for the reference simulation and for 30% of the mass flow exiting through the cabin outlet. When the outlet to the HVAC system is opened, the mass flow through the upper coolant jacket increases, naturally the velocity of the coolant increases most close to the cabin outlet.

Figure 4.16 shows the cell relative velocity in the lower coolant jacket. A velocity increase in the region below the IEM can be seen as well as a velocity decrease in the channels above the combustion chambers when coolant exits through the cabin outlet.

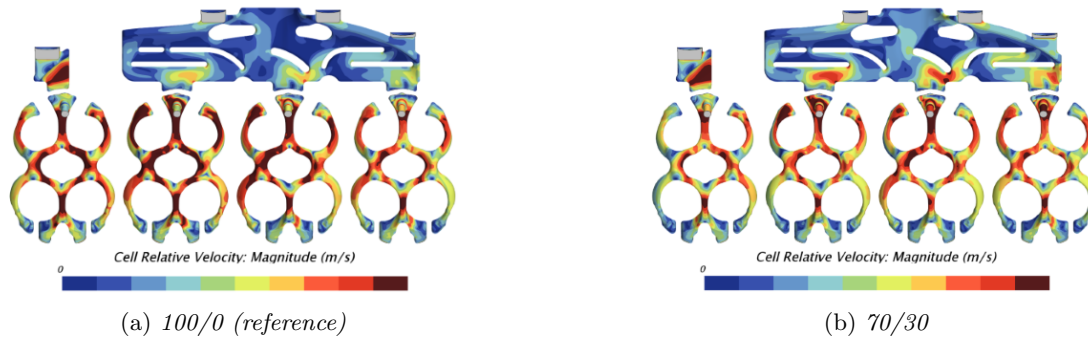


Figure 4.16: *Cell relative velocity in the lower part of the coolant jacket for 100% and 70% of the flow through the thermostat outlet*

In Figure 4.17 the heat extracted by each coolant jacket region is illustrated. An effect of the increased velocities in the upper coolant jacket and decreased velocities above the combustion chambers is that more heat is transferred to the coolant in the upper coolant jacket for increased flow to the cabin outlet while less heat is transferred above the combustion chambers. The heat transfer in the region below the IEM remains constant.

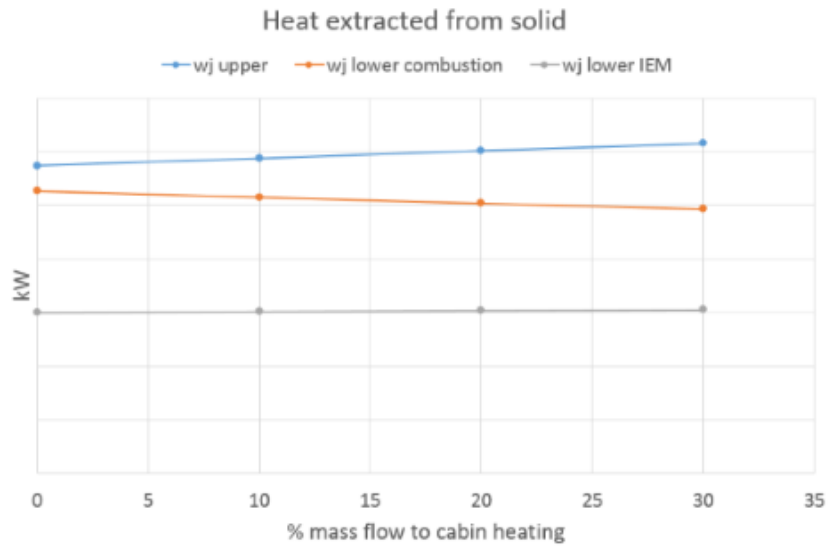


Figure 4.17: Heat transferred to coolant as a function of outflow distribution

Figure 4.18 shows the maximum temperature in each coolant jacket region for varying outflow distributions. The change in outflow distribution disrupts the flow field and this leads to instabilities on the maximum temperatures as stagnation points and recirculation regions change and move depending on the flow field. In Figure 4.18 the maximum temperature in the upper coolant jacket is much lower with 10% flow through the cabin outlet compared to the other distributions. The temperature in the region below the IEM remains almost constant while the temperature above the combustion chambers increases slightly after the cabin outlet is opened.

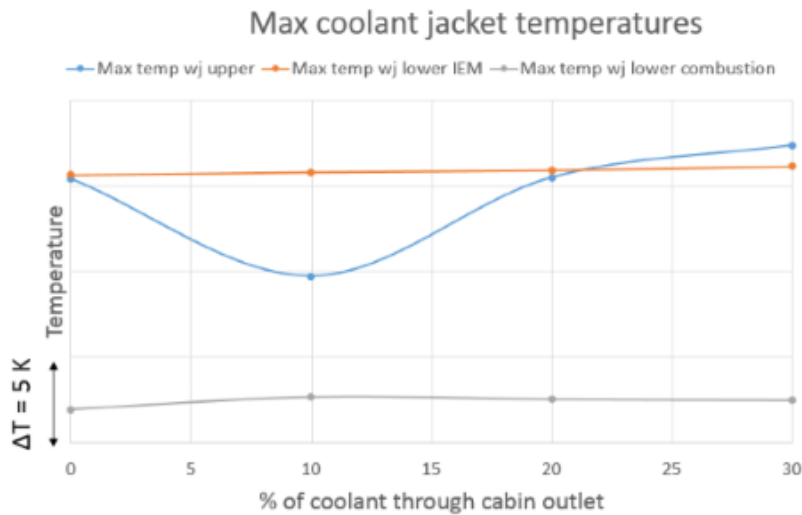


Figure 4.18: Maximum temperature on coolant jacket wall for different outflow distributions

In Figure 4.19 the temperature field of the upper coolant jacket is shown and the point of maximum temperature is shown as a black dot. Changes in the temperature field can be seen as the hotspots move around and the point of the maximum temperature is different for every outflow distribution. This indicates that the temperature of the coolant jacket is sensitive to mass flow distribution changes and that no single point can be characterised as more important than others.

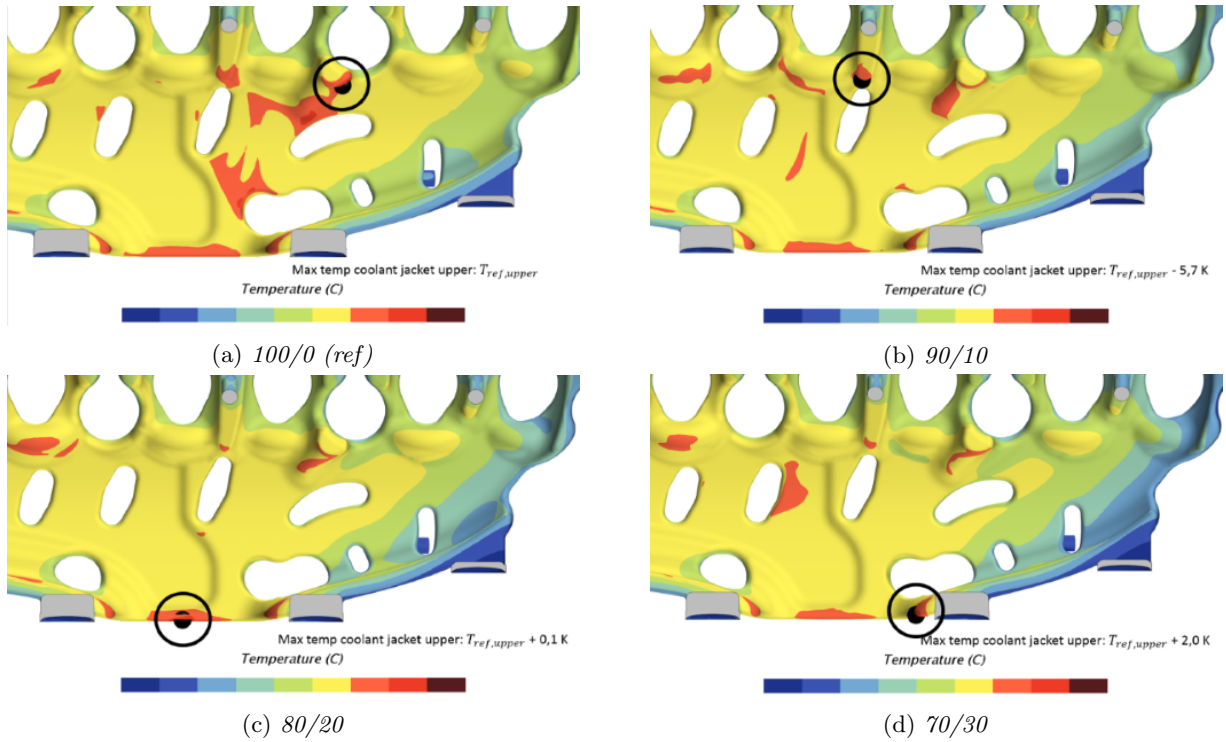


Figure 4.19: Local temperature field and maximum temperature on the upper coolant jacket wall for different outflow distributions

In Figure 4.20 the wall of the upper coolant jacket is divided into different areas depending on the wall temperature. Even if the outflow distribution do influence the location and size of the hotspots in the upper coolant jacket, the effect on the overall temperature distribution is small. A small decrease of areas with high temperatures can be seen for increased flow through the cabin outlet.

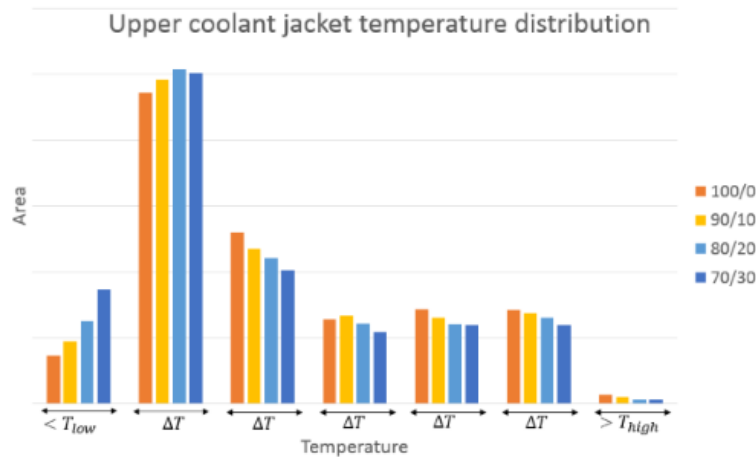


Figure 4.20: Temperature distribution in the upper coolant jacket

As illustrated in Figure 4.21 the maximum temperature on the gas side walls remain almost constant. Since the change of outflow distribution has a small effect on the overall temperature distribution in the coolant jacket, the gas side maximum temperatures are not significantly affected.

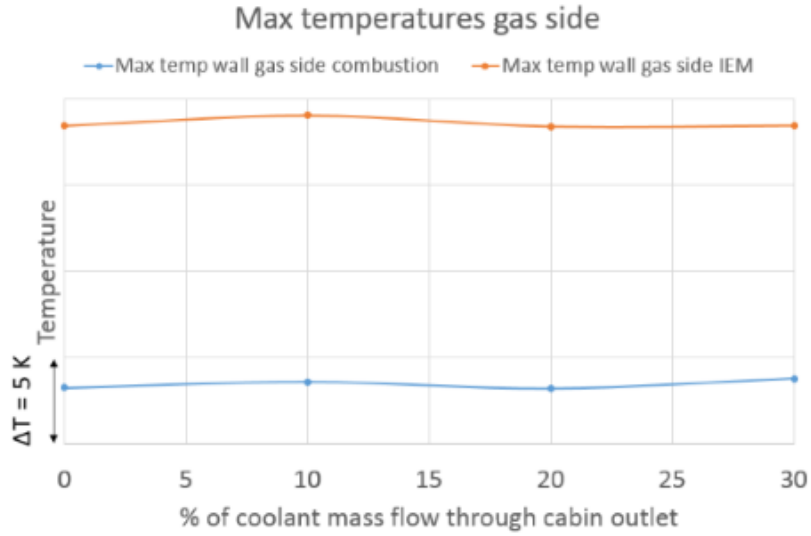


Figure 4.21: Maximum temperature on gas side wall for different outflow distributions

4.2.3 Pressure dependent saturation temperature

First a comparison between constant and pressure dependent saturation temperatures are analysed and then an analysis of pressure dependent saturation temperature for different outlet pressures is presented.

4.2.3.1 Constant vs pressure dependent saturation temperature

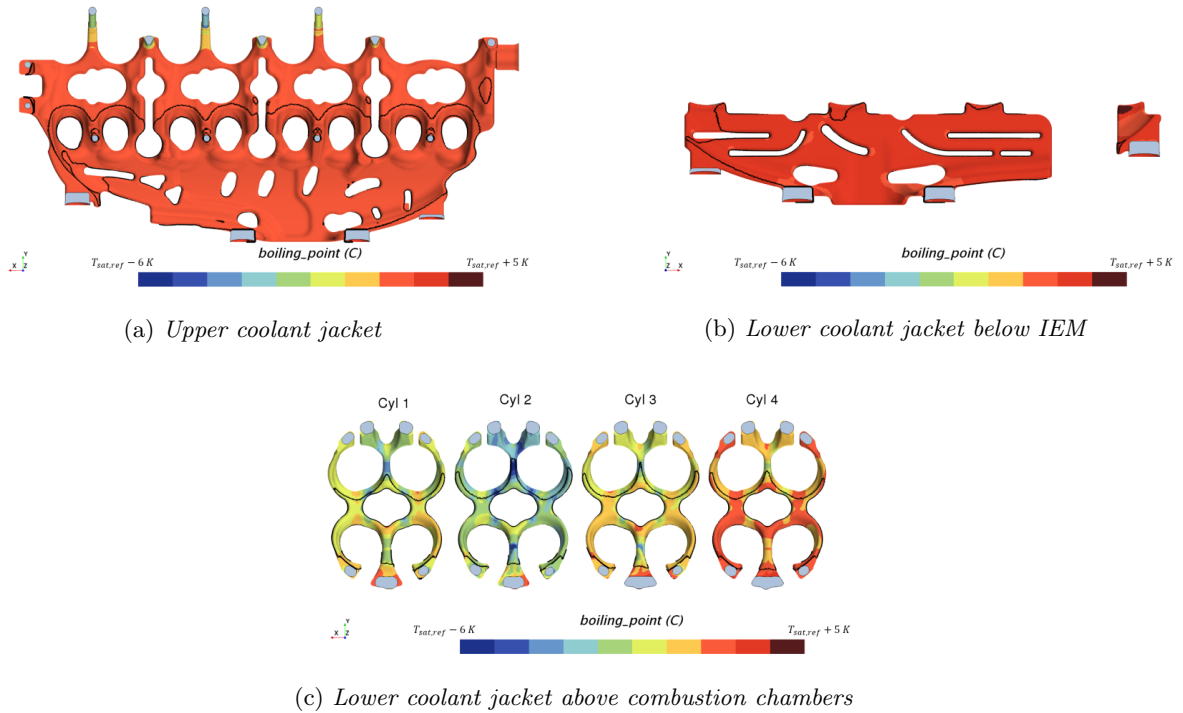


Figure 4.22: Saturation temperature in the coolant jacket with an outlet pressure at the thermostat of $P_{out,low}$

Figure 4.22 shows the saturation temperature in the different regions of the coolant jacket. The black lines illustrate the interface where boiling starts to occur. The saturation temperature in the coolant jacket is almost

uniform around $T_{sat,ref} + 2K$ in both the upper part of the coolant jacket and the region below the IEM. There are small regions where the pressure and thus the saturation temperature is lower, namely the channels in the upper coolant jacket leading to the cylinder block on the intake side (upper part of Figure 4.22a). However, these are regions where boiling does not take place. In the channels above the combustion chambers, significant pressure variations are present which leads to different saturation temperatures, both within the channels for each cylinder and between the cylinders.

Table 4.3 illustrates that, in the regions where boiling is present, the saturation temperature is nearly constant in both the upper coolant jacket and below the IEM. While a significant difference between the maximum and minimum saturation temperature can be seen in the region above the combustion chambers, both when the thermostat outlet pressure is $P_{out,low}$ and $P_{out,ref}$.

	Min boiling temperature		Max boiling temperature	
	$P_{out,low}$	$P_{out,ref}$	$P_{out,low}$	$P_{out,ref}$
Upper coolant jacket	$T_{sat,ref} + 1.5K$	$T_{sat,ref} + 14.1K$	$T_{sat,ref} + 2.9K$	$T_{sat,ref} + 15.1K$
Lower below IEM	$T_{sat,ref} + 2.0K$	$T_{sat,ref} + 14.6K$	$T_{sat,ref} + 3.9K$	$T_{sat,ref} + 15.7K$
Lower above combustion chambers	$T_{sat,ref} - 5.6K$	$T_{sat,ref} + 9.5K$	$T_{sat,ref} + 4.1K$	$T_{sat,ref} + 16.0K$

Table 4.3: Minimum and maximum boiling temperature in the region of the coolant jacket where boiling occurs

Despite the significant variation of boiling temperature in the channels above the combustion chambers, Table 4.4 shows that the heat transfer remains almost equal to when a constant boiling temperature is used. Figure 4.23 shows that the temperature in the coolant jacket above the combustion chambers for pressure dependent boiling temperature does not deviate from the temperature when constant boiling temperature is used.

	Saturation temperature		Thermostat outlet pressure	
	$T_{sat,ref}$	$T_{sat,ref} + 14K$	$P_{out,low}$	$P_{out,ref}$
Total heat transferred	$Q_{cj,comb}$	$1.00Q_{cj,comb}$	$1.00Q_{cj,comb}$	$1.00Q_{cj,comb}$
Heat transfer due to boiling	$Q_{b,cj,comb}$	$0.13Q_{b,cj,comb}$	$0.92Q_{b,cj,comb}$	$0.13Q_{b,cj,comb}$

Table 4.4: Heat transfer from solid to coolant jacket for constant and pressure dependent saturation temperature

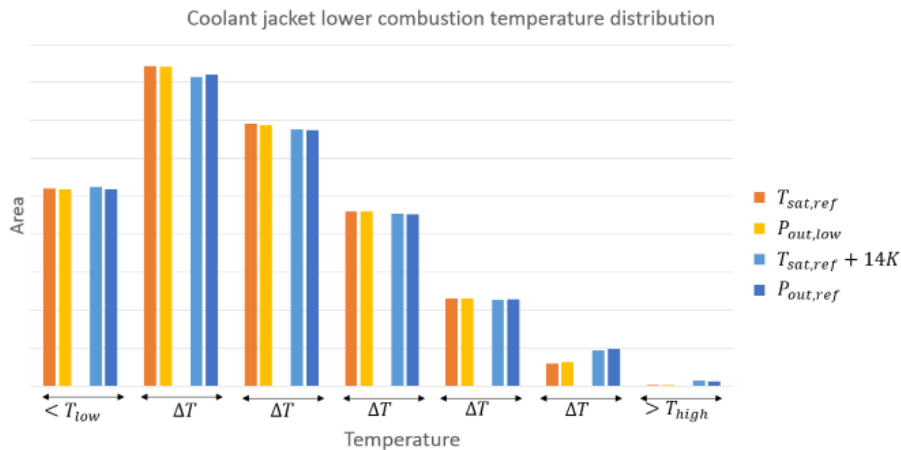


Figure 4.23: Temperature distribution of the coolant jacket channels above the combustion chambers for constant and pressure dependent saturation temperature

4.2.3.2 Different outlet pressures

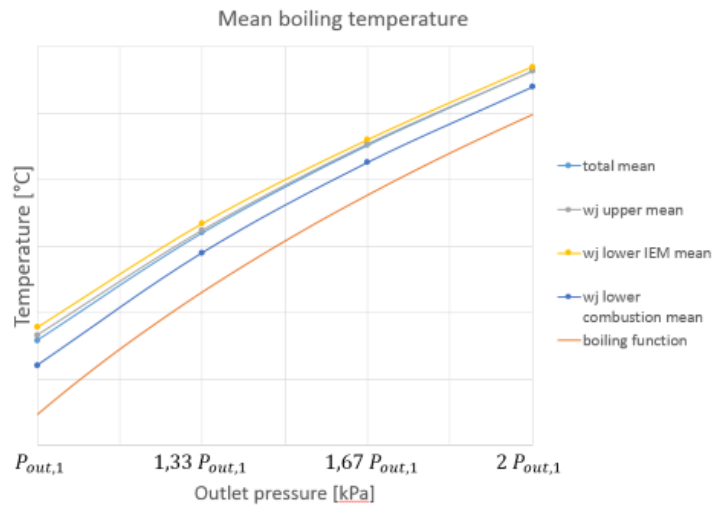


Figure 4.24: Mean saturation temperature in different parts of the coolant jacket for different pressures

The mean saturation temperature of the different regions of the coolant jacket is shown in Figure 4.24 as a function of outlet pressure. The local static pressure dependent saturation temperature is included for reference in red. As expected, the mean saturation temperatures increase with higher outlet pressures. The variations in saturation temperature within the coolant jacket is negligible compared to the effect that the outlet pressure has on the saturation temperature, as can be seen in Figures A.42, A.43 and A.44 in the Appendix.

In Figure 4.25 the surface integrated wall boiling heat flux is plotted. For increased outlet pressure, less heat is transferred to the coolant jacket as a result of boiling. This is due to the increased saturation temperature.

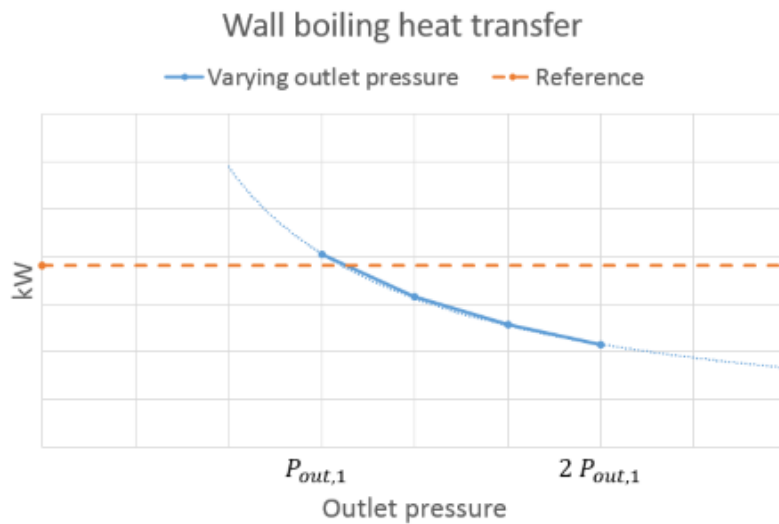


Figure 4.25: Heat transferred from the cylinder head solid to the coolant jacket due to boiling as a function of pressure in the thermostat pressure

The decreased boiling heat transfer also means that the temperature can increase further at the wall without the vapour bubbles transporting the heat to the bulk of the coolant flow. Figure 4.26 shows how the maximum

temperature in the coolant jacket increases with increased outlet pressure.

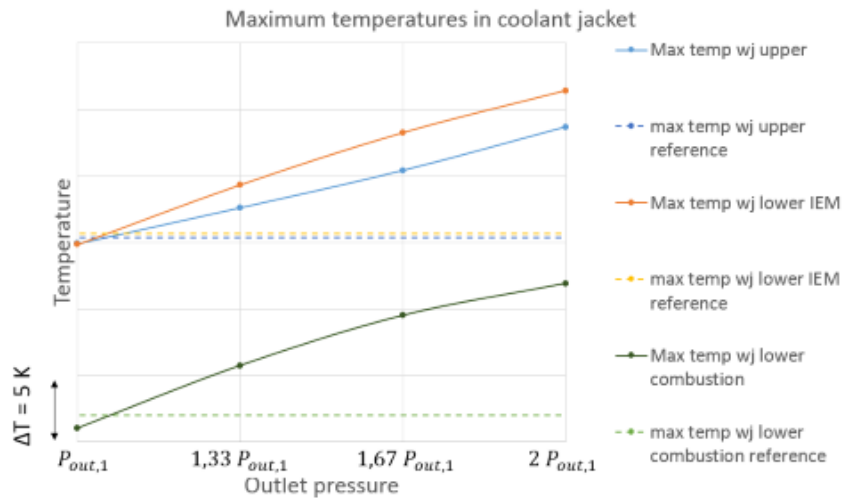


Figure 4.26: *Maximum temperatures in the different regions of the coolant jacket as functions of thermostat outlet pressure*

With increased temperatures on the coolant jacket walls, the temperature on the gas side walls increases as well as can be seen in Figure 4.27. While an increased saturation temperature decreases the risk of excessive boiling, the drawback of this is that the solid temperature in the cylinder head increases.

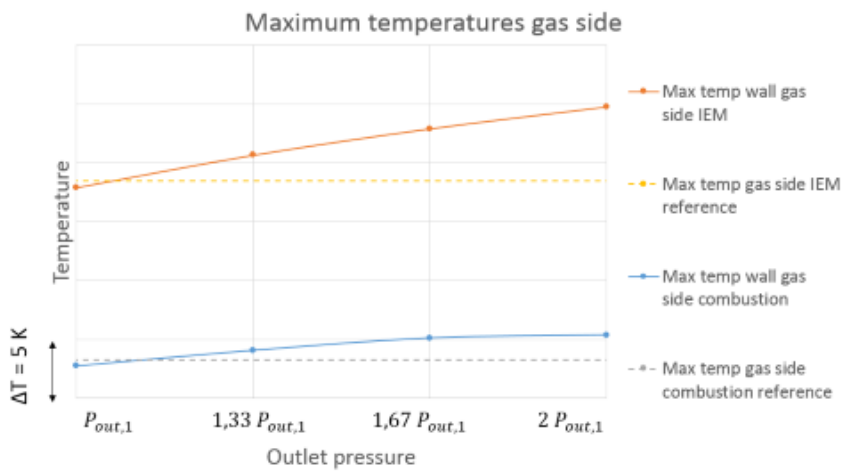


Figure 4.27: *Maximum temperatures on the gas side walls of the IEM and combustion chamber top as function of thermostat outlet pressure*

4.2.4 Thermal conductivity

	Reference	k_{mid}	k_{low}
Upper coolant jacket	$T_{ref,upper}$	$T_{ref,upper} + 0.5K$	$T_{ref,upper} + 2.3K$
Lower coolant jacket below IEM	$T_{ref,cj-IEM}$	$T_{ref,cj-IEM} + 0.2K$	$T_{ref,cj-IEM} + 1.5K$
Lower coolant jacket above combustion chambers	$T_{ref,cj-comb}$	$T_{ref,cj-comb} + 0.4K$	$T_{ref,cj-comb} + 0.7K$
Gas side top of combustion chambers	$T_{ref,gas-comb}$	$T_{ref,gas-comb} + 3.1K$	$T_{ref,gas-comb} + 17.2K$
Gas side IEM	$T_{ref,gas-IEM}$	$T_{ref,gas-IEM} + 2.1K$	$T_{ref,gas-IEM} + 12.6K$

Table 4.5: Maximum temperatures in the cylinder head for different thermal conductivities

As mentioned in Section 3.4.2, a high thermal conductivity means easier heat transfer and lower temperature gradient for a given heat flux. Table 4.5 shows the maximum temperature of the walls on both the coolant side and the gas side. The reference simulation and the simulation with the thermal conductivity k_{mid} show similar maximum temperatures on the coolant side, with slightly higher temperatures on the gas side for the k_{mid} case. On the gas side the temperature difference is more apparent. As the thermal conductivity of the reference case is higher, this is expected.

Following the same reasoning, it is expected for the simulation with a thermal conductivity of k_{low} to have higher temperatures on the gas side than k_{mid} or k_{ref} .

In Figure 4.28 the temperature and temperature derivative in the vertical direction are plotted along the line in Figure 4.13a. The temperature gradient is larger for the simulation with the low thermal conductivity compared to the other two simulations, as expected.

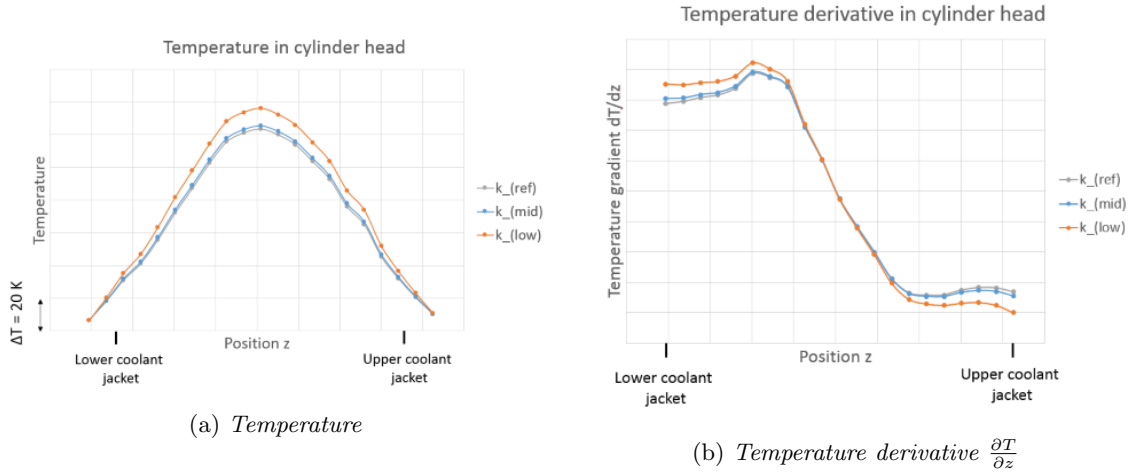


Figure 4.28: Temperature and temperature derivative in the cylinder head for different thermal conductivities

In Table 4.6 a slight reduction in the heat transferred to the coolant in the cylinder head can be observed when the thermal conductivity is decreased.

	Reference	k_{mid}	k_{low}
Upper coolant jacket	$Q_{cj,upper}$	$0.99Q_{cj,upper}$	$0.97Q_{cj,upper}$
Lower coolant jacket below IEM	$Q_{cj,IEM}$	$0.99Q_{cj,IEM}$	$0.97Q_{cj,IEM}$
Lower coolant jacket above combustion chambers	$Q_{cj,comb}$	$0.99Q_{cj,comb}$	$0.96Q_{cj,comb}$
Total	Q_{ref}	$0.99Q_{ref}$	$0.97Q_{ref}$

Table 4.6: Heat transferred to coolant in the cylinder head for different thermal conductivities

4.3 Geometrical changes

Due to time constraints, the analyses of the geometrical changes should be considered preliminary. Further analysis is needed, both on how displacements of the coolant jacket and surface topology affect the heat transfer in the cylinder head.

4.3.1 Displacement

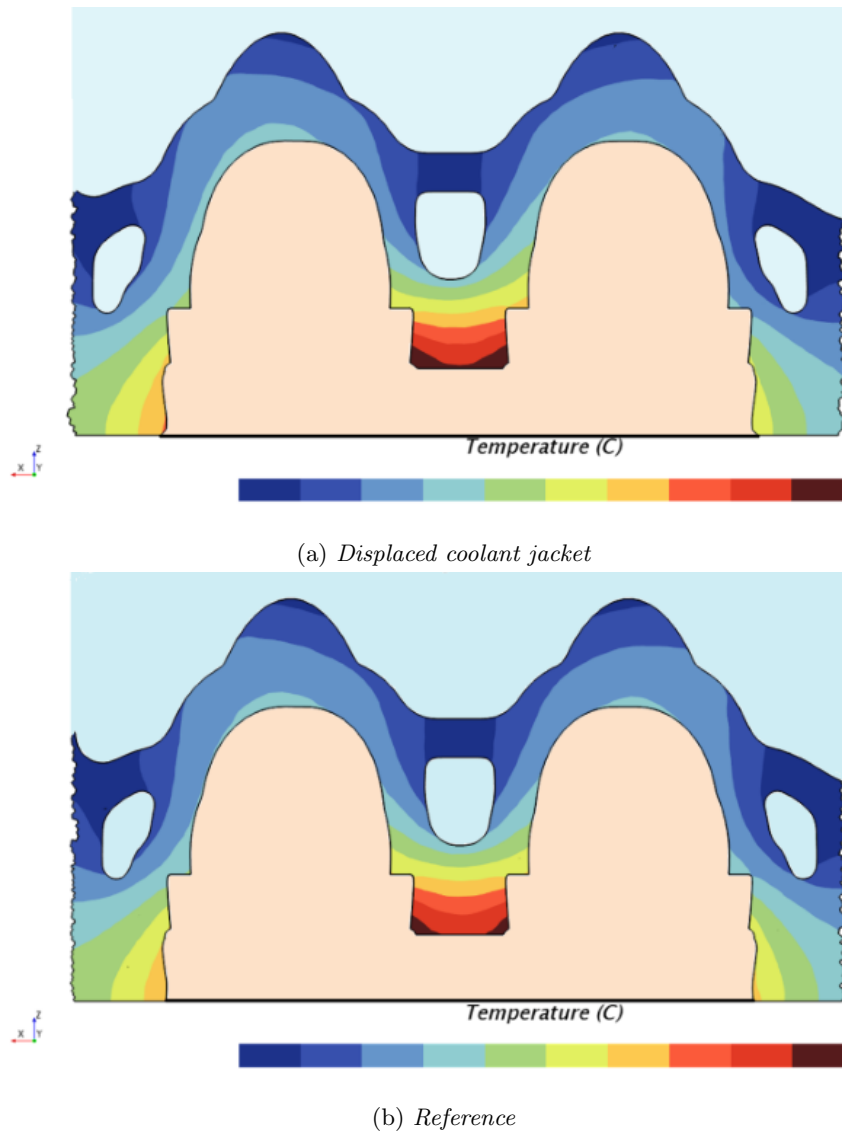


Figure 4.29: Temperature field in the solid between the exhaust gas and coolant on the plane illustrated in Figure 3.6 (the orange region is the exhaust gases and light blue regions are coolant)

In Figure 4.29 a displacement of the temperature field can be seen between the displaced coolant jacket and the reference. The temperature on the coolant side remains constant and the temperature field of the solid follows the displaced coolant jacket. This causes the gas side wall temperature to decrease on the side the coolant jacket is moved towards while the temperature increases on the opposite side.

Judging from Figure 4.29 the temperature gradient appears to remain constant compared to the reference case. However, the change in material thickness could lead to a unforeseen change in thermal stresses within the structure.

4.3.2 Surface topology modification

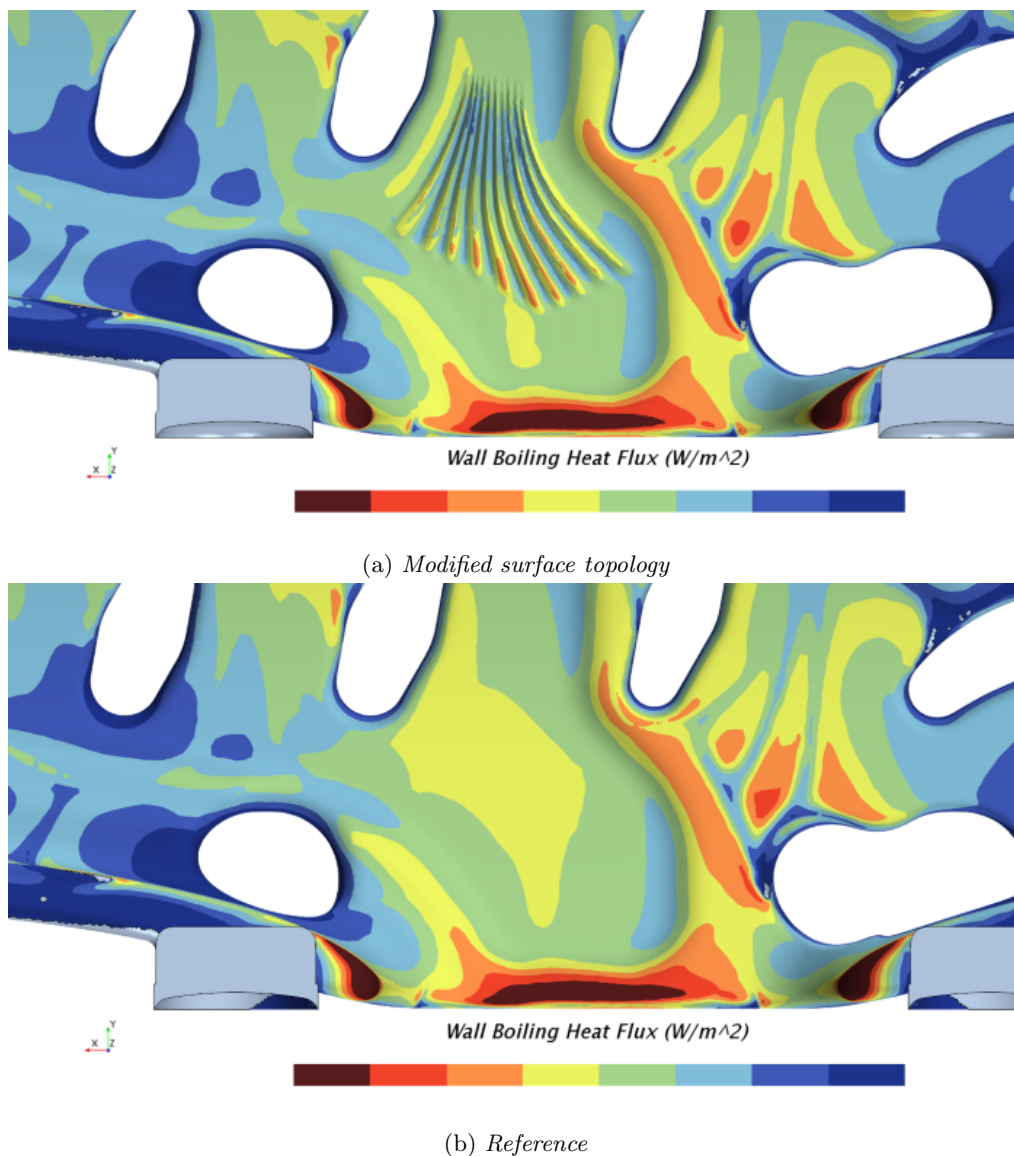


Figure 4.30: *Wall boiling heat flux in upper part of coolant jacket close to exhaust flange for modified and reference surface topology*

In Figure 4.30 the wall boiling heat flux on the upper coolant jacket in the vicinity of the exhaust flange is shown for both the modified surface and the reference. On average, the wall boiling heat flux is lower on the modified surface compared to the reference simulation. However, small areas of elevated wall boiling heat flux can be seen on the modified surface. These areas are closer to the IEM compared to the surrounding areas and the reference geometry.

The surface topology modification seems to have a larger effect on the region further away from the exhaust flange, where the hills are closer together, compared to closer to the exhaust flange, where the hills are further apart.

Table 4.7 summarises the comparison between the reference simulation and the modified, within the rectangle in Figure 3.7. 7% more heat is transferred to the coolant on the modified surface compared to the reference. At the same time, since the area in this region is increased, the surface average wall boiling heat flux is 18% lower for the modified surface compared to the reference simulation.

In critical regions, where the wall boiling heat flux is close to the critical heat flux (see Figure 2.4, modifying the surface topology can reduce the wall boiling heat flux in order to have a safe margin against the critical heat flux.

	Area	Surface integrated wall boiling heat flux	Surface average wall boiling heat flux
Reference	A_{ref}	$Q_{b,ref,local}$	$q_{b,ref,local}$
Modified surface	$1.30A_{ref}$	$1.07Q_{b,ref,local}$	$0.82q_{b,ref,local}$

Table 4.7: Wall boiling heat flux comparison for the area enclosed by the rectangle in Figure 3.7 between the modified surface topology and the reference case

5 Conclusions

From the parametric study, it has been found that the temperature within the cylinder head decreases with increased mass flow. Reduced temperatures for increased mass flow is seen on both the coolant jacket walls and the gas/solid interfaces. With increased mass flow, the heat transfer from the cylinder head to the coolant increases slightly. However, since stagnation regions still exist, regions with high wall temperatures (and high wall boiling heat flux) are difficult to remove by simply increasing mass flow. This is true both in the coolant jacket and on the gas/solid interface. Mass flow rate has a very small effect on the temperature in critical regions if the geometry of the coolant jacket is inappropriate.

Changes in mass flow distribution significantly alters the flow field in the coolant jacket, resulting in unsteady variations in maximum temperatures and the locations of these depending on the distribution. Especially in the regions around the IEM. While the mass flow distribution has a significant effect on local temperature and boiling intensity, the global effects on the temperature distribution and heat transfer in the coolant jacket are minor. Therefore, the temperatures on the gas/solid interface is not significantly affected by variations in mass flow distribution. It should however be noted that local critical points can lead to engine failure. Therefore, the distribution of outlet mass flow can have significant effect on engine durability.

Increasing the reference pressure (increasing saturation temperature) naturally reduces the wall boiling heat flux. However, it also leads to a significant increase in temperature in the coolant jacket. A small temperature increase occurs on the gas/solid interface as well. So while increasing the coolant system pressure can reduce the risk of excessive boiling, it also leads to higher solid temperatures, which are the main task of the cooling system to reduce. However, since this study uses a boiling model that does not take the insulating effect of intense boiling, increasing the pressure may reduce temperatures by avoiding excessive boiling and thus limiting the insulating effect.

There is no significant difference in temperature or wall boiling heat flux when using a local static pressure based saturation temperature compared to a global constant saturation temperature. In the regions enveloping the IEM, where boiling is significant, the pressure is almost constant resulting in a nearly constant saturation temperature in these regions. In the channels above the combustion chambers, the pressure variations are enough to cause significant variations in saturation temperature. However, the variations in saturation temperature does not lead to significant differences in wall temperature or wall boiling heat flux compared to a constant saturation temperature.

Changing the thermal conductivity of the solid results in different temperature gradients within the cylinder head. While the temperature on the coolant jacket walls remain roughly constant for different thermal conductivities, the temperature on the gas/solid interface increase significantly for decreased thermal conductivity. A lower thermal conductivity also lead to a slightly reduced amount of heat transferred to the coolant.

Changing the surface topology to increase the area of the coolant jacket in certain regions reduces the average heat flux in that region. This can be used to reduce the boiling intensity in regions where the boiling is close to the critical heat flux. In the simulation results analysed in this master thesis the effect of the surface topology modification is larger in the region where the hills are closer together than where they are further apart. One cause of this is probably that the relative area increase is larger when the hills are closer than when they are further apart. A more detailed analysis of how surface topology modifications affect coolant flow and temperatures should be performed in order to find the positive and negative effects of surface topology change.

The coolant temperature is not significantly affected by a horizontal displacement. The effect on the temperature on the gas/solid interface is more apparent. Change in material thickness may affect thermal stresses in the cylinder head. More analyses on how displacements affect the temperature field in the engine is needed.

5.1 Recommendations

Since there are stagnation regions leading to hotspots both for low mass flows and for high mass flows, simply increasing mass flow is an inefficient way to decrease temperature in critical regions. It is more important to create geometries that prevent stagnation regions. Preventing stagnation regions also allow the coolant jacket to be moved closer to the gas side which enables better cooling in critical areas on the gas side.

The channels above the combustion chambers maintain high velocities throughout the entire region relatively well. This could indicate that a concept with small channels could improve the cooling around the IEM as

well as velocities and thus convection increases. However, the pressure variations within the channels above the combustion chambers are quite significant, possibly leading to larger variation of saturation temperature around the IEM as well if the same concept is adopted. This could lead to the difference between the constant and local pressure dependent saturation temperature becoming significant.

When it comes to boiling heat flux, Rohsenow's boiling heat flux correlation has a limited range for where it is accurate. When simulating regions with high wall temperatures, a different model which is able to take the critical heat flux into account should be used when possible. However, such a model is likely to be more computationally expensive as more variables must be taken into account.

6 Future work

In this study, most focus has been on the non geometrical parameters. Further studies on how geometrical variations affect the heat transfer within the cylinder head is needed. When it comes to displacements, different directions and perhaps larger displacements (to magnify effects) could be of interest to find out how sensitive the temperature field of the cylinder head is to production variations of the coolant jacket. This should be coupled with FE analysis of the cylinder head to see how large effects a displacement has on the durability of the coolant jacket.

A deeper analysis on how the surface topology affects the coolant flow could quantify the effect it has on the heat transfer within the coolant jacket. There are infinite ways to modify the surface topology. Therefore a study on different surface topologies could give increased understanding on how the heat transfer is affected. A further analysis on how the surface topology affect the flow field, both locally and globally, should be performed as well as studying how the pressure is affected. Depending on the effect surface topology has on the pressure, a pressure dependent saturation temperature should be considered. The reduced surface averaged wall boiling heat flux should also be compared with the probably higher production cost for a more complex topology.

References

- [1] W. M. Rohsenow. *A method of correlating heat transfer data for surface boiling of liquids*. Technical report. Massachusetts Institute of Technology, 1951.
- [2] C. Mazur et al. Understanding the drivers of fleet emission reduction activities of the German car manufacturers. *Environmental Innovation and Societal Transitions* **16** (2015), 3–21.
- [3] N. Fraser et al. Challenges for Increased Efficiency through Gasoline Engine Downsizing. *SAE International Journal of Engines* **2(1)** (2009), 991–1008. DOI: 10.4271/2009-01-1053.
- [4] M. H. Westbrook. *The Electric Car: development and future of battery, hybrid and fuel-cell cars*. The Institution of Engineering and Technology, 2001. ISBN: 978-1-849-19174-6.
- [5] C. Stan. *Alternative Propulsion for Automobiles*. Springer International Publishing, 2017. ISBN: 978-3-319-31930-8.
- [6] D. Takahashi et al. Combustion Development to Realize High Thermal Efficiency Engines. *SAE International Journal of Engines* **9(3)** (2016), 1486–1493. DOI: 10.4271/2016-01-0693.
- [7] S. Fontanezi, G. Cicalese, and A. Tiberi. Combined In-cylinder/CHT Analyses for the Accurate Estimation of the Thermal Flow Field of a High Performance Engine for Sport Car Applications (2013). DOI: 10.4271/2013-01-1088.
- [8] R. Stone. *Introduction to Internal Combustion Engines*. 4th ed. Palgrave Macmillan, 2012. ISBN: 978-0-230-57663-6.
- [9] S. D’Ambrosio et al. Impact on Performance, Emissions and Thermal Behavior of a New Integrated Exhaust Manifold Cylinder Head Euro 6 Diesel Engine. *SAE International Journal of Engines* **6(3)** (2013), 1814–1833. DOI: 10.4271/2013-24-0128.
- [10] M. Bovo. Comparative thermal analysis of an engine with conventional and integrated exhaust manifold (2019).
- [11] D. J. Jonhs. *Thermal Stress Analyses*. Pergamon Press Ltd, 1965. ISBN: 978-1-4832-1361-3. DOI: 10.1016/C2013-0-08286-2.
- [12] A. Lanin and I. Fedik. *Thermal Stress Resistance of Materials*. Springer, 1965. ISBN: 978-3-540-71399-9.
- [13] N. E. Dowling. *Mechanical Behavior of Materials*. 4th ed. Pearson Education Limited, 2013. ISBN: 978-0-273-76455-7.
- [14] Y. I. Cho et al. *Handbook of heat transfer*. Ed. by W. M. Rohsenow, J. P. Hartnett, and Y. I. Cho. 3rd ed. McGraw-Hill Education, 1998. Chap. 1. Basic concepts of heat transfer. ISBN: 978-0-070-53555-8.
- [15] V. K. Dhir. Boiling heat transfer. *Annual Review of Fluid Mechanics* **30** (1998), 365–401. ISSN: 00664189.
- [16] S. G. Kandlikar. *Multiphase flow handbook*. Ed. by F. E. Michaelides, C. T. Crowe, and J. D. Schwarzkopf. 2nd ed. CRC-Press, Taylor & Francis Group, 2017. Chap. 8. Boiling. ISBN: 978-1-498-70100-6.
- [17] F. Öhrby. “Numerical modeling of subcooled nucleate flow boiling in engine cooling systems”. MA thesis. Chalmers University of Technology, 2014.
- [18] L. Davidson. *Fluid mechanics, turbulent flow and turbulence modelling*. Chalmers University of Technology, Mar. 25, 2019.
- [19] H. K. Versteeg and W. Malalasekera. *An Introduction to Computational Fluid Dynamics. The Finite Volume Method*. 2nd ed. Pearson Education Limited, 2007. ISBN: 978-0-13-127498-3.
- [20] M. Bovo. “Principles of Heat Transfer in Internal Combustion Engines from a Modeling standpoint”. PhD thesis. Chalmers University of Technology, 2014.
- [21] *Simcenter Star-CCM+ Documentation Version 13.04.010*. Siemens PLM Software. 2018.
- [22] M. M. Patil, A. Pise, and N. Gokale. *Simulation of Conjugate Heat Transfer (CHT) Between Engine Head and Cooling Medium of Diesel Engine*. SAE Technical Paper 2015-01-1665. 2015. DOI: 10.4271/2015-01-1662.
- [23] F. Meng et al. A stable and accurate partitioned algorithm for conjugate heat transfer. *Journal of Computational Physics* **344** (2017), 51–85. DOI: 10.1016/j.jcp.2017.04.052.
- [24] G. R. Warrier and V. K. Dhir. Heat Transfer and Wall Heat Flux Partitioning During Subcooled Flow Nucleate Boiling—A Review. *Journal of Heat Transfer* **128(12)** (2006), 1243–1256. DOI: 10.1115/1.2349510.
- [25] *Glythermin NF*. Technical Information TI/EVO 1023. BASF. 2007.

A Appendix

A.1 Reference simulation

Flow field

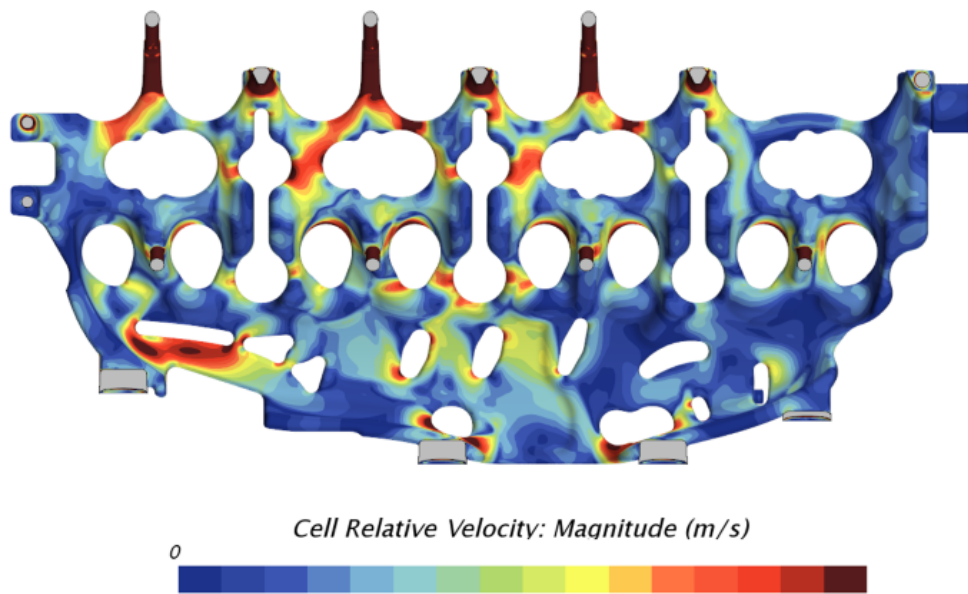


Figure A.1: *Cell relative velocity upper coolant jacket*

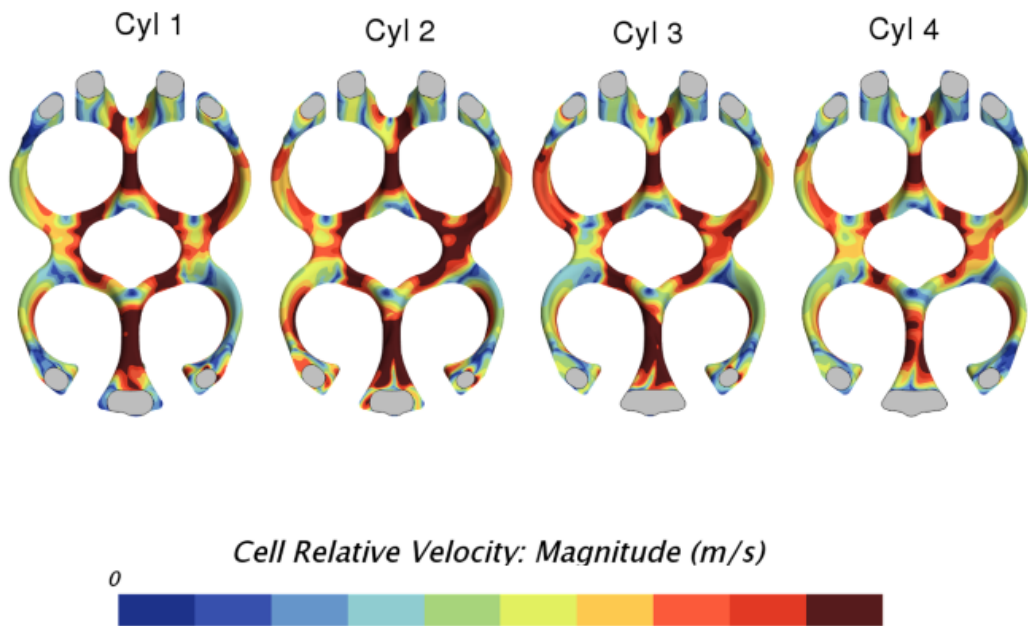


Figure A.2: *Cell relative velocity lower coolant jacket above combustion chambers*

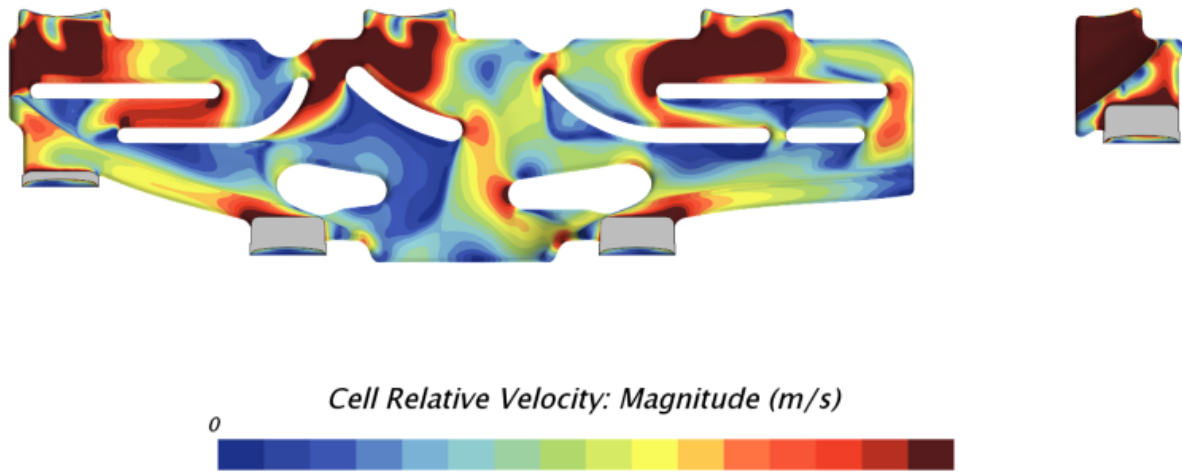


Figure A.3: Cell relative velocity lower coolant jacket below IEM

Temperature

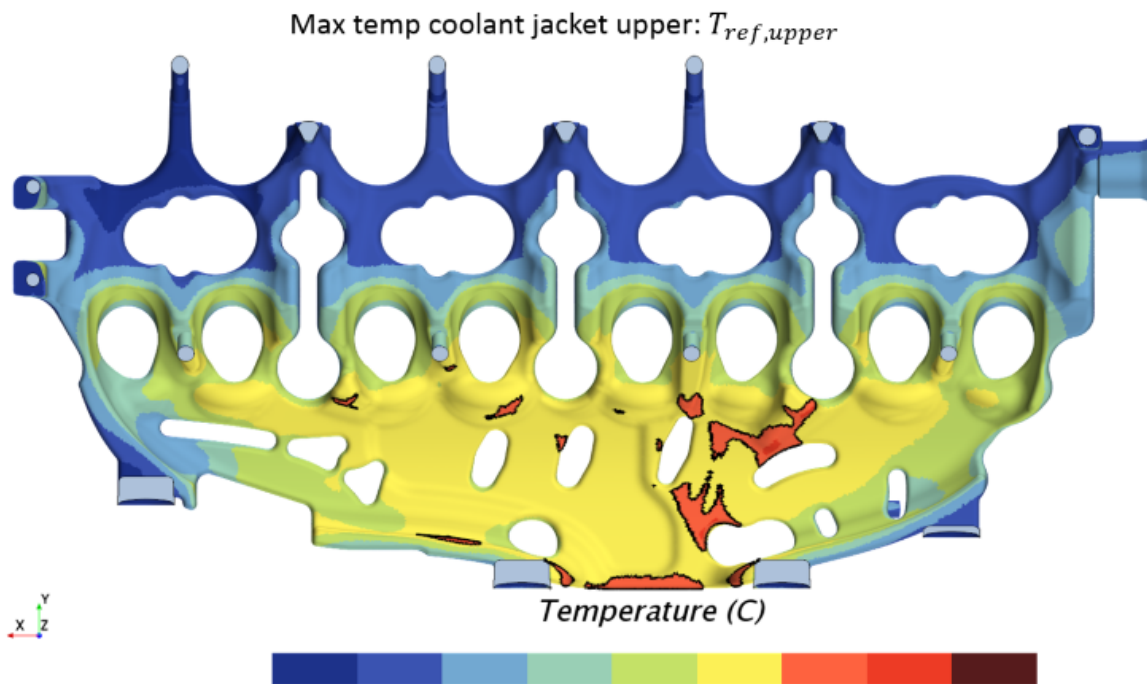


Figure A.4: Temperature field upper coolant jacket

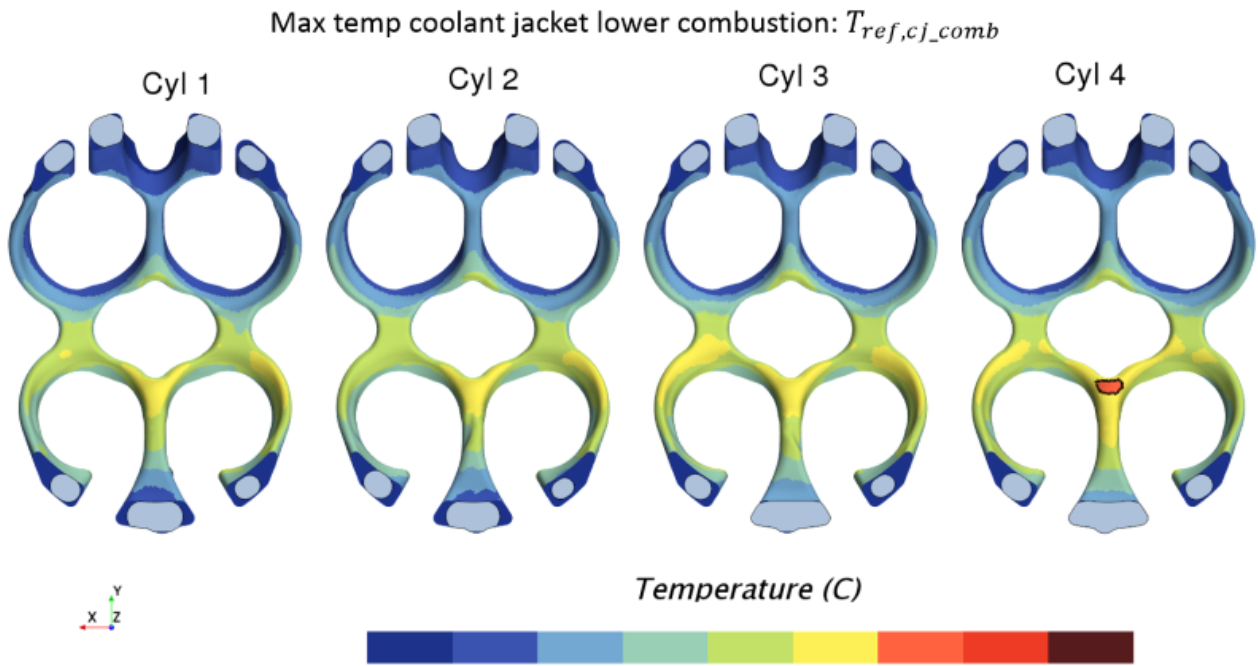


Figure A.5: *Temperature field lower coolant jacket above combustion chambers*

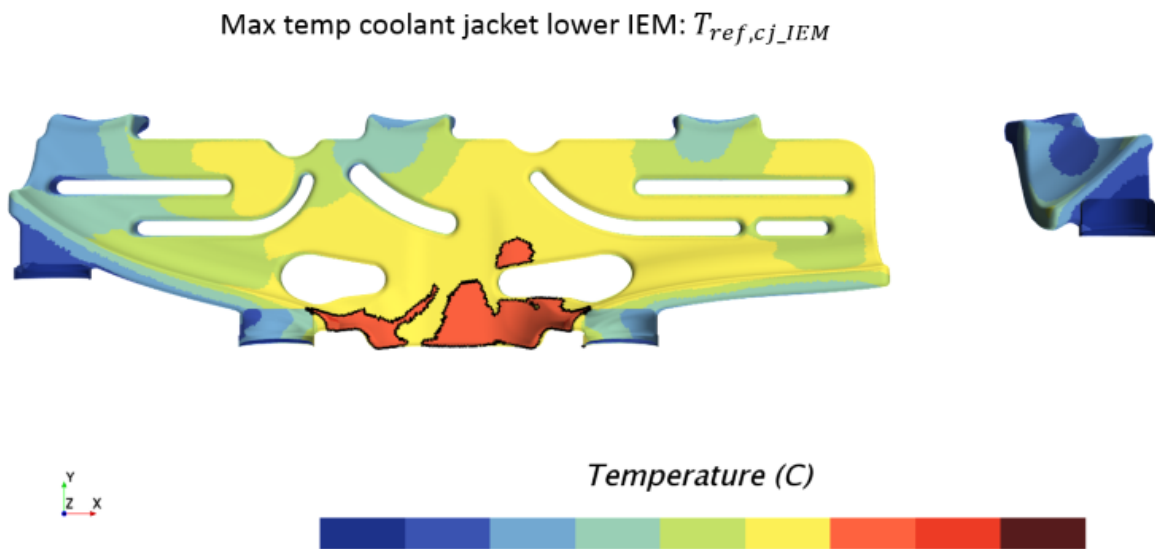


Figure A.6: *Temperature field lower coolant jacket below IEM*

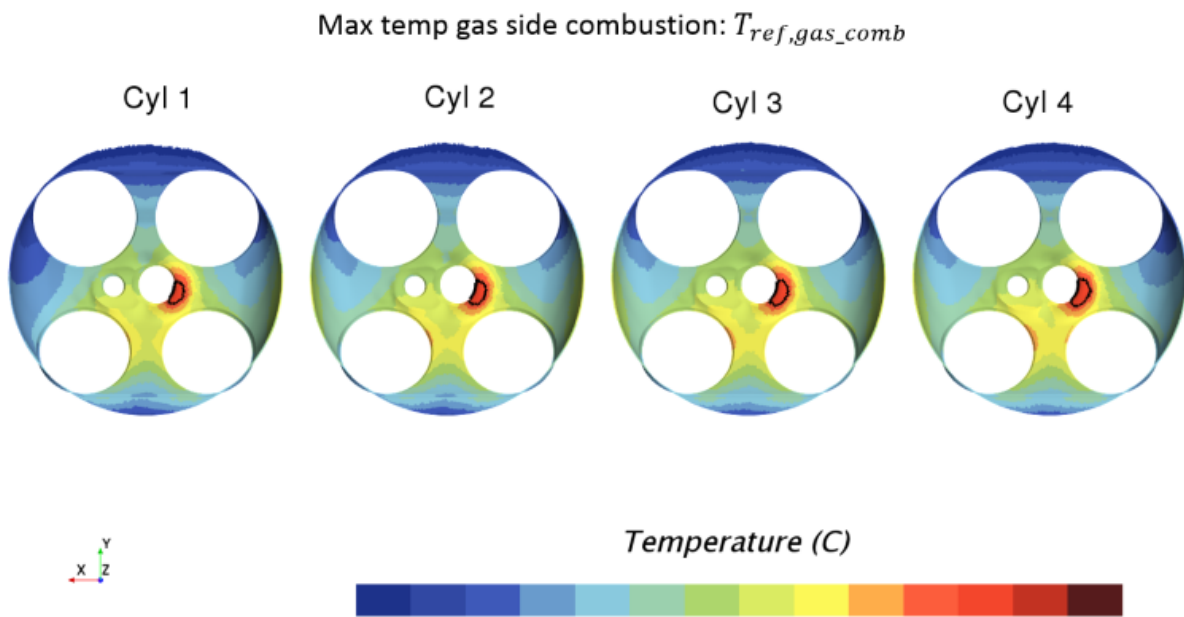


Figure A.7: *Temperature field gas/solid interface at top of combustion chambers*

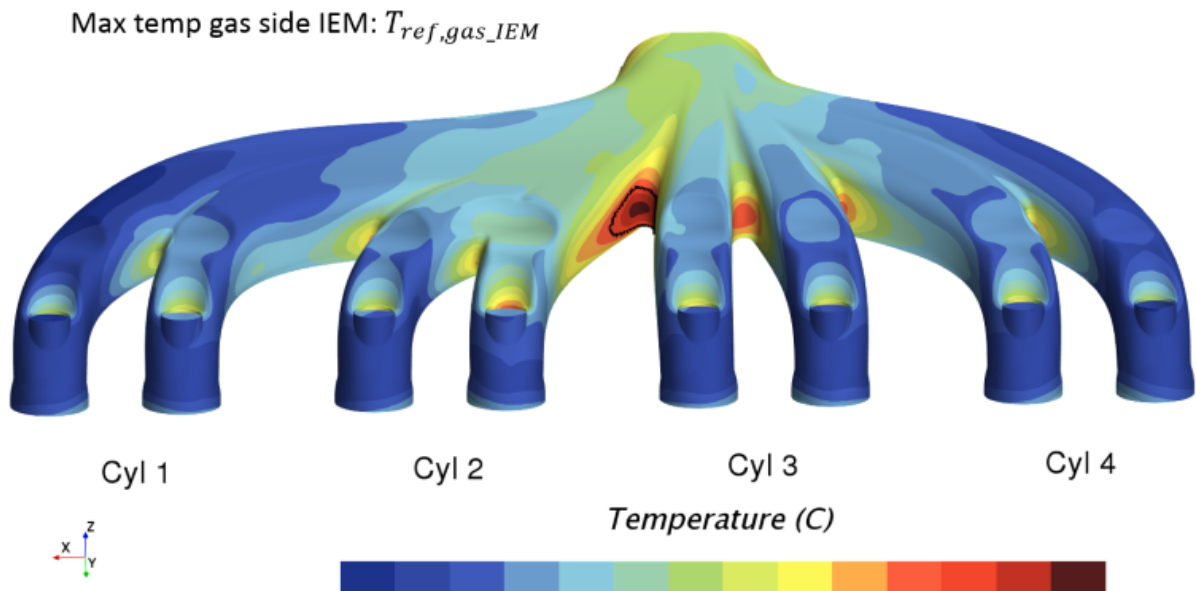


Figure A.8: *Temperature field gas/solid interface at IEM*

Heat flux

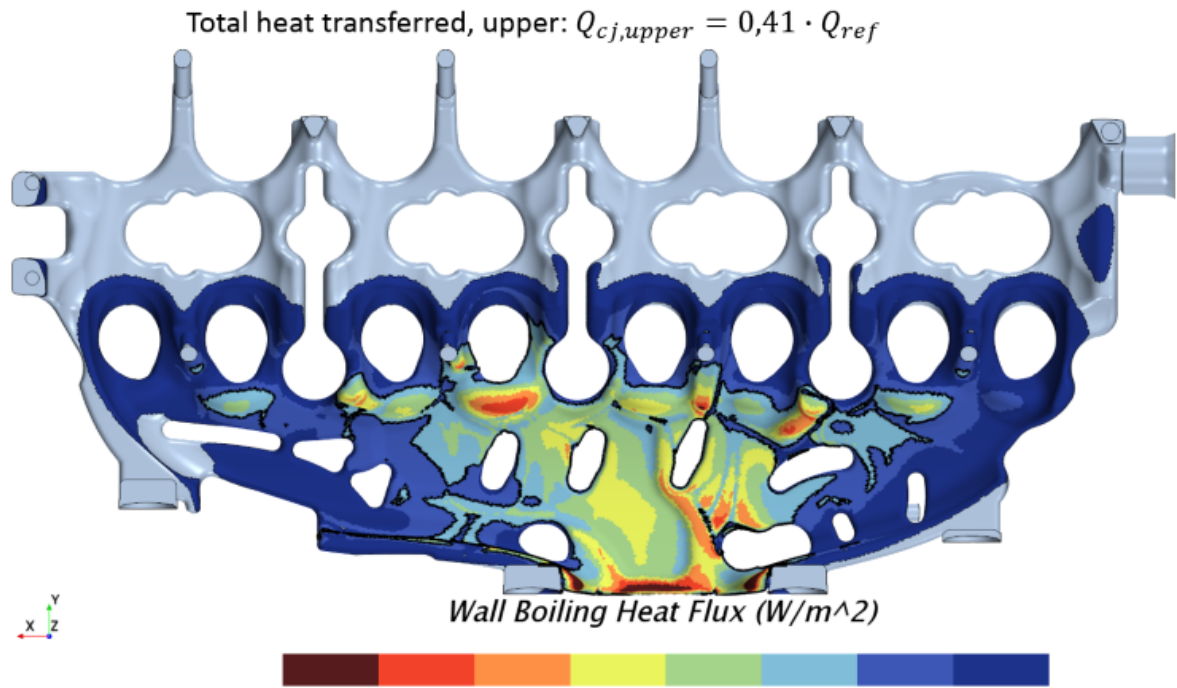


Figure A.9: Wall boiling heat flux upper coolant jacket

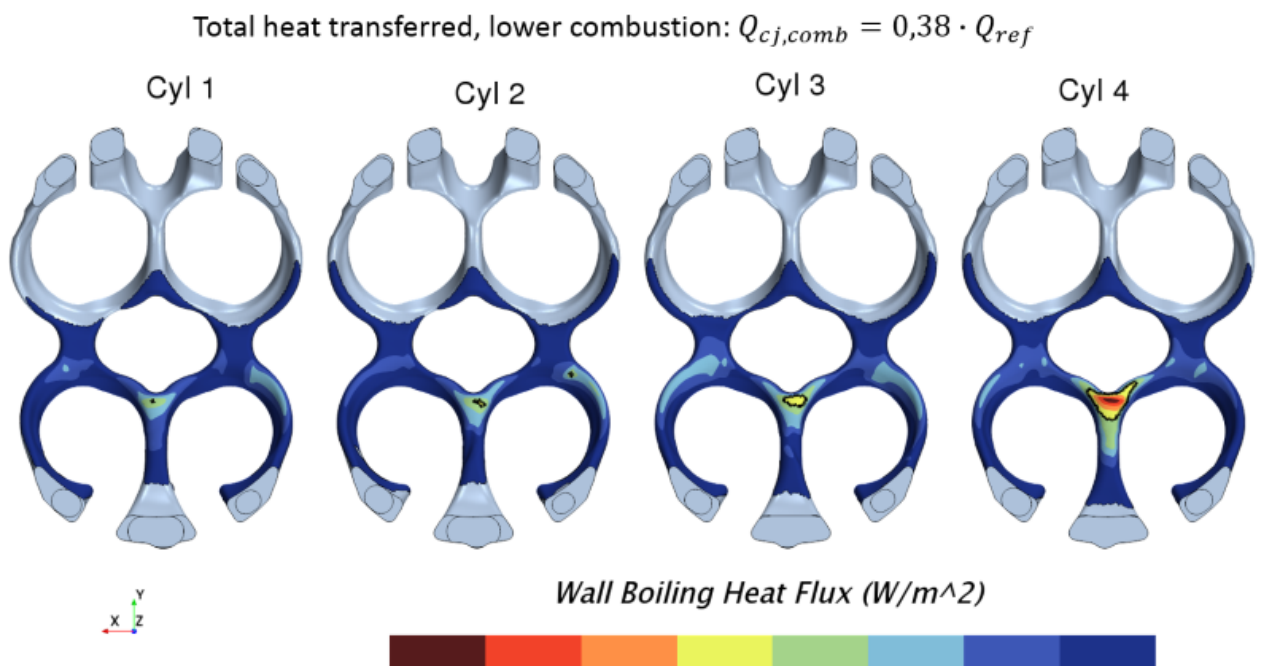


Figure A.10: Wall boiling heat flux lower coolant jacket above combustion chambers

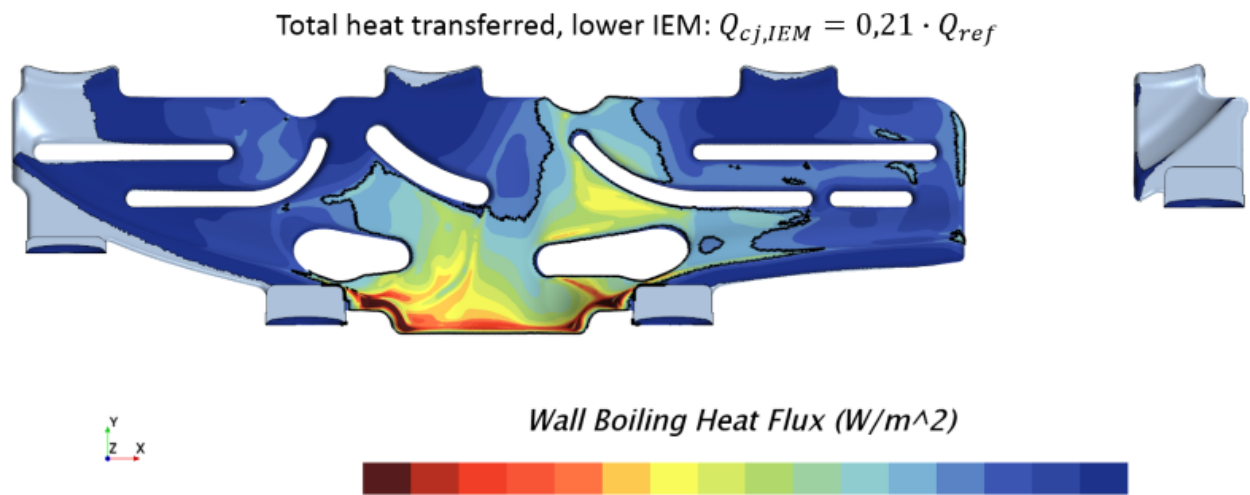


Figure A.11: *Wall boiling heat flux lower coolant jacket below IEM*

A.2 Mass flow rate

Flow field

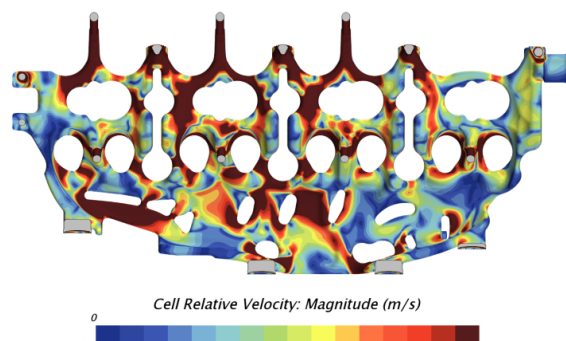
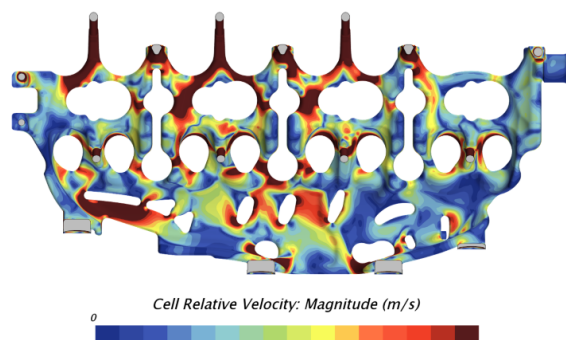
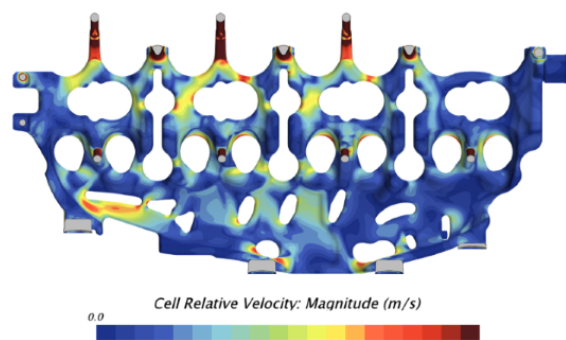
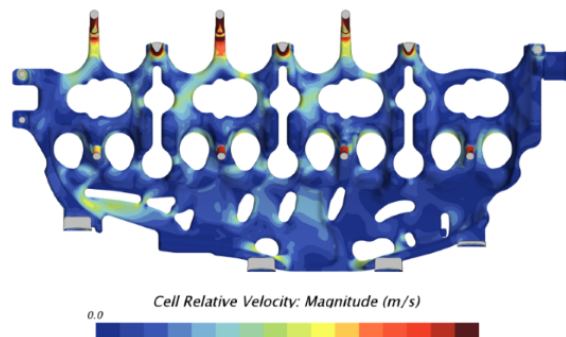
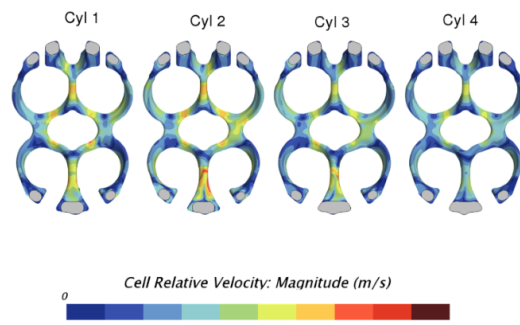
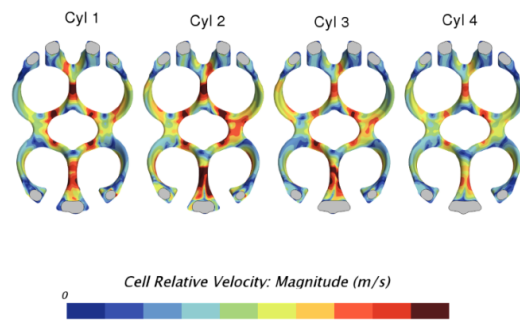


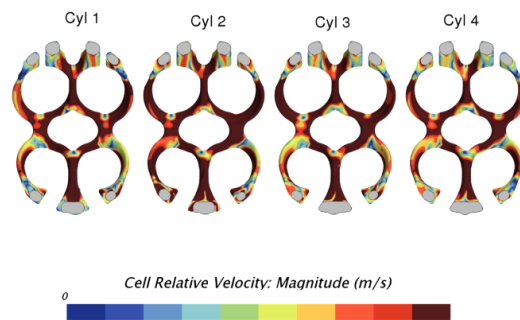
Figure A.12: Cell relative velocity in upper coolant jacket



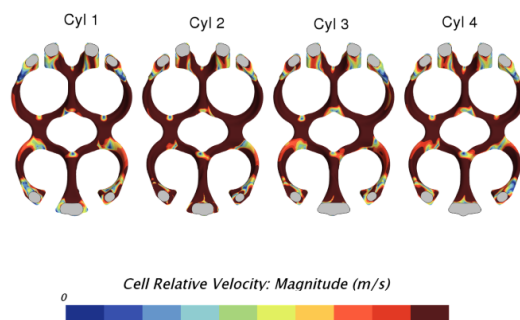
(a) $0.5\dot{m}_{ref}$



(b) $0.75\dot{m}_{ref}$



(c) $1.5\dot{m}_{ref}$



(d) $2\dot{m}_{ref}$

Figure A.13: *Cell relative velocity in lower coolant jacket above combustion chambers*

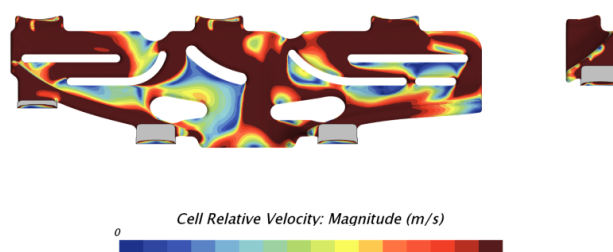
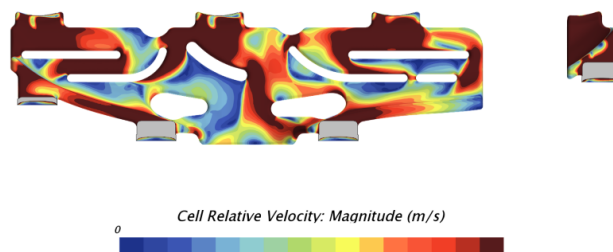
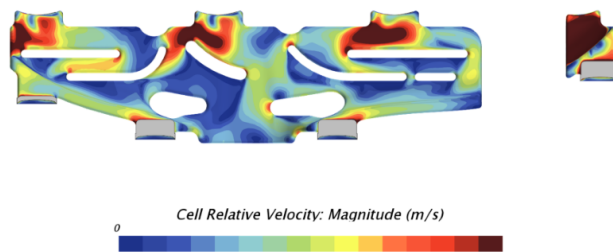
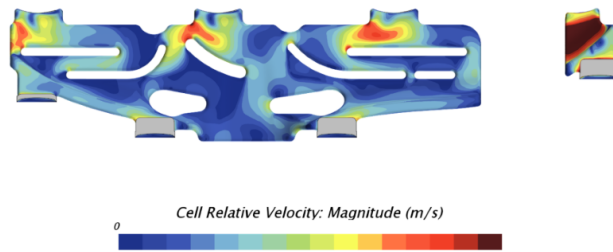


Figure A.14: Cell relative velocity in lower coolant jacket below IEM

Temperature

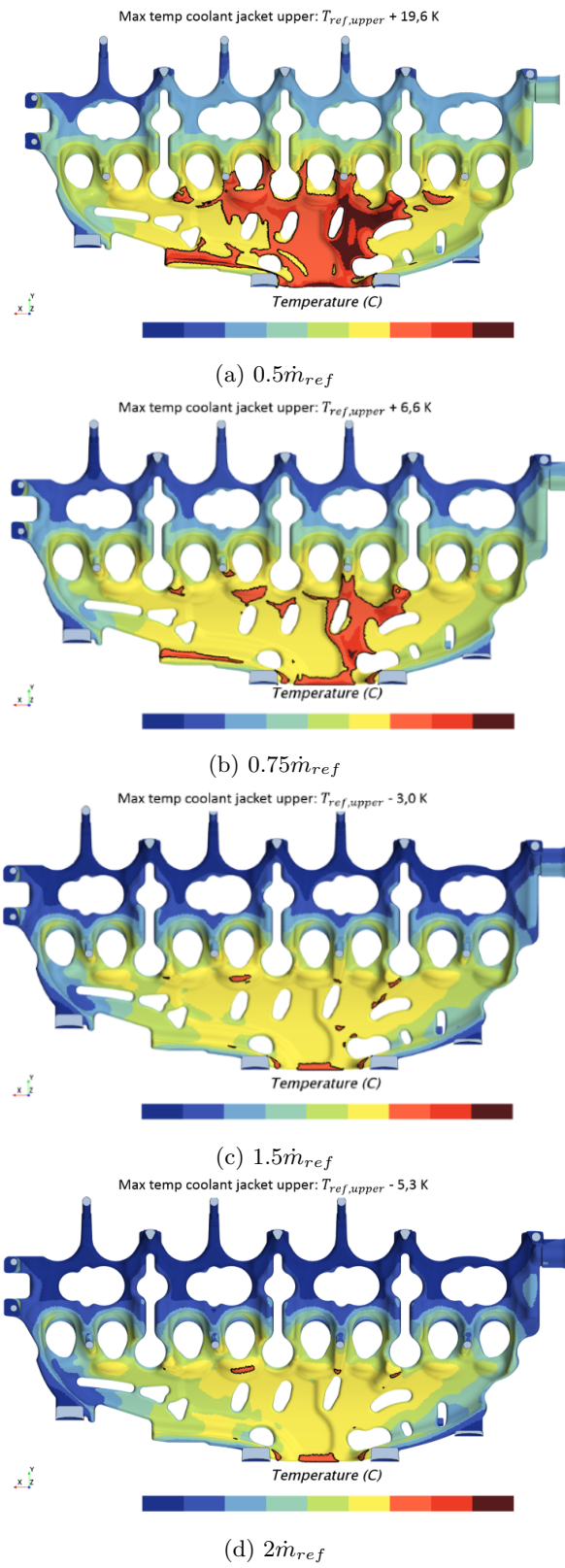
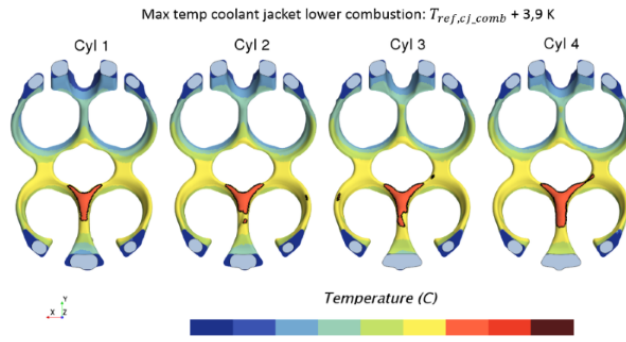
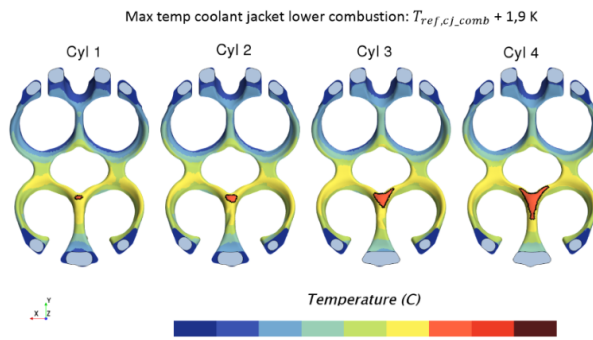


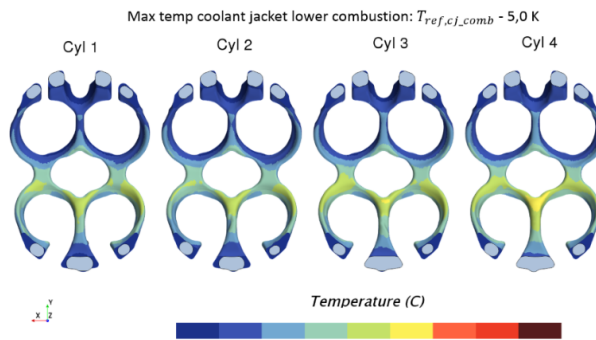
Figure A.15: *Temperature field in upper coolant jacket*



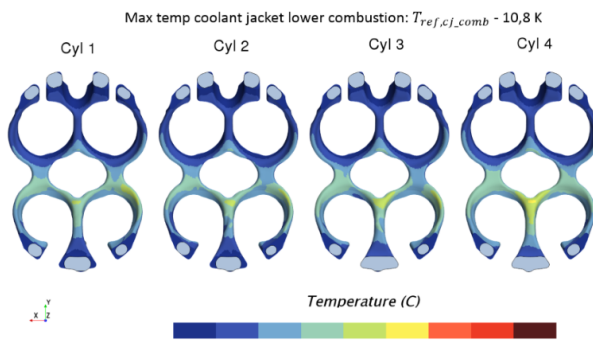
(a) $0.5\dot{m}_{ref}$



(b) $0.75\dot{m}_{ref}$

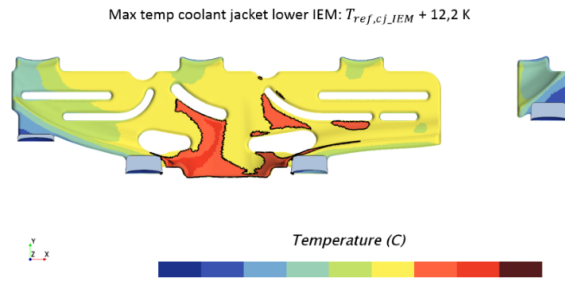


(c) $1.5\dot{m}_{ref}$

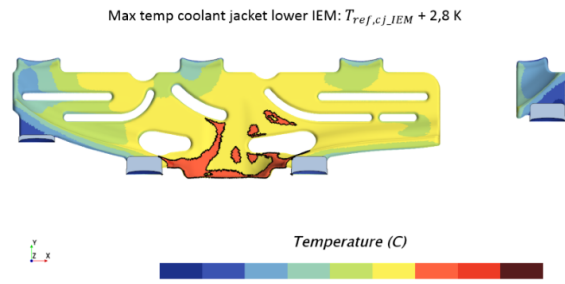


(d) $2\dot{m}_{ref}$

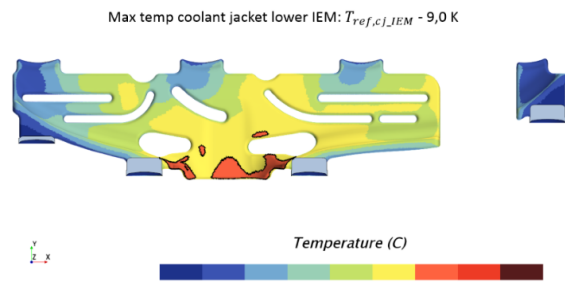
Figure A.16: *Temperature field in lower coolant jacket above combustion chambers*



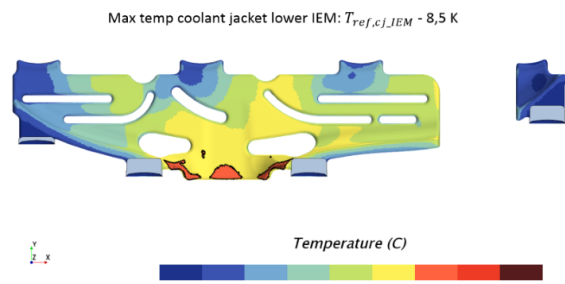
(a) $0.5\dot{m}_{ref}$



(b) $0.75\dot{m}_{ref}$

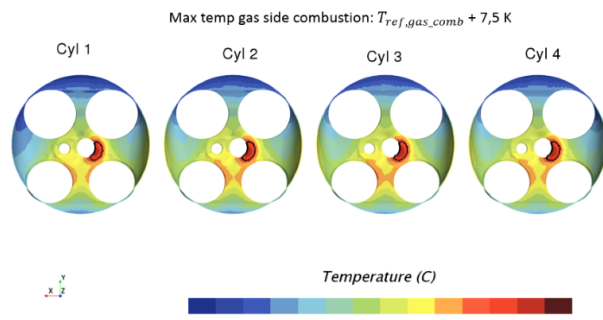


(c) $1.5\dot{m}_{ref}$

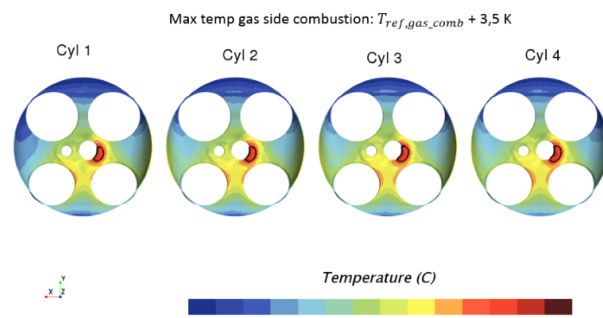


(d) $2\dot{m}_{ref}$

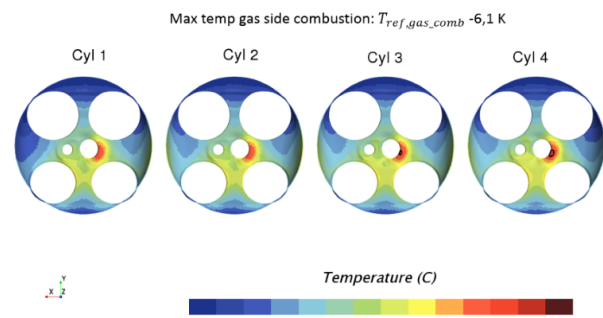
Figure A.17: *Temperature field in lower coolant jacket below IEM*



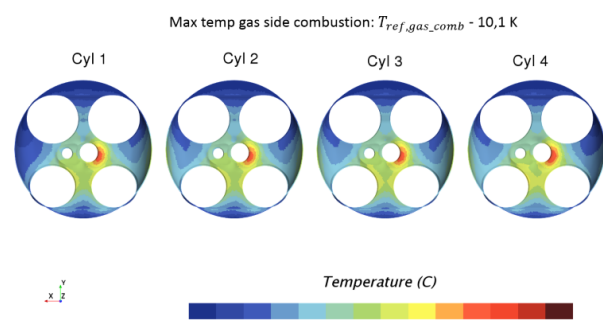
(a) $0.5\dot{m}_{ref}$



(b) $0.75\dot{m}_{ref}$

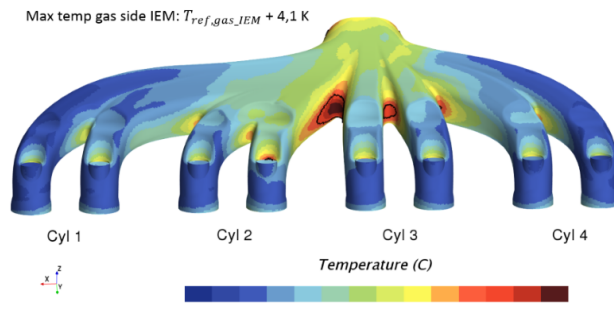


(c) $1.5\dot{m}_{ref}$

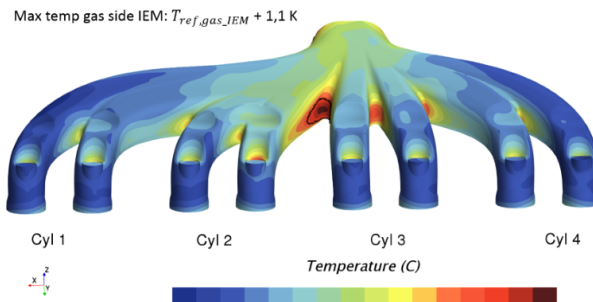


(d) $2\dot{m}_{ref}$

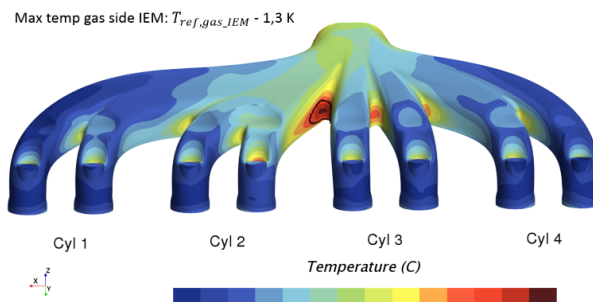
Figure A.18: *Temperature field on gas/solid interface at top of combustion chambers*



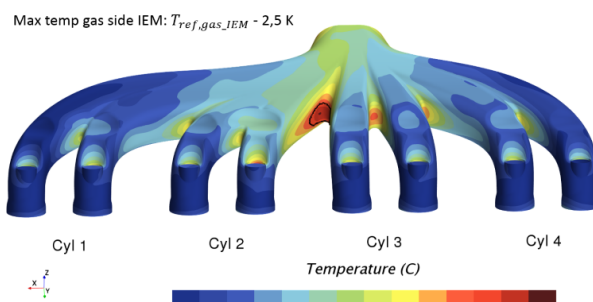
(a) $0.5\dot{m}_{ref}$



(b) $0.75\dot{m}_{ref}$



(c) $1.5\dot{m}_{ref}$



(d) $2\dot{m}_{ref}$

Figure A.19: *Temperature field on gas/solid interface at IEM*

Heat flux

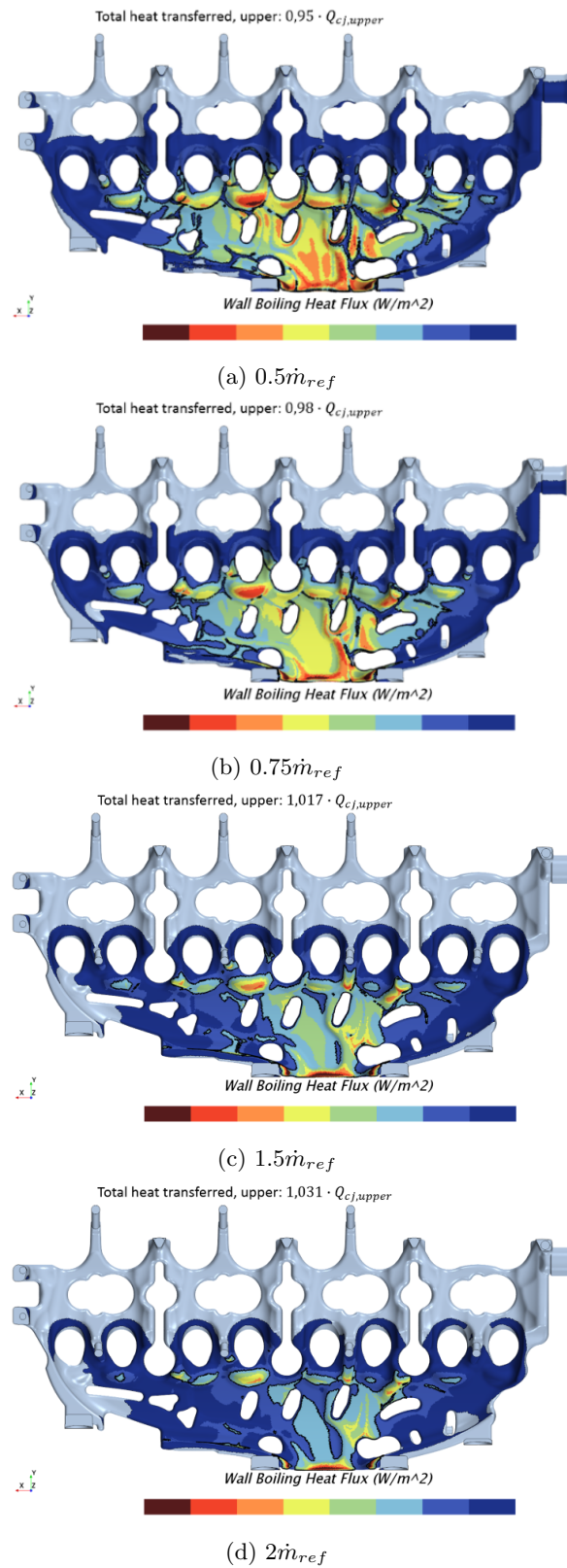


Figure A.20: Wall boiling heat flux in upper coolant jacket

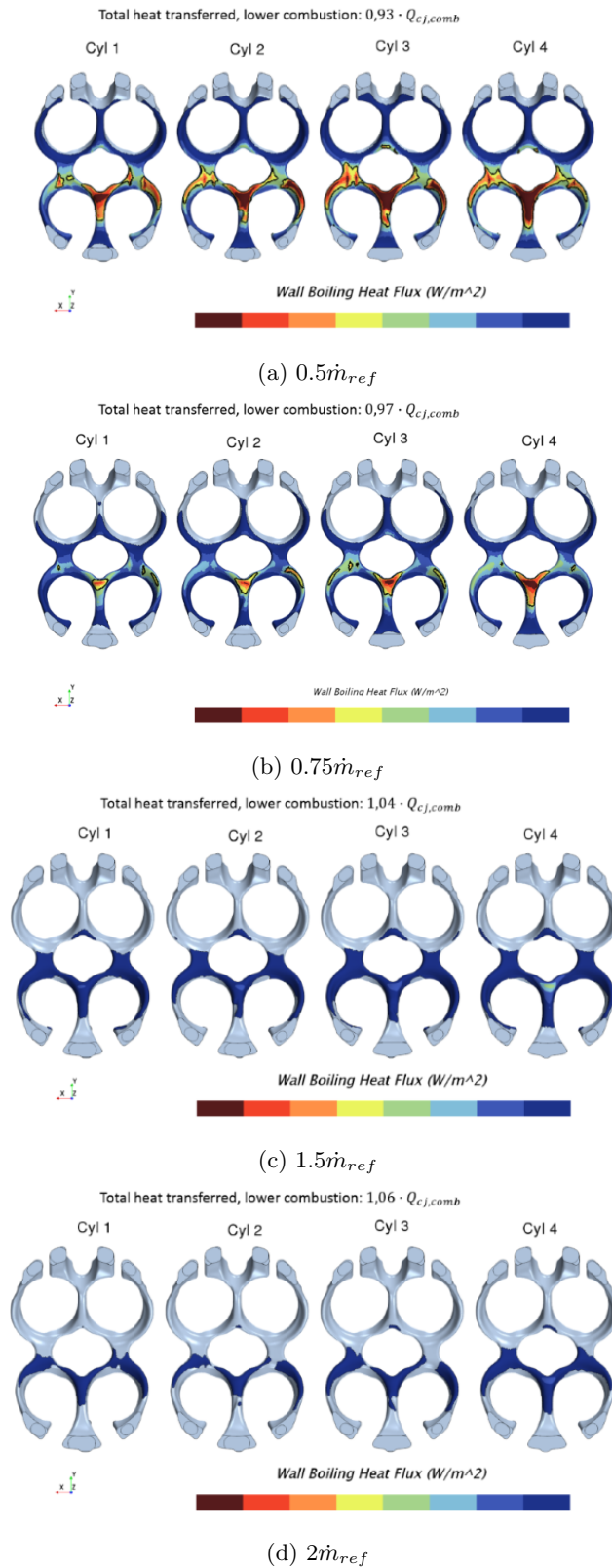
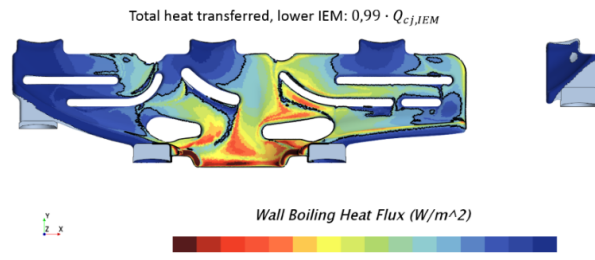
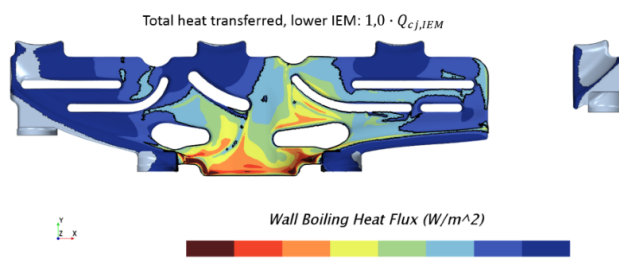


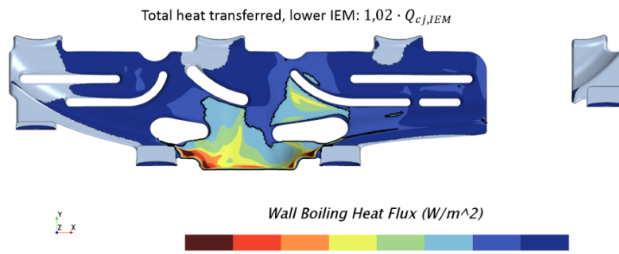
Figure A.21: Wall boiling heat flux in lower coolant jacket above combustion chambers



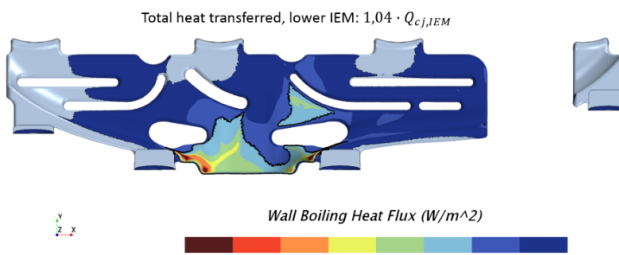
(a) $0,5\dot{m}_{ref}$



(b) $0,75\dot{m}_{ref}$



(c) $1,5\dot{m}_{ref}$

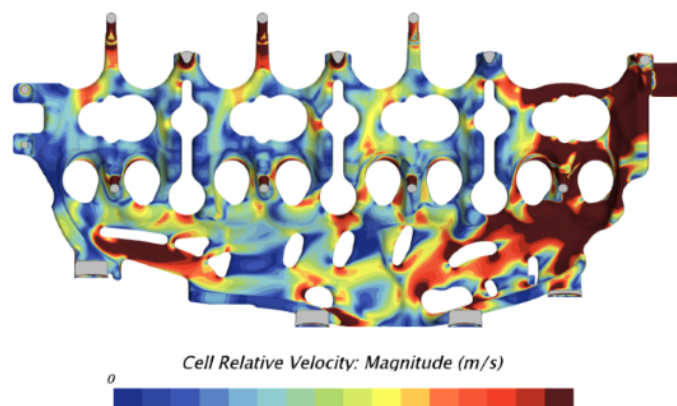


(d) $2\dot{m}_{ref}$

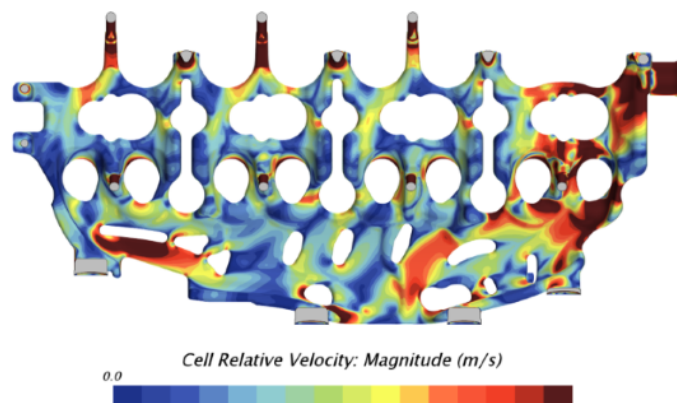
Figure A.22: Wall boiling heat flux in lower coolant jacket below IEM

A.3 Mass flow distribution

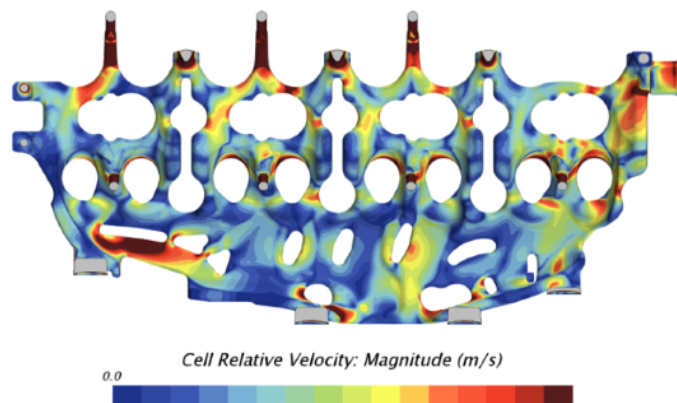
Flow field



(a) 70/30 distribution

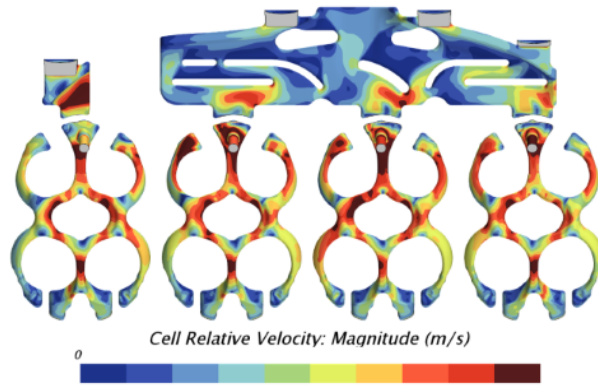


(b) 80/20 distribution

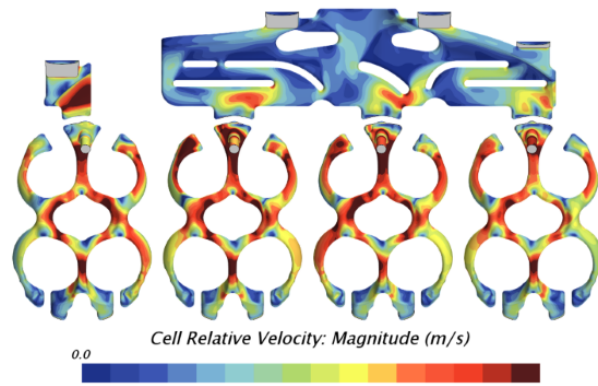


(c) 90/10 distribution

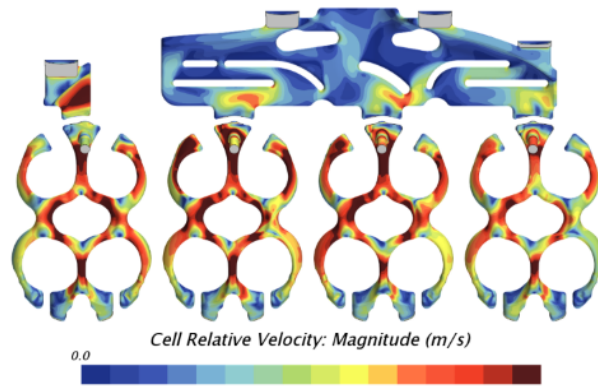
Figure A.23: Cell relative velocity in upper coolant jacket



(a) 70/30 distribution



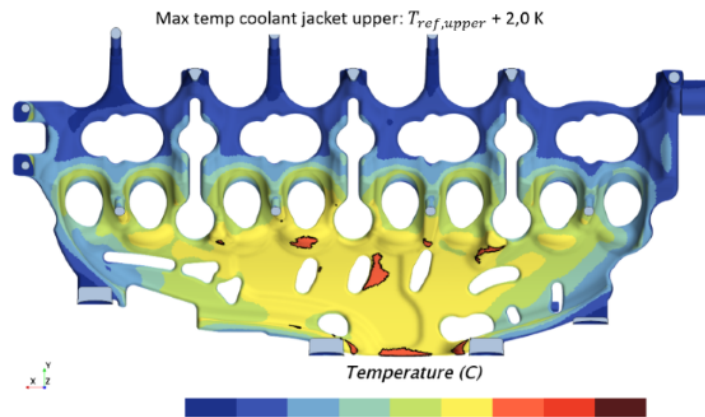
(b) 80/20 distribution



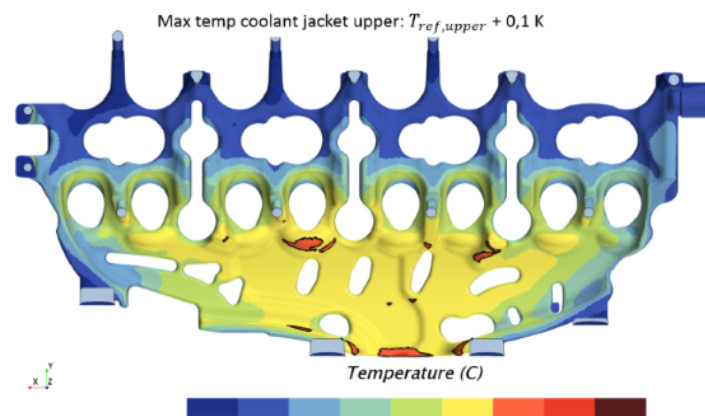
(c) 90/10 distribution

Figure A.24: Cell relative velocity in lower coolant jacket

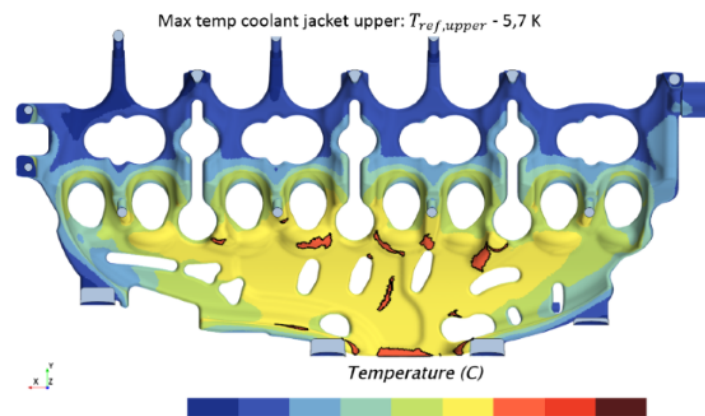
Temperature



(a) 70/30 distribution



(b) 80/20 distribution



(c) 90/10 distribution

Figure A.25: *Temperature field in upper coolant jacket*

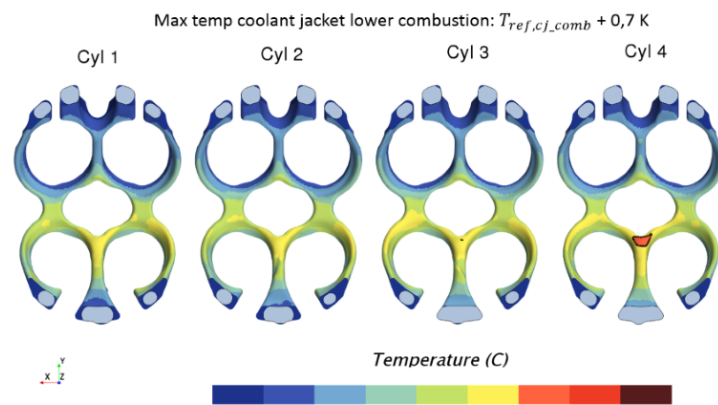
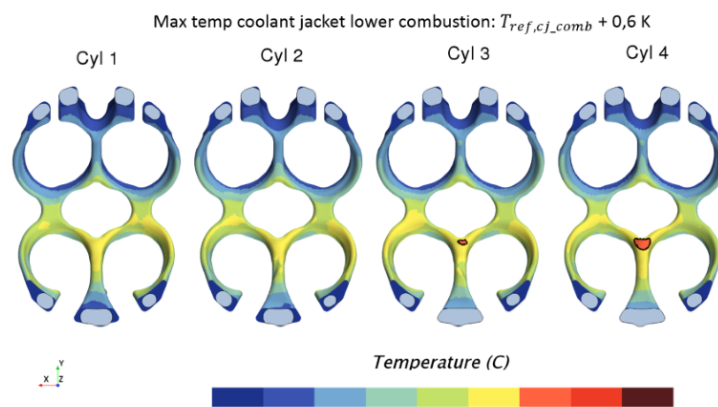
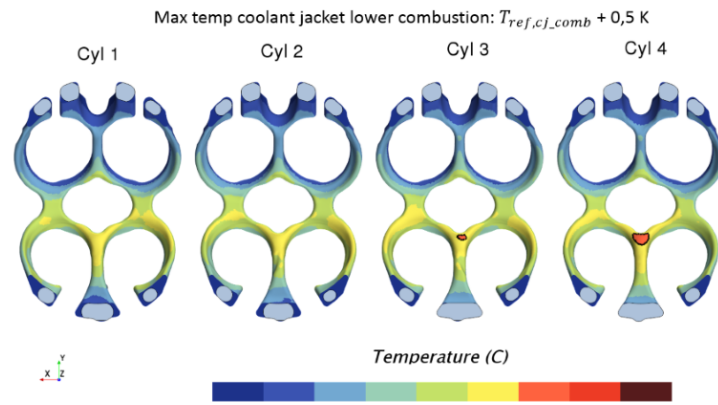
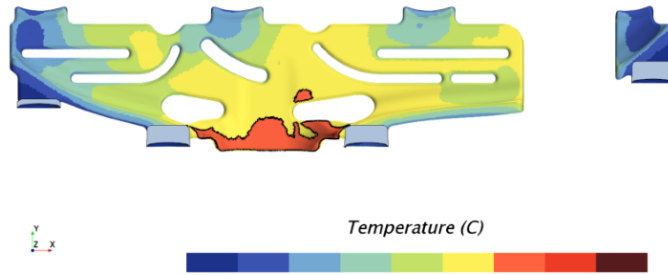


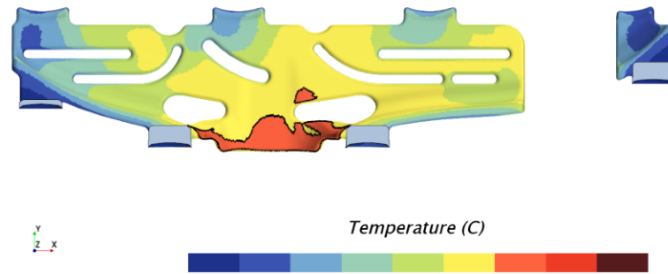
Figure A.26: *Temperature field in lower coolant jacket above combustion chambers*

Max temp coolant jacket lower IEM: $T_{ref,cj_IEM} + 0,5$ K



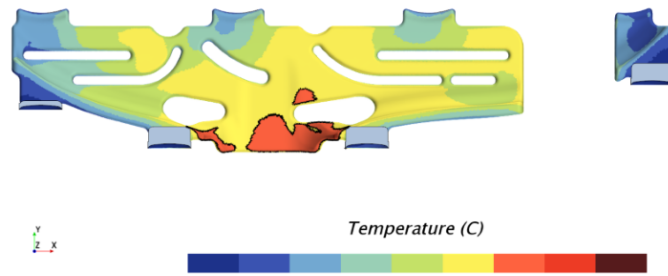
(a) 70/30 distribution

Max temp coolant jacket lower IEM: $T_{ref,cj_IEM} + 0,3$ K



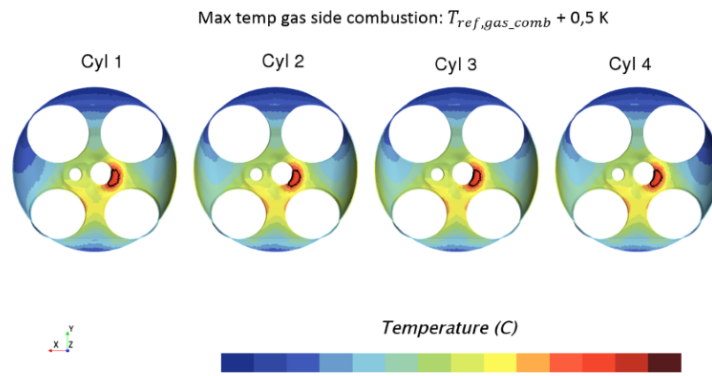
(b) 80/20 distribution

Max temp coolant jacket lower IEM: $T_{ref,cj_IEM} + 0,2$ K

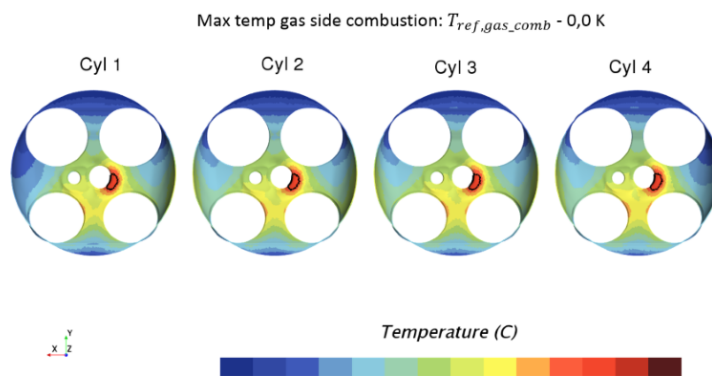


(c) 90/10 distribution

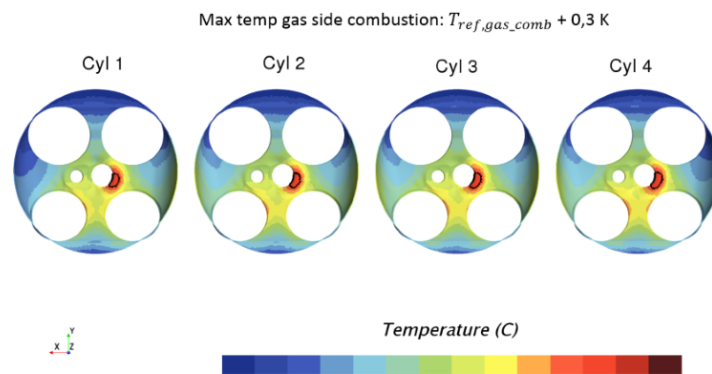
Figure A.27: Temperature field in lower coolant jacket below IEM



(a) 70/30 distribution

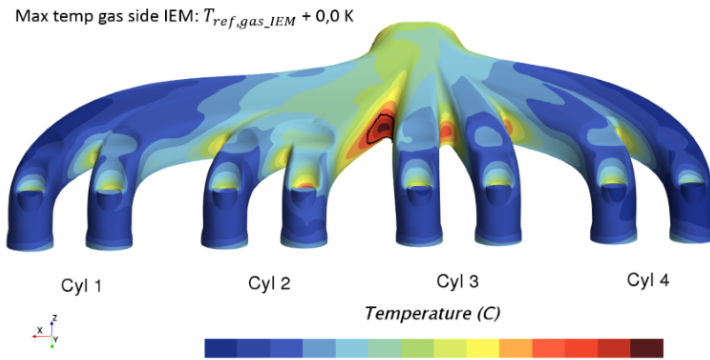


(b) 80/20 distribution

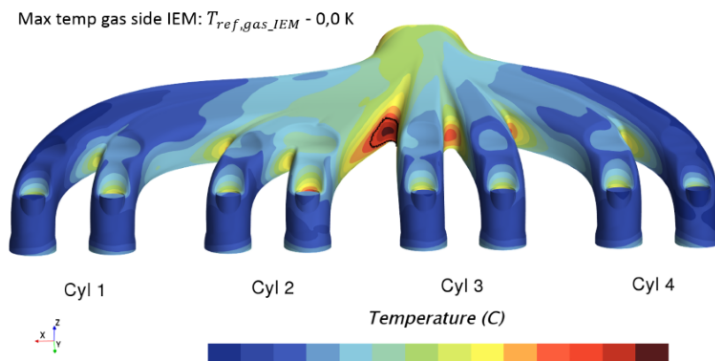


(c) 90/10 distribution

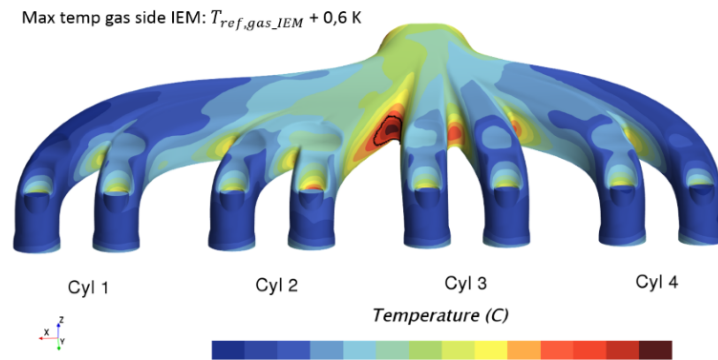
Figure A.28: Temperature field on gas/solid interface at top of combustion chambers



(a) 70/30 distribution



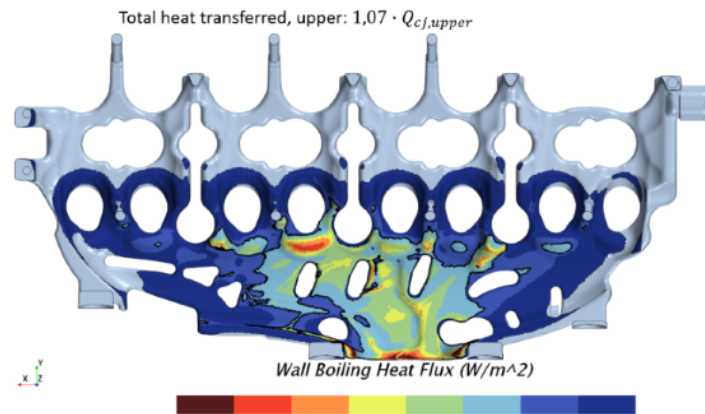
(b) 80/20 distribution



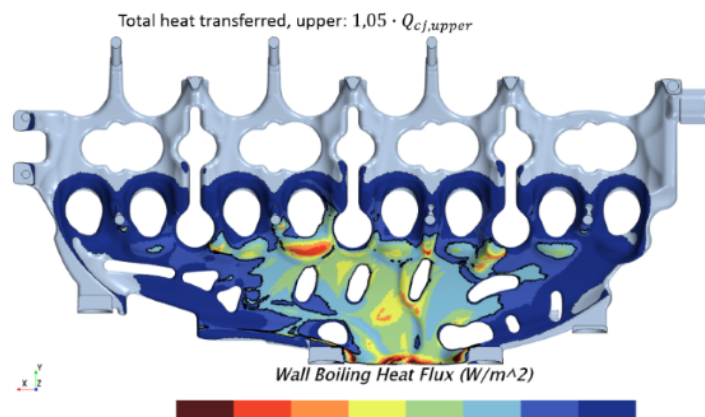
(c) 90/10 distribution

Figure A.29: Temperature field on gas/solid interface at IEM

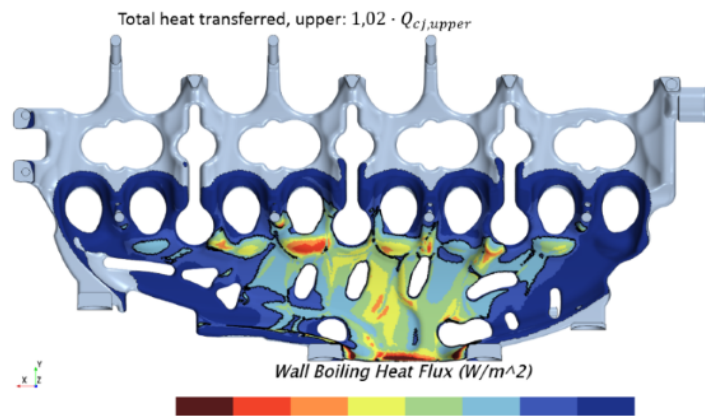
Heat flux



(a) 70/30 distribution

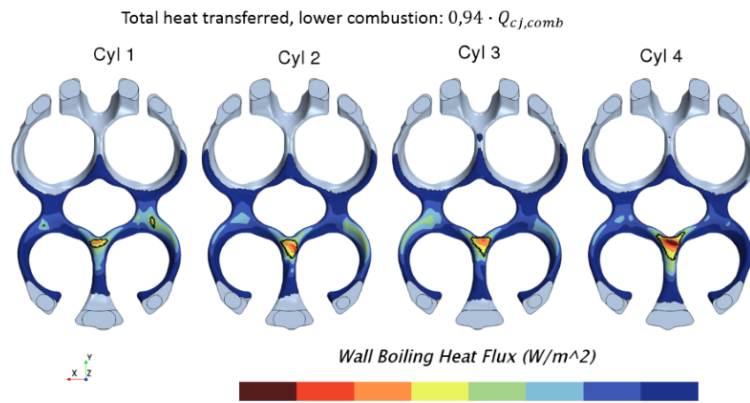


(b) 80/20 distribution

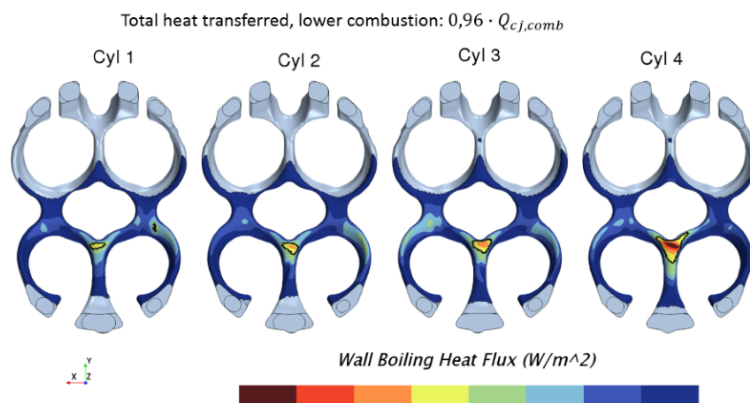


(c) 90/10 distribution

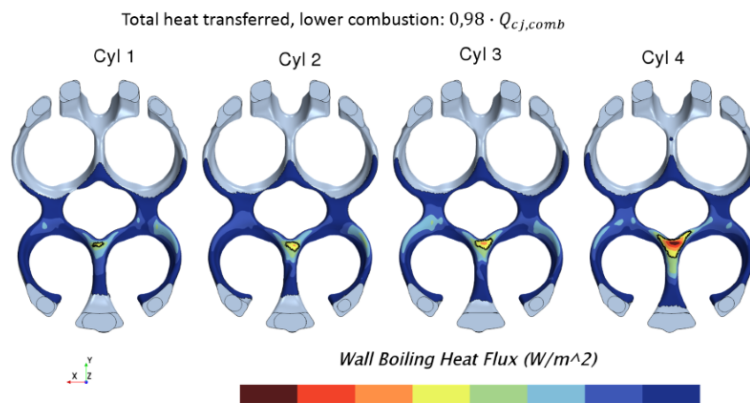
Figure A.30: Wall boiling heat flux in upper coolant jacket



(a) 70/30 distribution

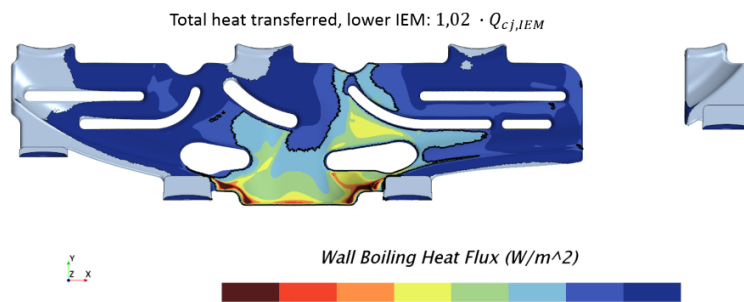


(b) 80/20 distribution

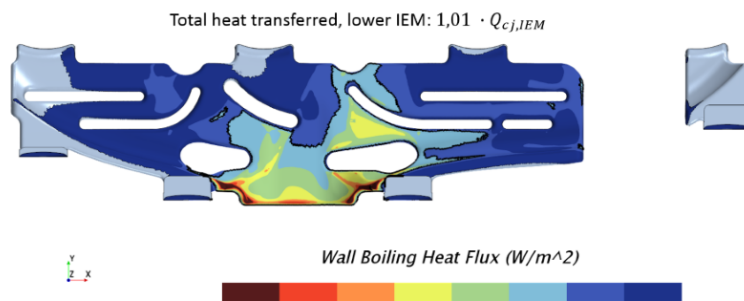


(c) 90/10 distribution

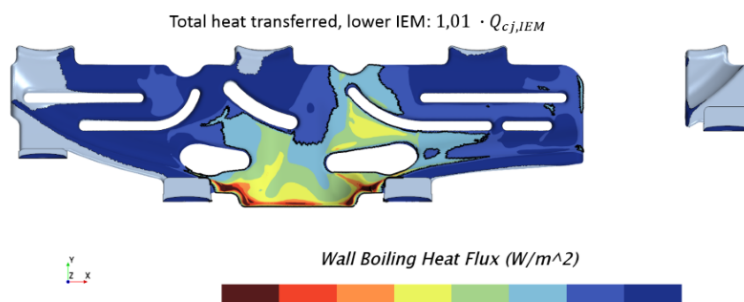
Figure A.31: Wall boiling heat flux in lower coolant jacket above combustion chambers



(a) 70/30 distribution



(b) 80/20 distribution

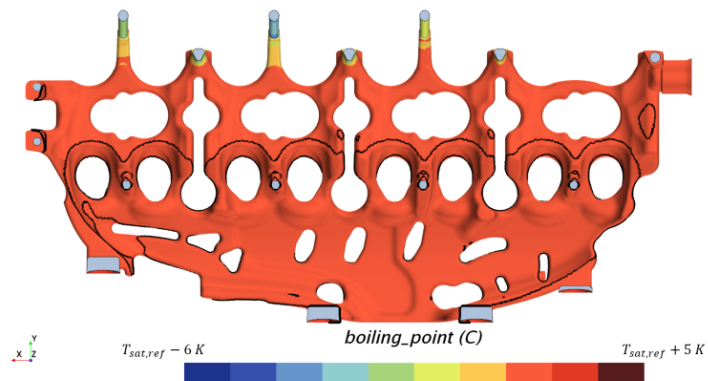


(c) 90/10 distribution

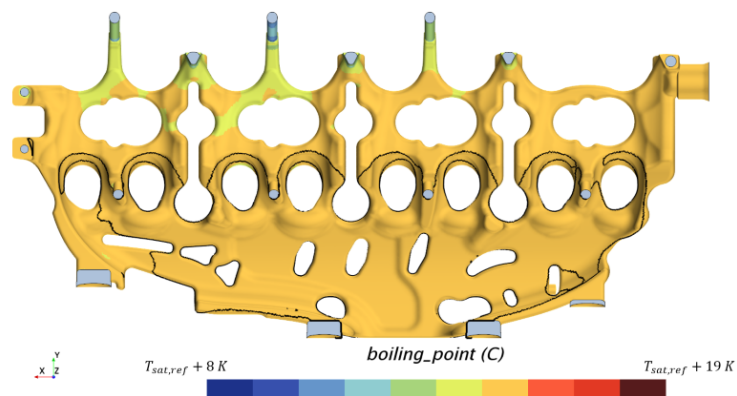
Figure A.32: Wall boiling heat flux in lower coolant jacket below IEM

A.4 Constant vs pressure dependent saturation temperature

Saturation temperature

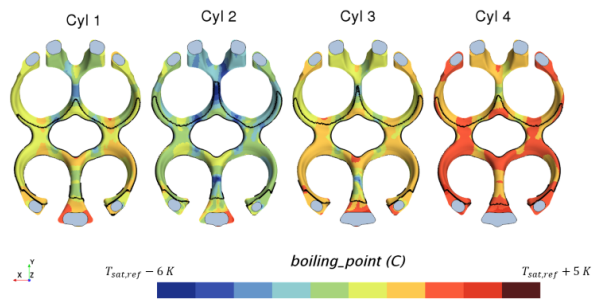


(a) $P_{out,low}$

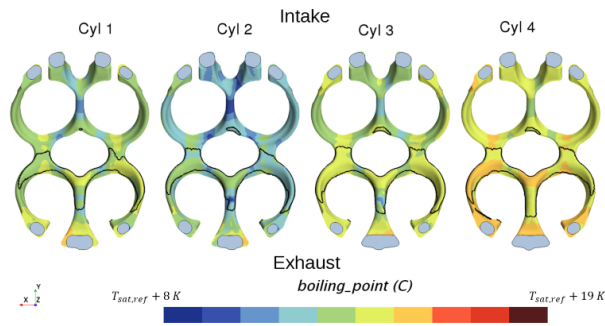


(b) $P_{out,ref}$

Figure A.33: Saturation temperature in upper coolant jacket

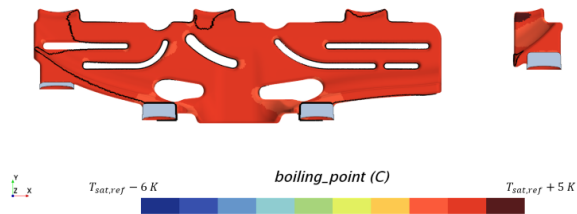


(a) $P_{out,low}$

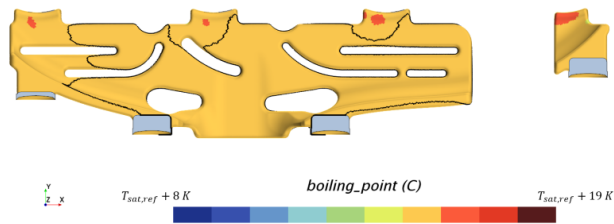


(b) $P_{out,ref}$

Figure A.34: Saturation temperature in lower coolant jacket above combustion chambers



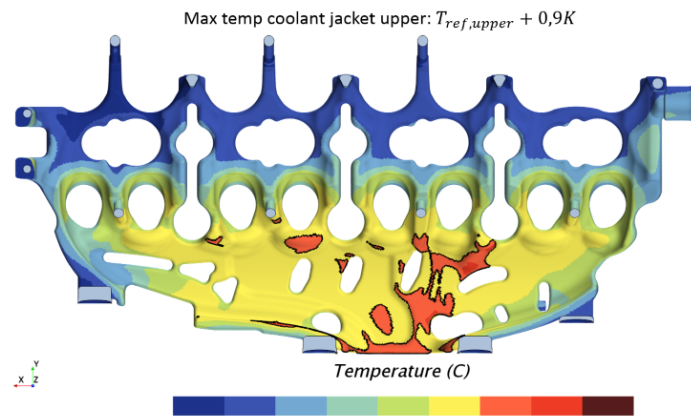
(a) $P_{out,low}$



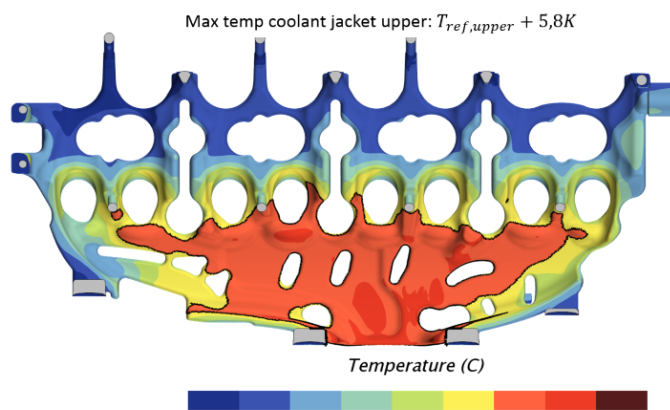
(b) $P_{out,ref}$

Figure A.35: Saturation temperature in lower coolant jacket below IEM

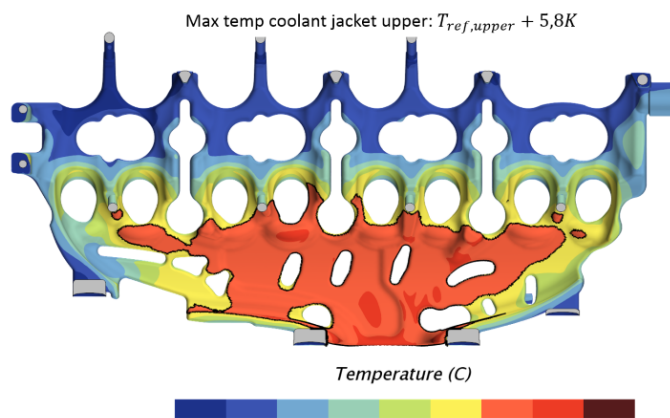
Temperature



(a) $P_{out,low}$

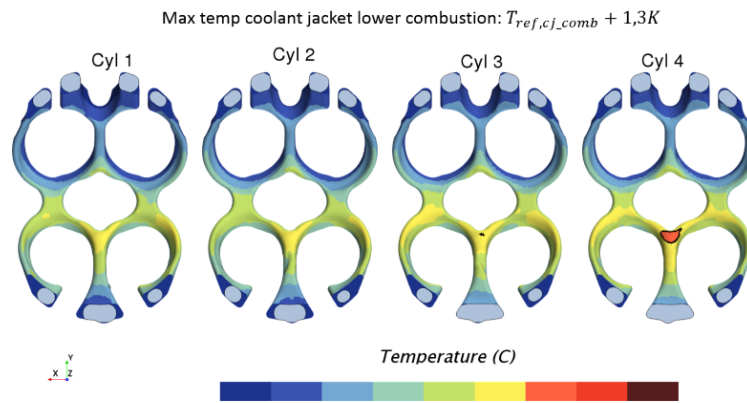


(b) $P_{out,ref}$

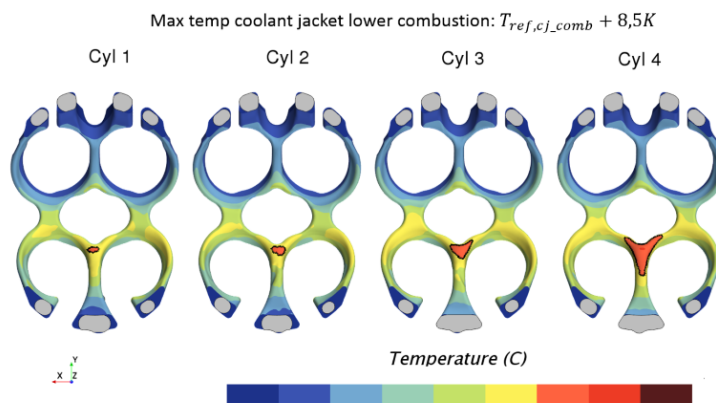


(c) $T_{sat,ref} + 14K$

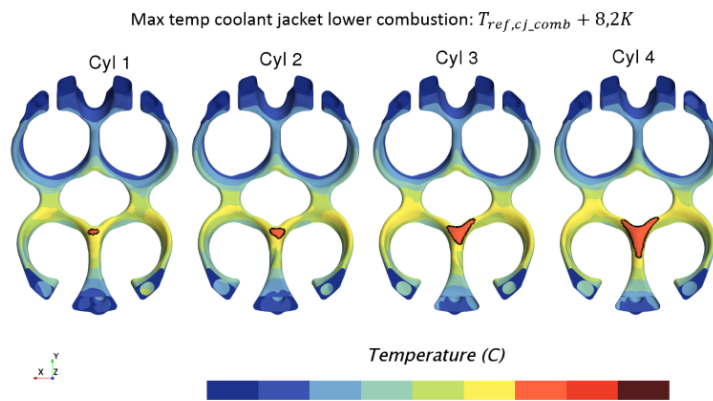
Figure A.36: *Temperature field in upper coolant jacket*



(a) $P_{Out,low}$



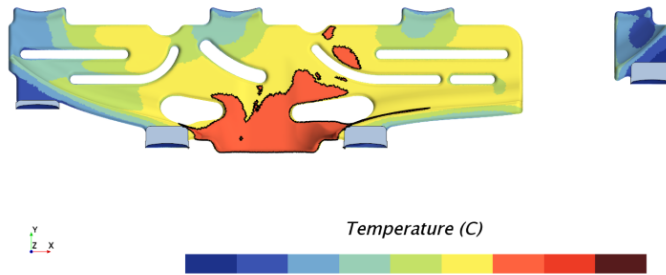
(b) $P_{Out,ref}$



(c) $T_{sat,ref} + 14K$

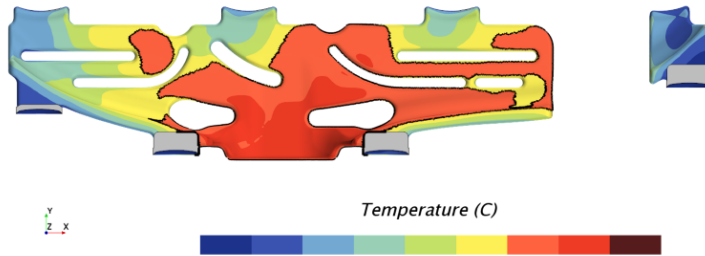
Figure A.37: *Temperature field in lower coolant jacket above combustion chambers*

Max temp coolant jacket lower IEM: $T_{ref,cj_IEM} + 1,6K$



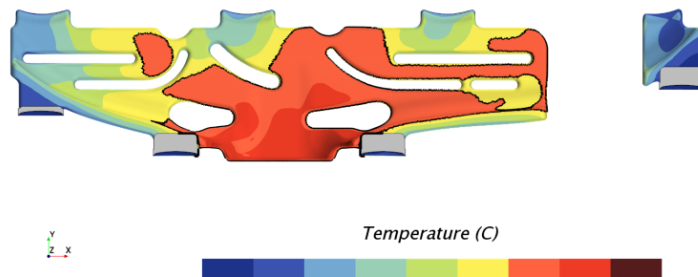
(a) $P_{out,low}$

Max temp coolant jacket lower IEM: $T_{ref,cj_IEM} + 8,9K$



(b) $P_{out,ref}$

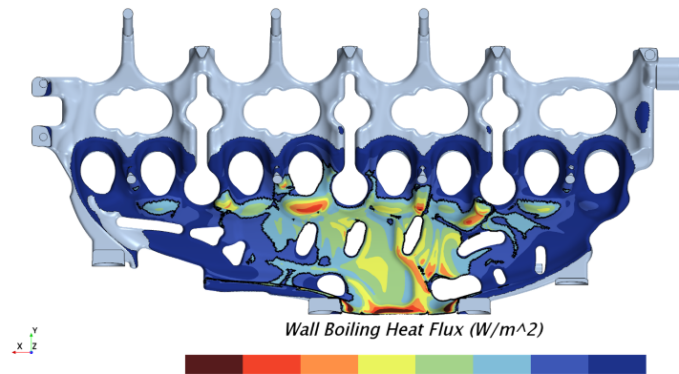
Max temp coolant jacket lower IEM: $T_{ref,cj_IEM} + 8,0K$



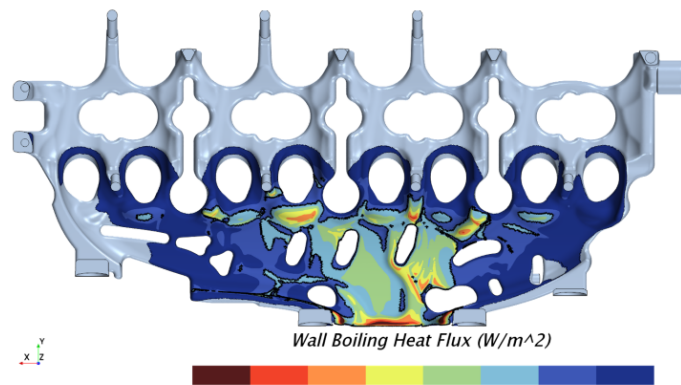
(c) $T_{sat,ref} + 14K$

Figure A.38: Temperature field in lower coolant jacket below IEM

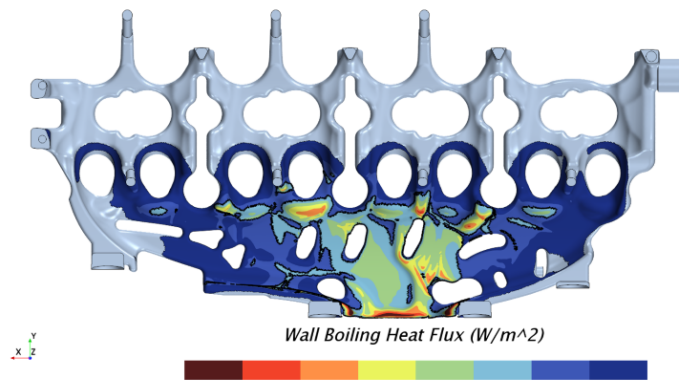
Heat flux



(a) $P_{out,low}$

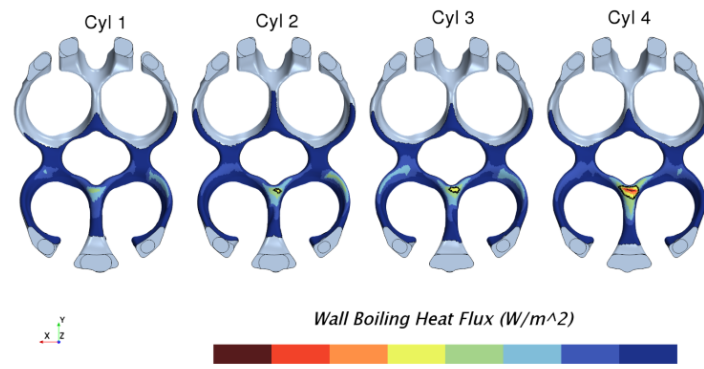


(b) $P_{out,ref}$

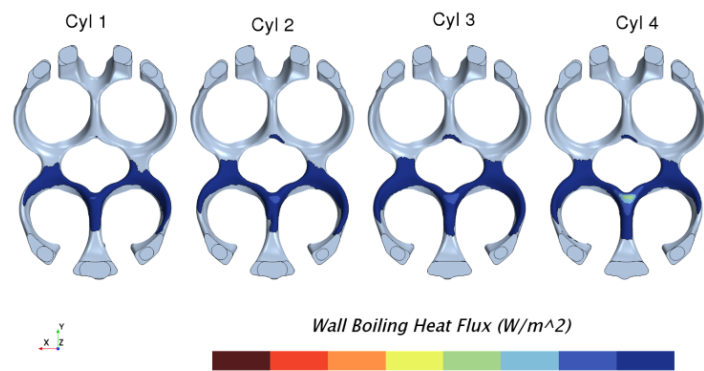


(c) $T_{sat,ref} + 14K$

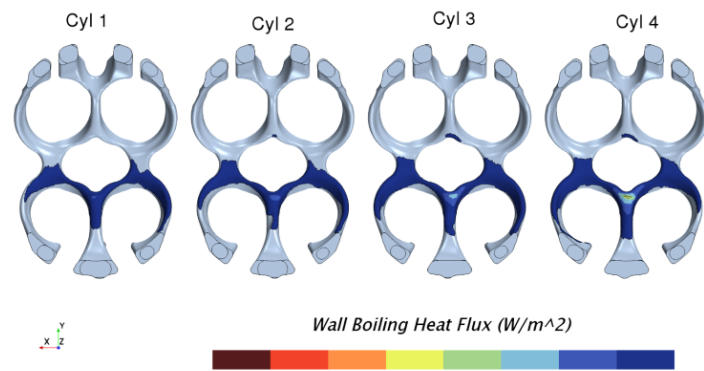
Figure A.39: Wall boiling heat flux in upper coolant jacket



(a) $P_{out,low}$



(b) $P_{out,ref}$



(c) $T_{sat,ref} + 14K$

Figure A.40: Wall boiling heat flux in lower coolant jacket above combustion chambers

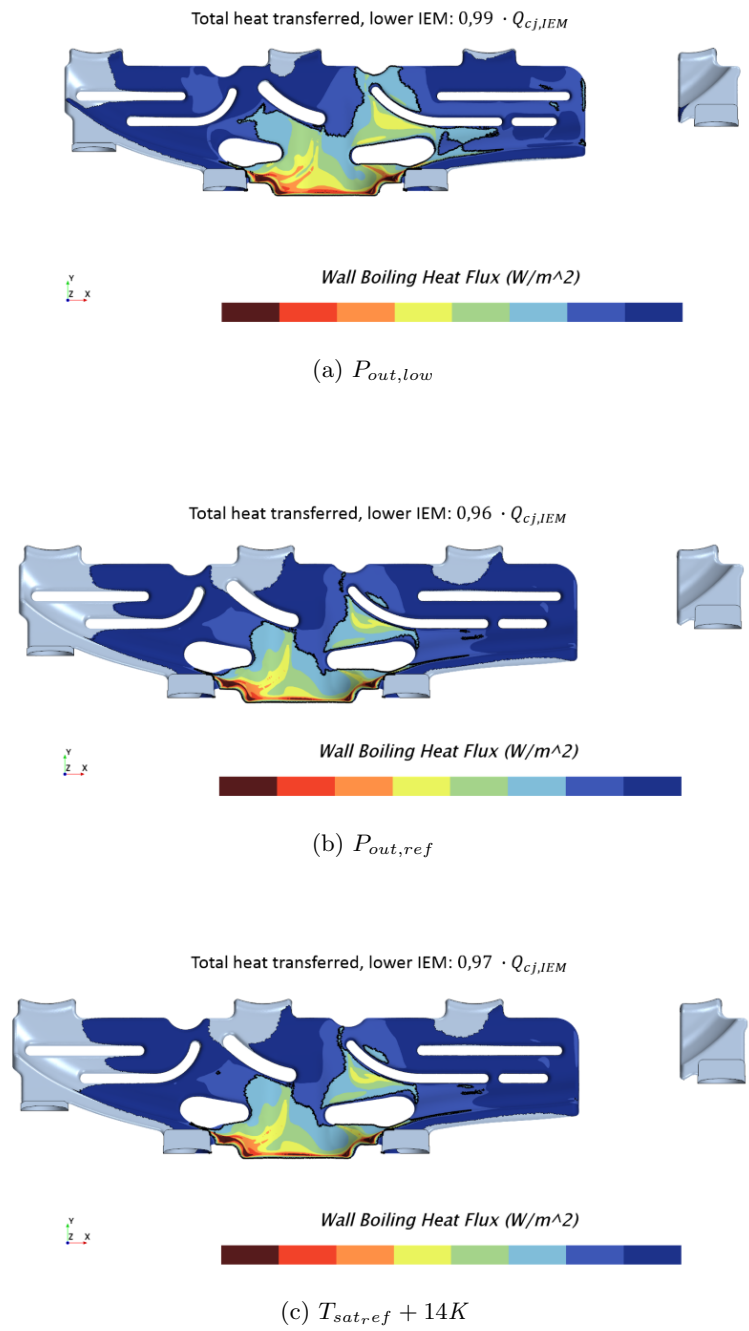
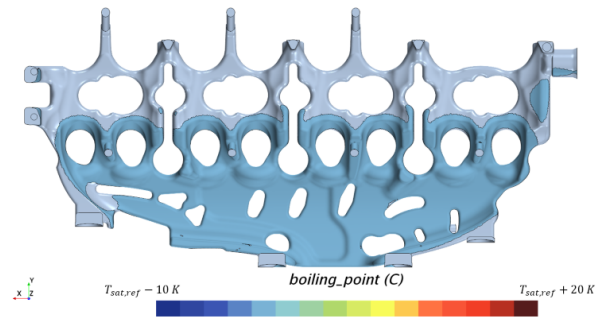


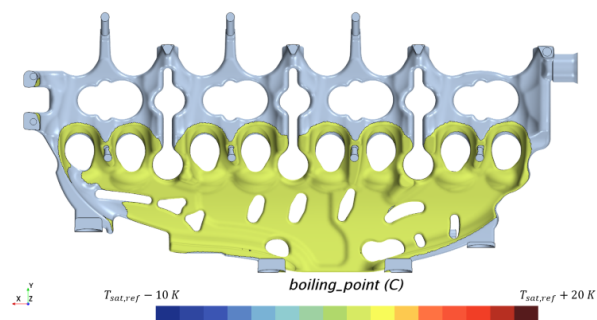
Figure A.41: Wall boiling heat flux in lower coolant jacket below IEM

A.5 Outlet pressure

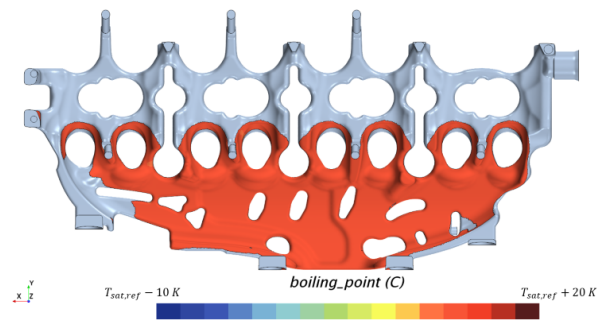
Saturation temperature



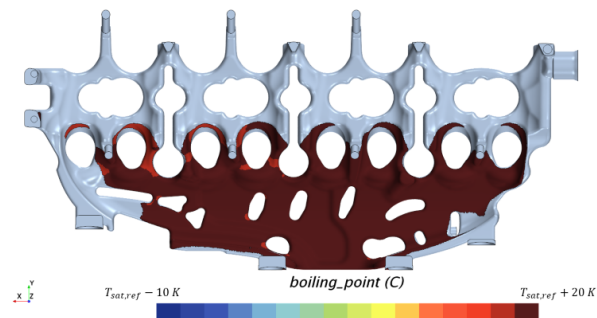
(a) $P_{out,1}$



(b) $1.33P_{out,1}$

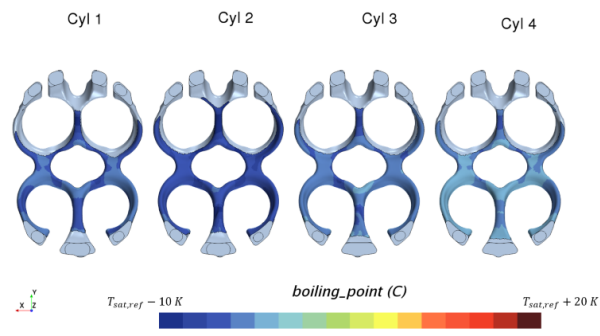


(c) $1.67P_{out,1}$

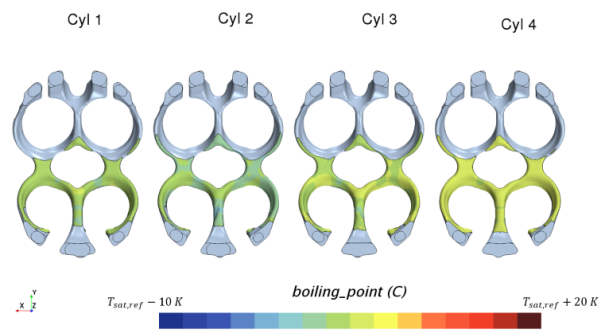


(d) $2P_{out,1}$

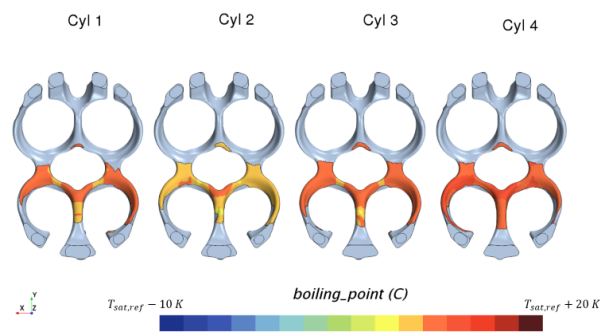
Figure A.42: Saturation temperature in upper coolant jacket



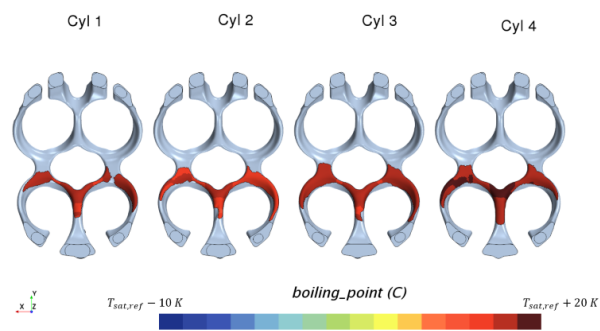
(a) $P_{Out,1}$



(b) $1.33P_{Out,1}$

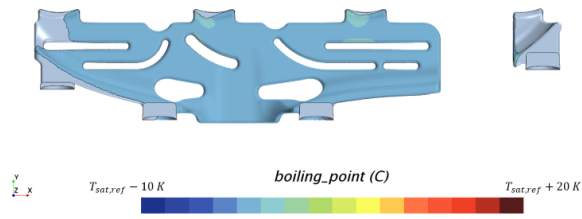


(c) $1.67P_{Out,1}$

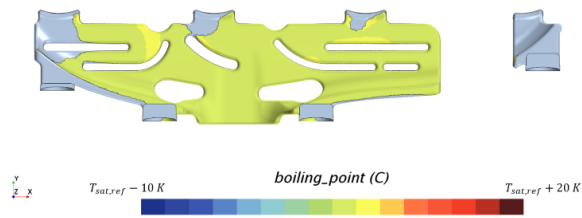


(d) $2P_{Out,1}$

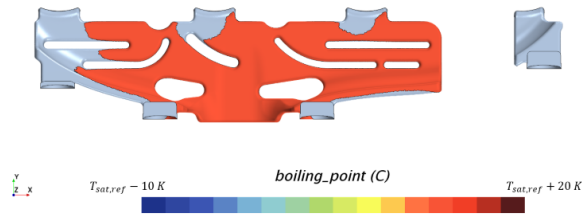
Figure A.43: Saturation temperature in lower coolant jacket above combustion chambers



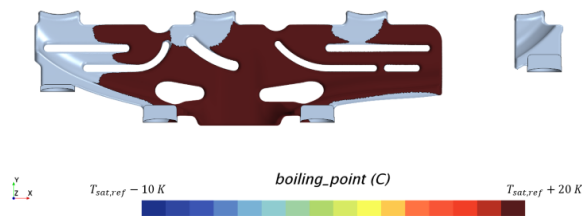
(a) $P_{out,1}$



(b) $1.33P_{out,1}$



(c) $1.67P_{out,1}$



(d) $2P_{out,1}$

Figure A.44: Saturation temperature in upper coolant jacket

Temperature

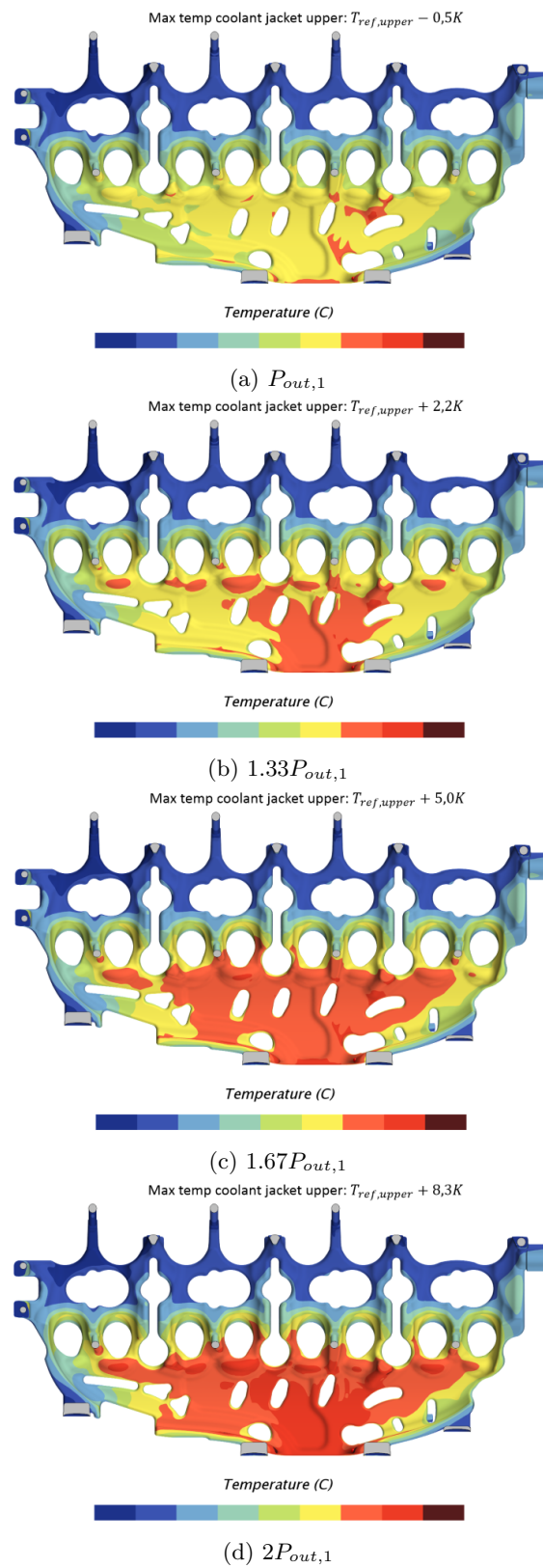
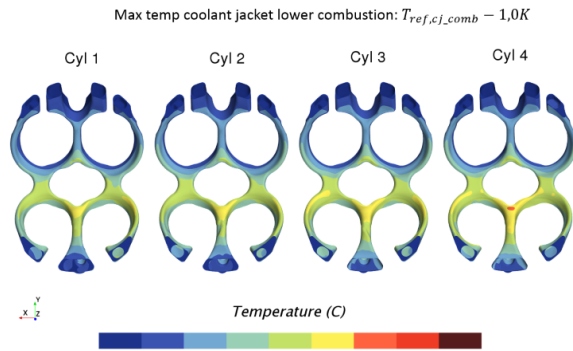
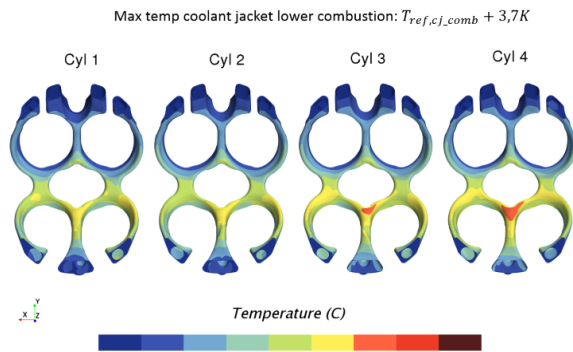


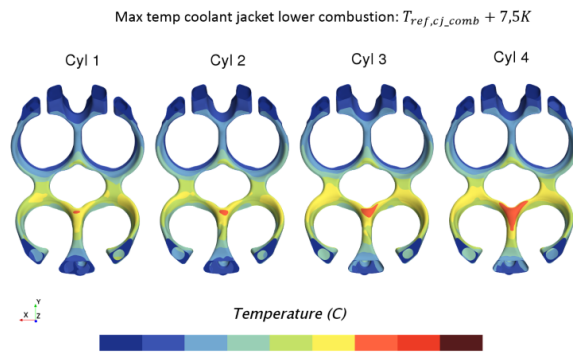
Figure A.45: *Temperature field in upper coolant jacket*



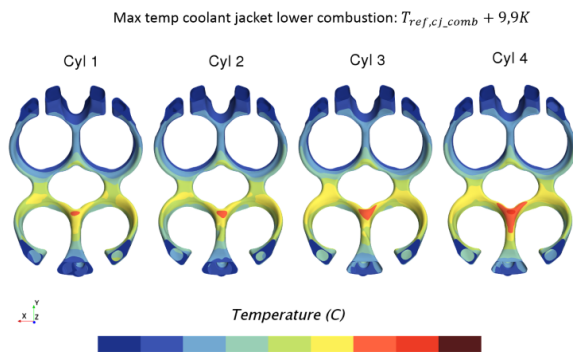
(a) $P_{out,1}$



(b) $1.33P_{out,1}$



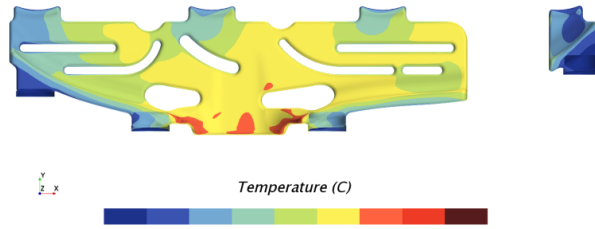
(c) $1.67P_{out,1}$



(d) $2P_{out,1}$

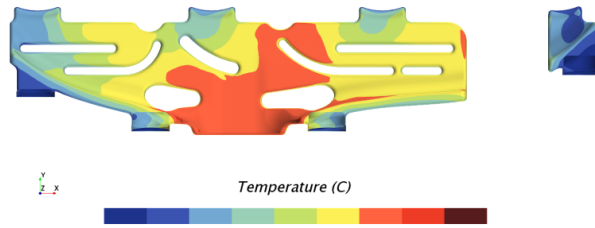
Figure A.46: *Temperature field in lower coolant jacket above combustion chambers*

Max temp coolant jacket lower IEM: $T_{ref,cj,IEM} - 0,8K$



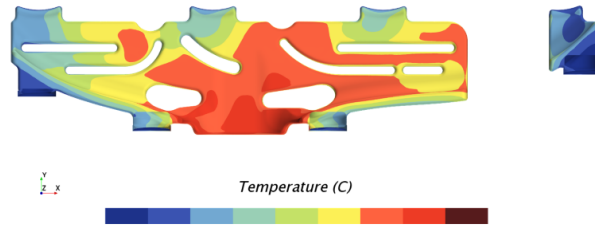
(a) $P_{out,1}$

Max temp coolant jacket lower IEM: $T_{ref,cj,IEM} + 3,7K$



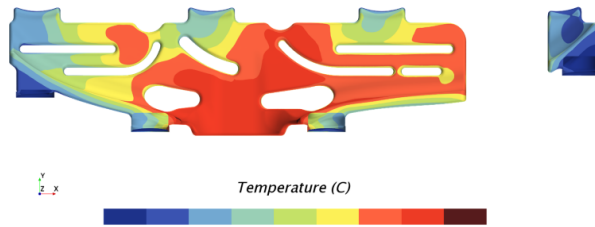
(b) $1.33P_{out,1}$

Max temp coolant jacket lower IEM: $T_{ref,cj,IEM} + 7,6K$



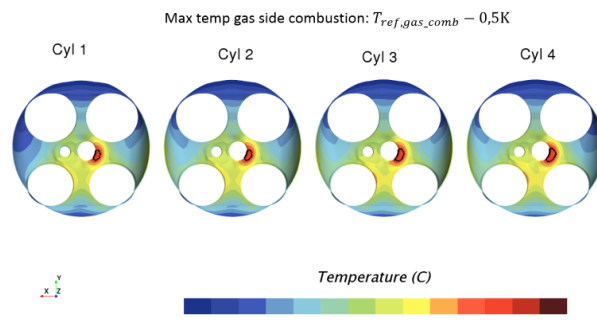
(c) $1.67P_{out,1}$

Max temp coolant jacket lower IEM: $T_{ref,cj,IEM} + 10,8K$

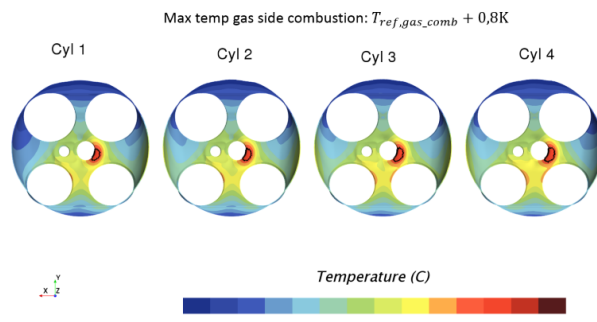


(d) $2P_{out,1}$

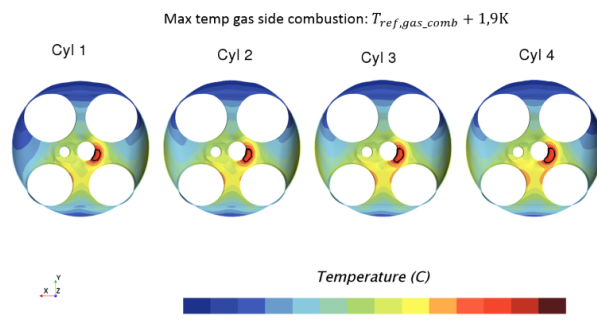
Figure A.47: *Temperature field in lower coolant jacket below IEM*



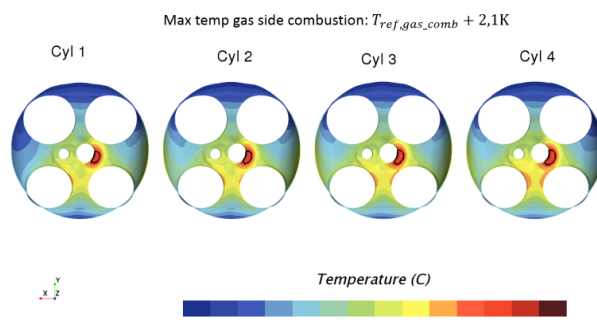
(a) $P_{out,1}$



(b) $1.33P_{out,1}$

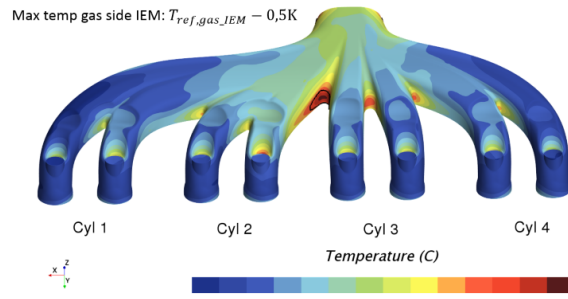


(c) $1.67P_{out,1}$

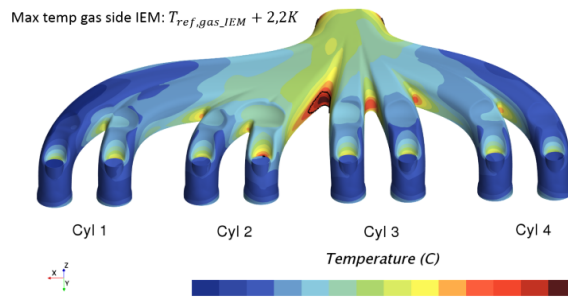


(d) $2P_{out,1}$

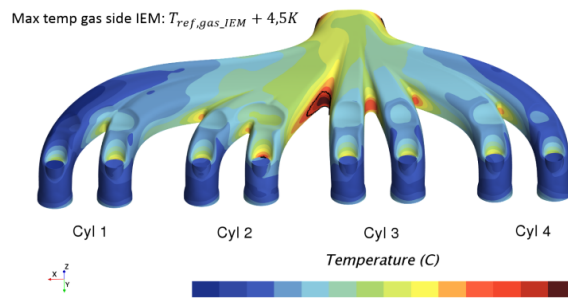
Figure A.48: *Temperature field on gas/solid interface at top of combustion chambers*



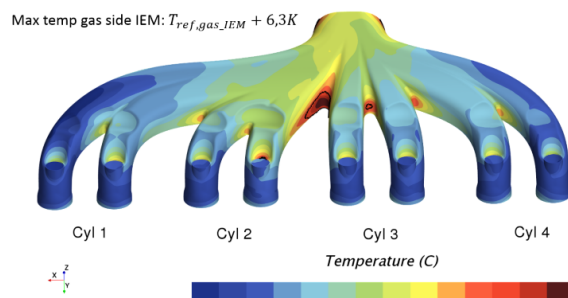
(a) $P_{out,1}$



(b) $1.33P_{out,1}$



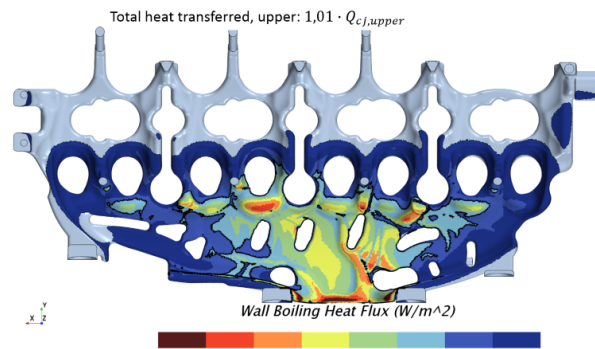
(c) $1.67P_{out,1}$



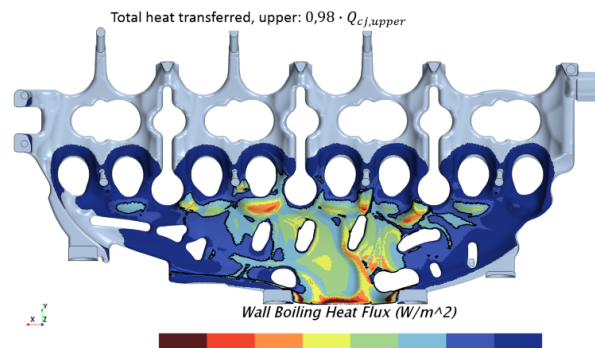
(d) $2P_{out,1}$

Figure A.49: *Temperature field on gas/solid interface at IEM*

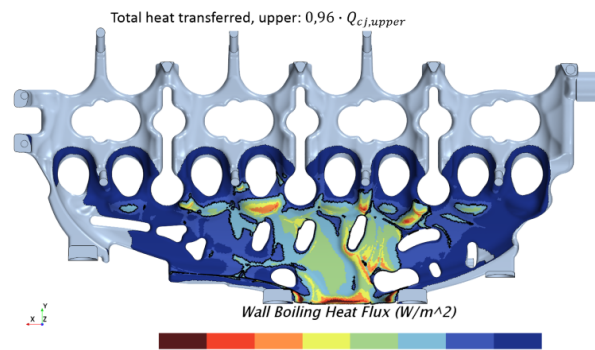
Heat flux



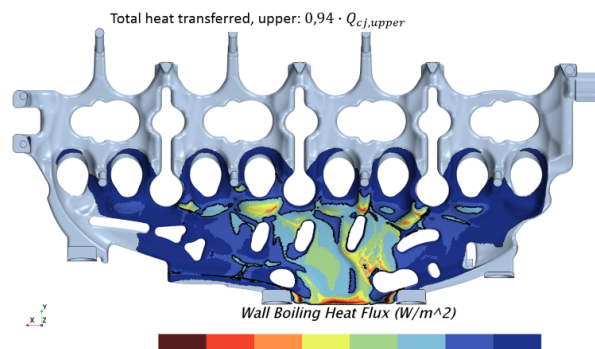
(a) $P_{out,1}$



(b) $1,33P_{out,1}$

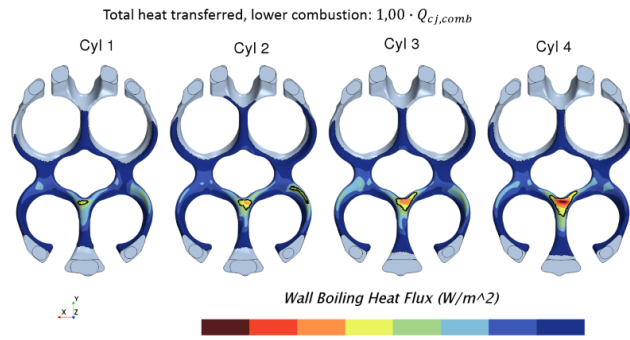


(c) $1,67P_{out,1}$

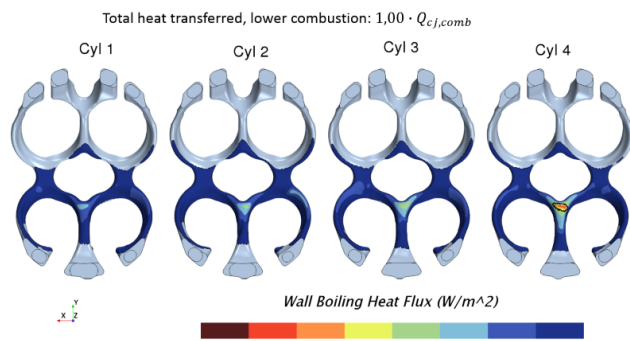


(d) $2P_{out,1}$

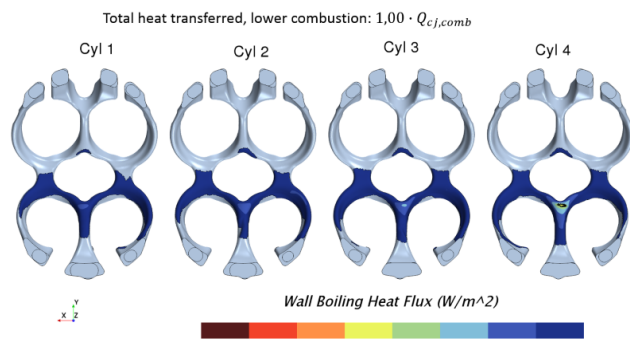
Figure A.50: Wall boiling heat flux in upper coolant jacket



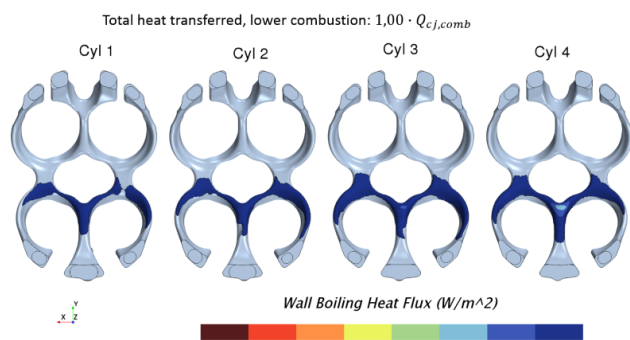
(a) $P_{out,1}$



(b) $1.33P_{out,1}$

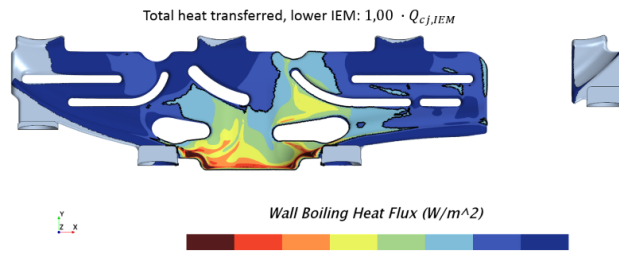


(c) $1.67P_{out,1}$

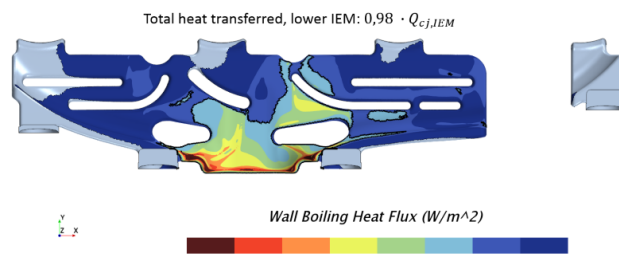


(d) $2P_{out,1}$

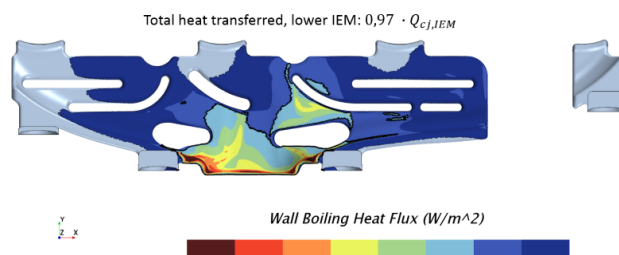
Figure A.51: Wall boiling heat flux in lower coolant jacket above combustion chambers



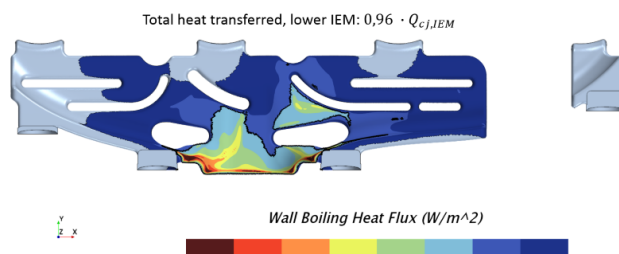
(a) $P_{out,1}$



(b) $1.33P_{out,1}$



(c) $1.67P_{out,1}$



(d) $2P_{out,1}$

Figure A.52: Wall boiling heat flux in lower coolant jacket below IEM

A.6 Thermal conductivity

Temperature

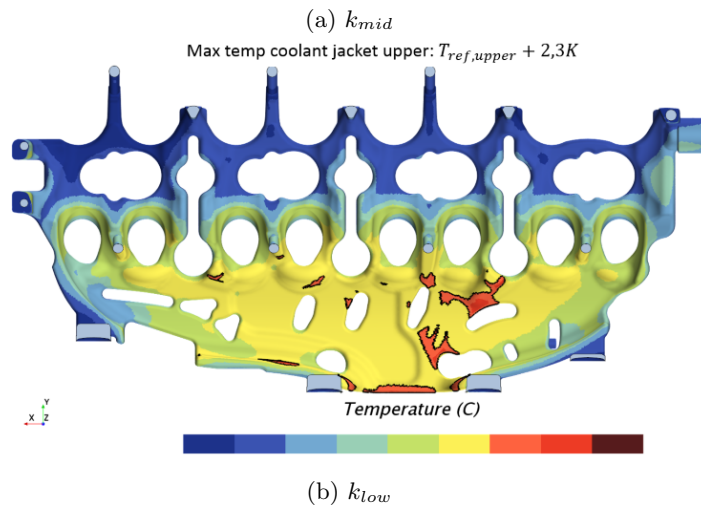
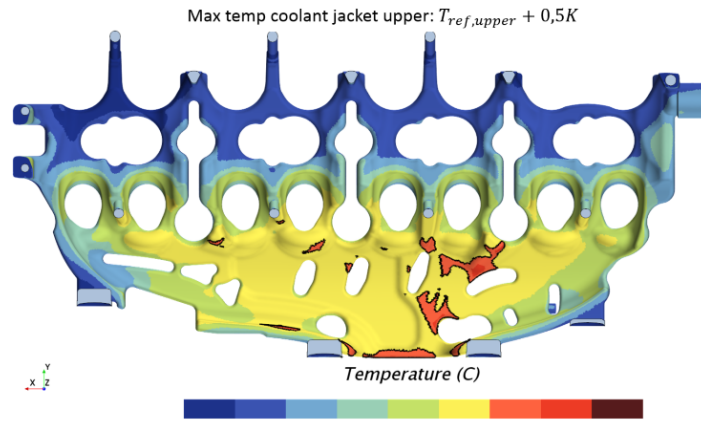
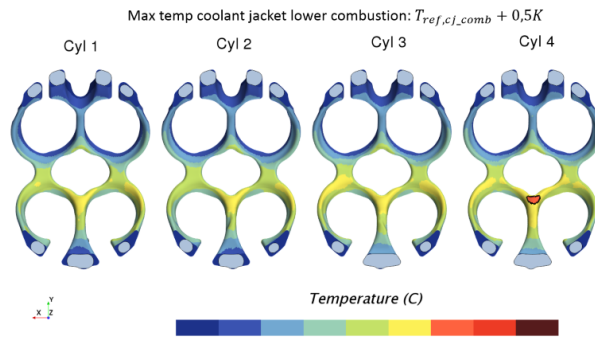
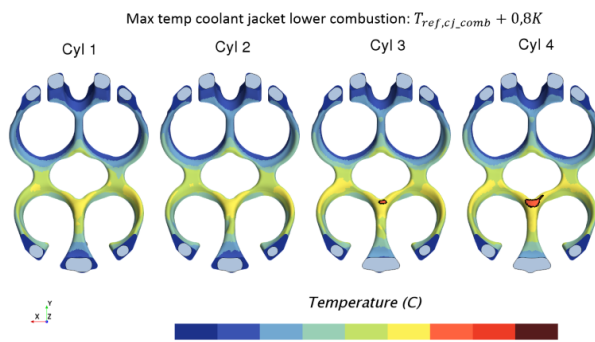


Figure A.53: *Temperature field in upper coolant jacket*

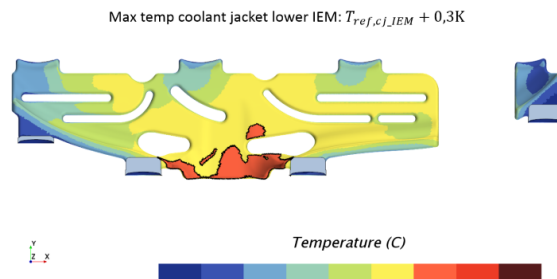


(a) k_{mid}

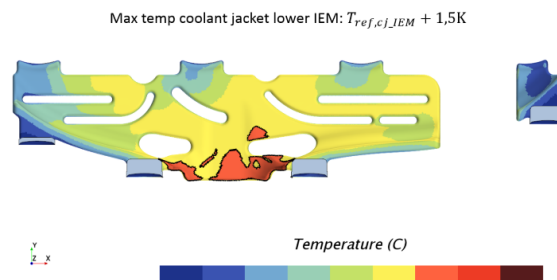


(b) k_{low}

Figure A.54: *Temperature field in lower coolant jacket above combustion chambers*



(a) k_{mid}



(b) k_{low}

Figure A.55: *Temperature field in lower coolant jacket below IEM*

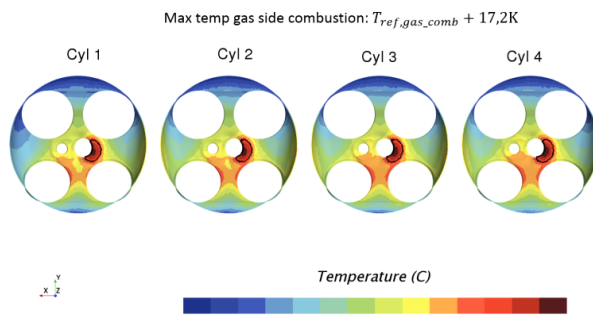
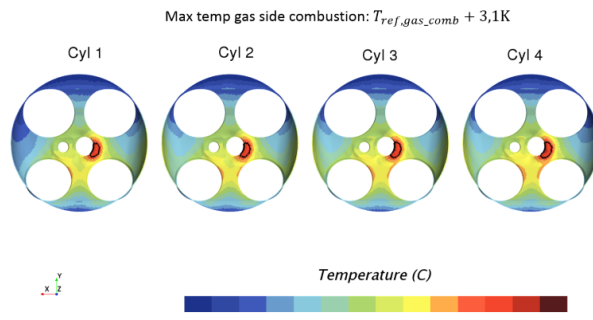


Figure A.56: Temperature field on gas/solid interface at top of combustion chambers

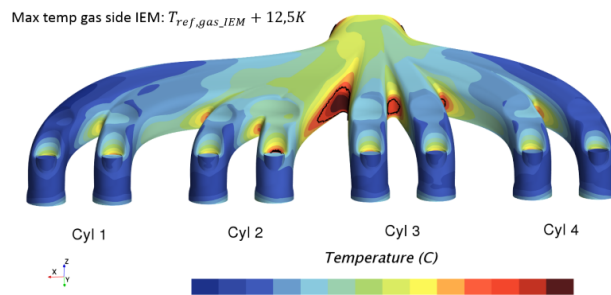
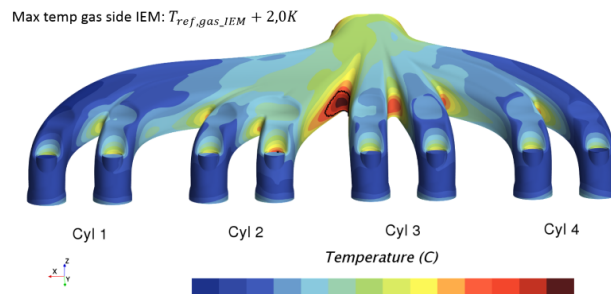
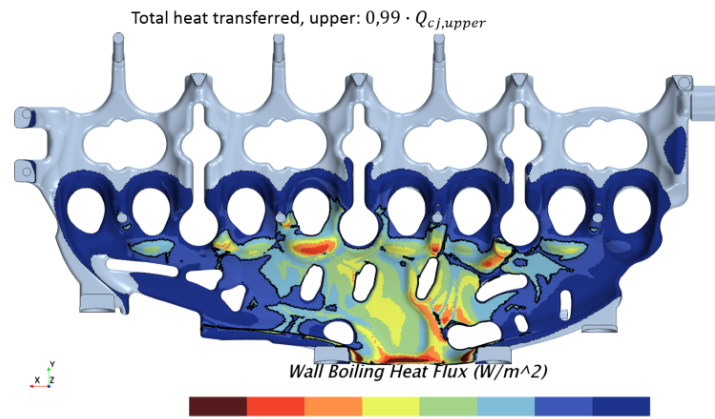
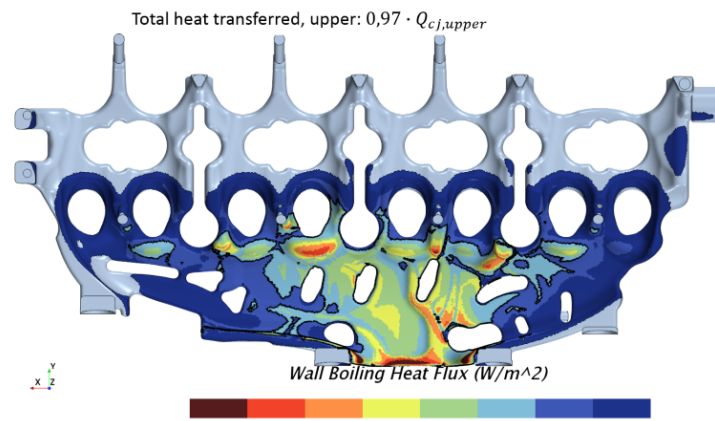


Figure A.57: Temperature field on gas/solid interface at IEM

Heat flux

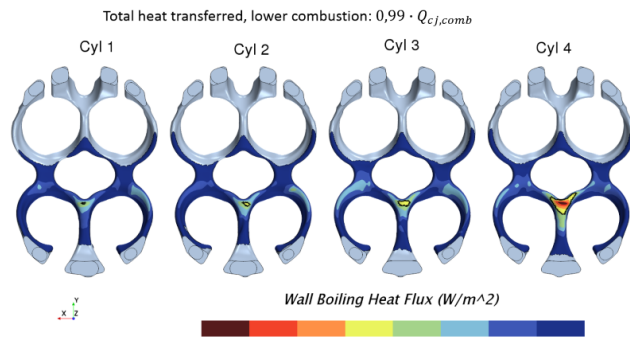


(a) k_{mid}

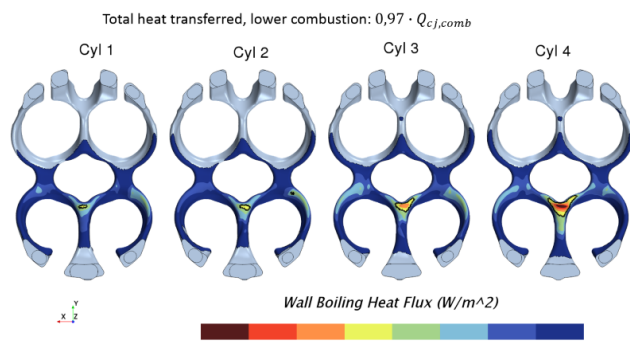


(b) k_{low}

Figure A.58: Wall boiling heat flux in upper coolant jacket

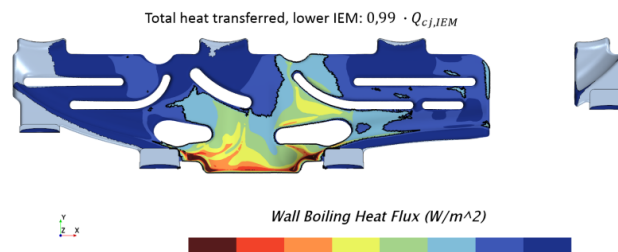


(a) k_{mid}

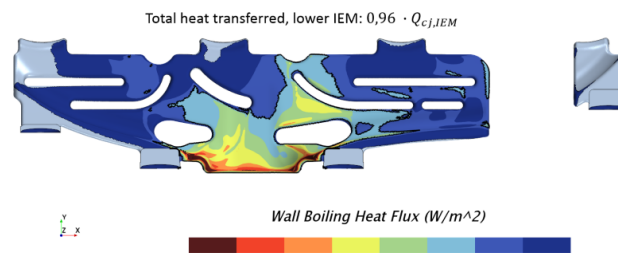


(b) k_{low}

Figure A.59: Wall boiling heat flux in lower coolant jacket above combustion chambers



(a) k_{mid}



(b) k_{low}

Figure A.60: Wall boiling heat flux in lower coolant jacket below IEM

A.7 Displacement

Temperature

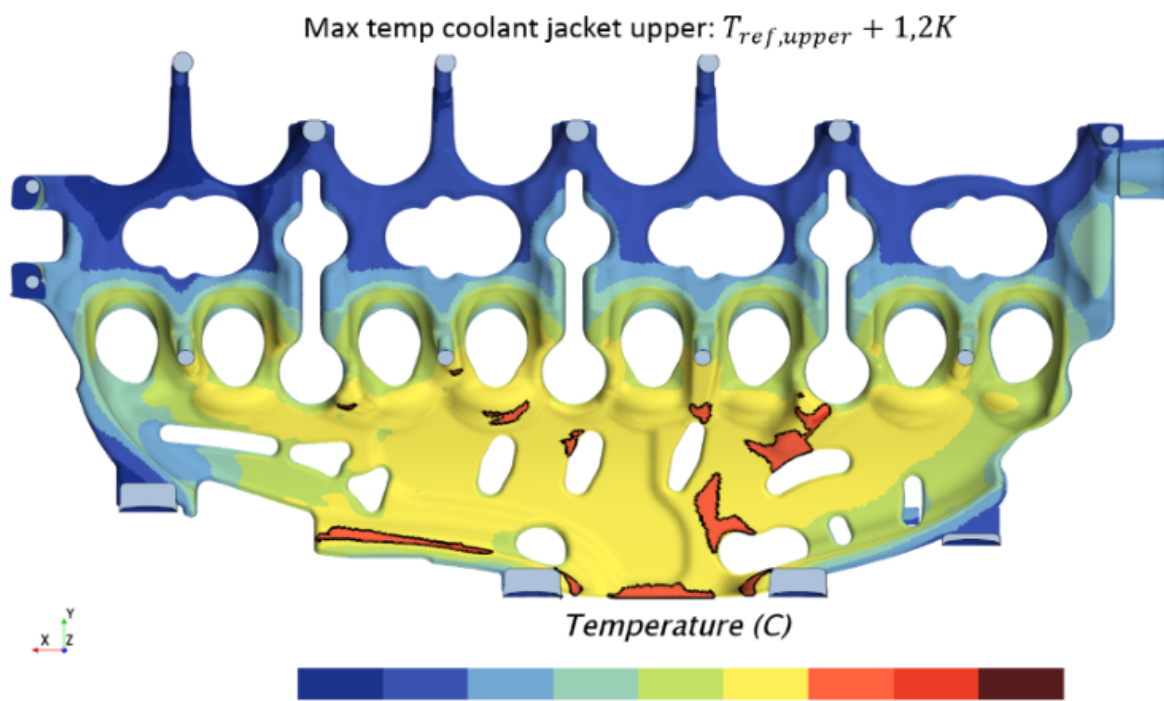


Figure A.61: *Temperature field upper coolant jacket*

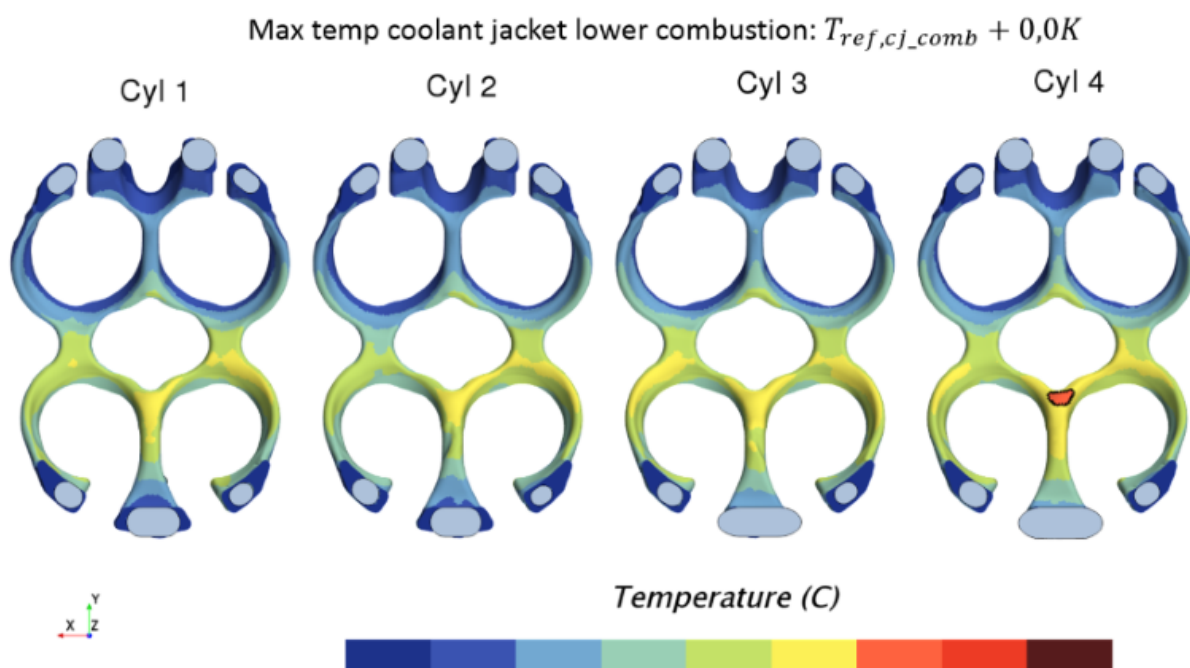


Figure A.62: *Temperature field lower coolant jacket above combustion chambers*

Max temp coolant jacket lower IEM: $T_{ref,cj_IEM} + 0,7K$

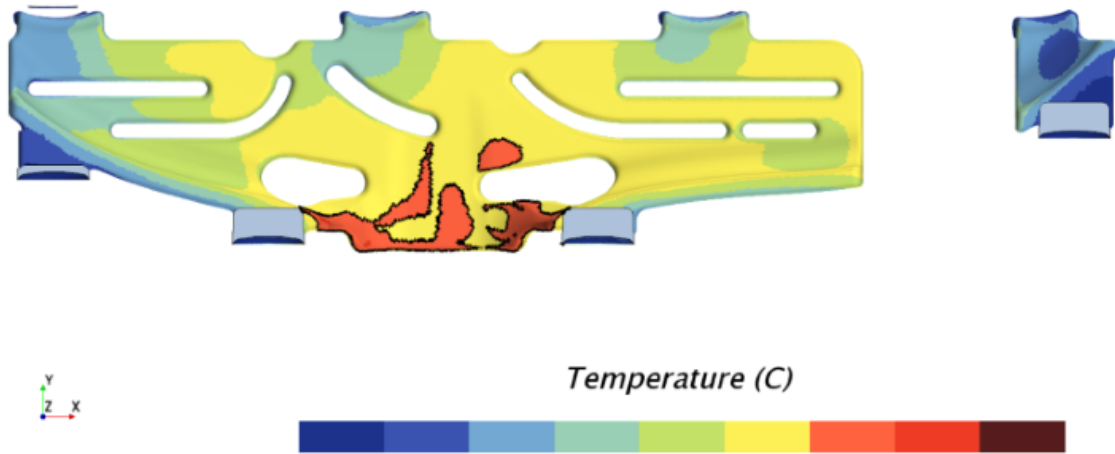


Figure A.63: *Temperature field lower coolant jacket below IEM*

Max temp gas side combustion: $T_{ref,gas_comb} - 2,6K$

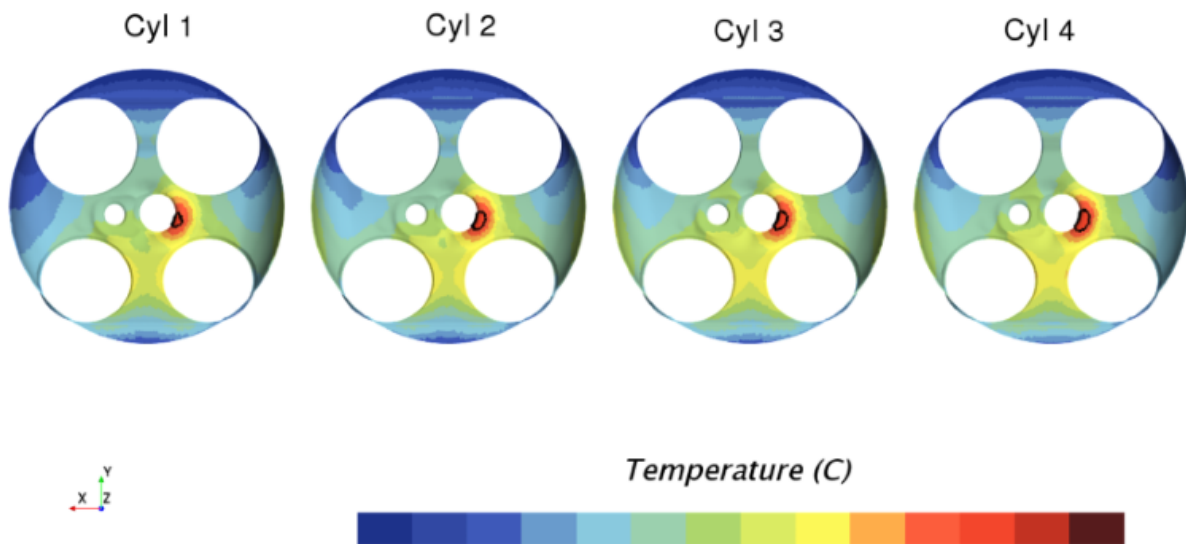


Figure A.64: *Temperature field gas/solid interface at top of combustion chambers*

Max temp gas side IEM: $T_{ref,gas_IEM} - 1,2K$

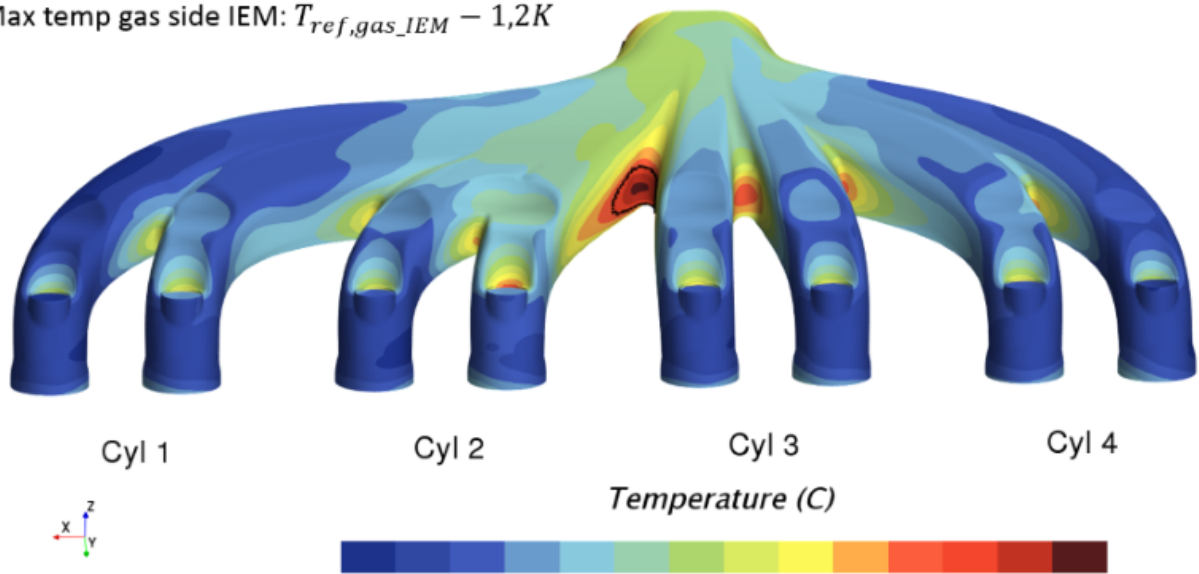


Figure A.65: *Temperature field gas/solid interface at IEM*

Heat flux

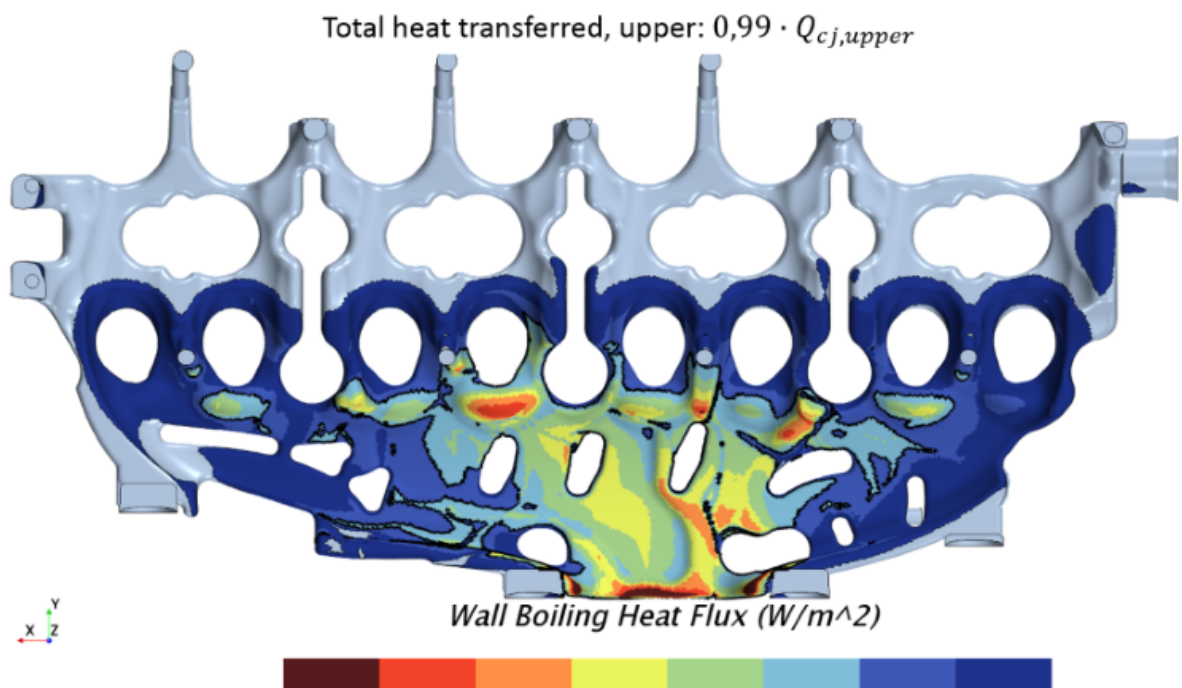


Figure A.66: *Wall boiling heat flux upper coolant jacket*

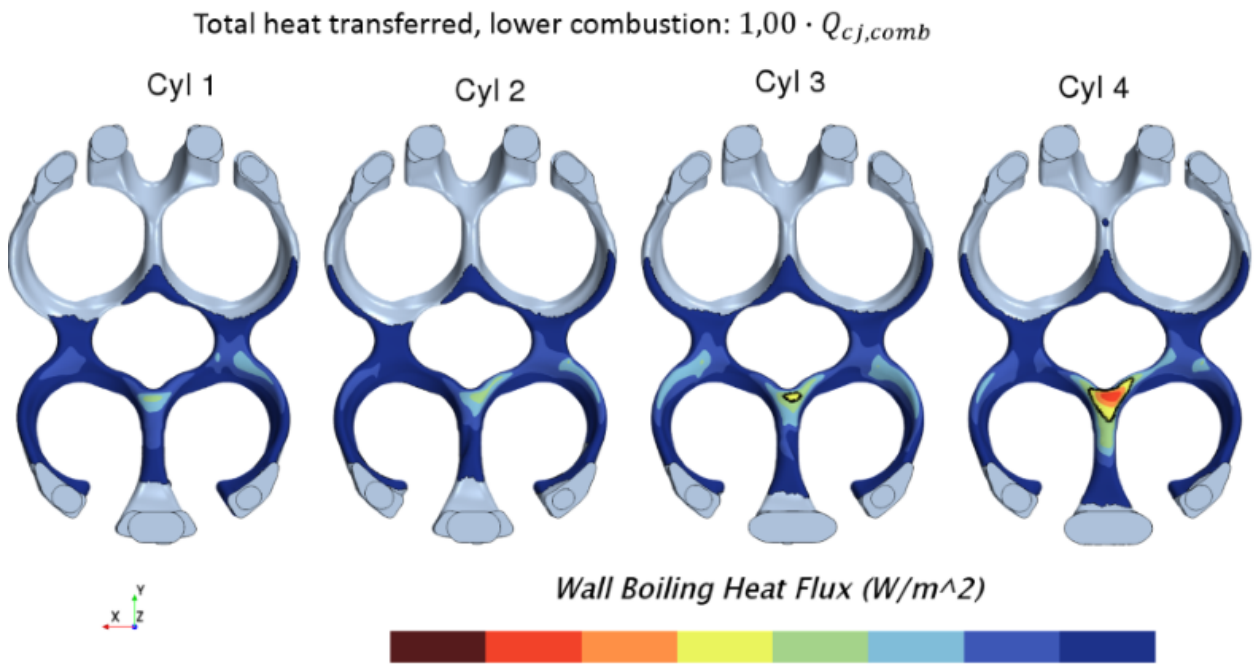


Figure A.67: *Wall boiling heat flux lower coolant jacket above combustion chambers*

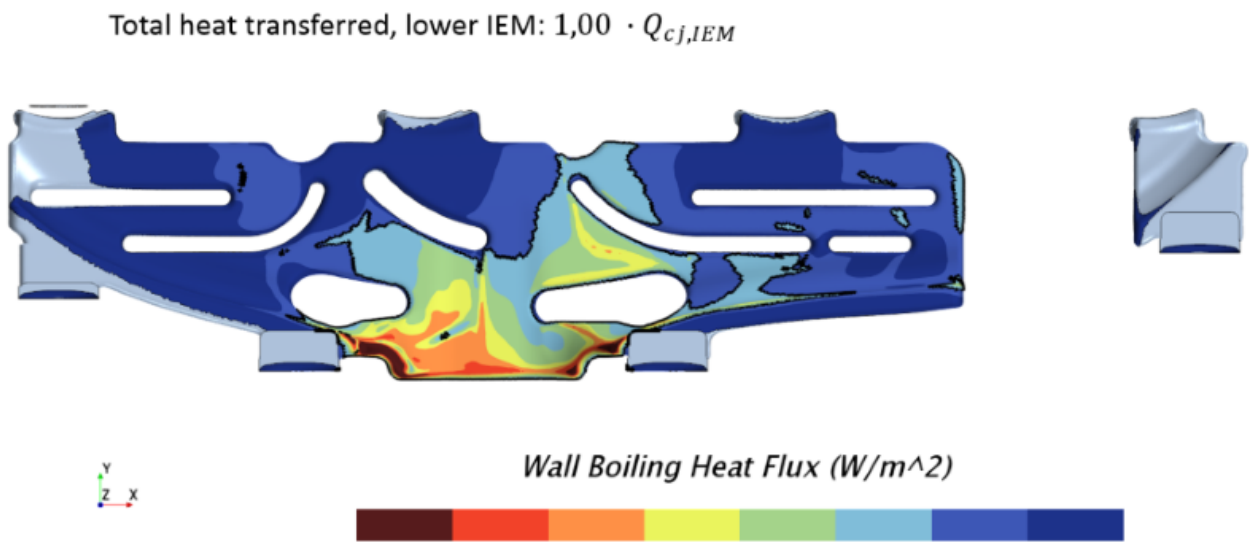
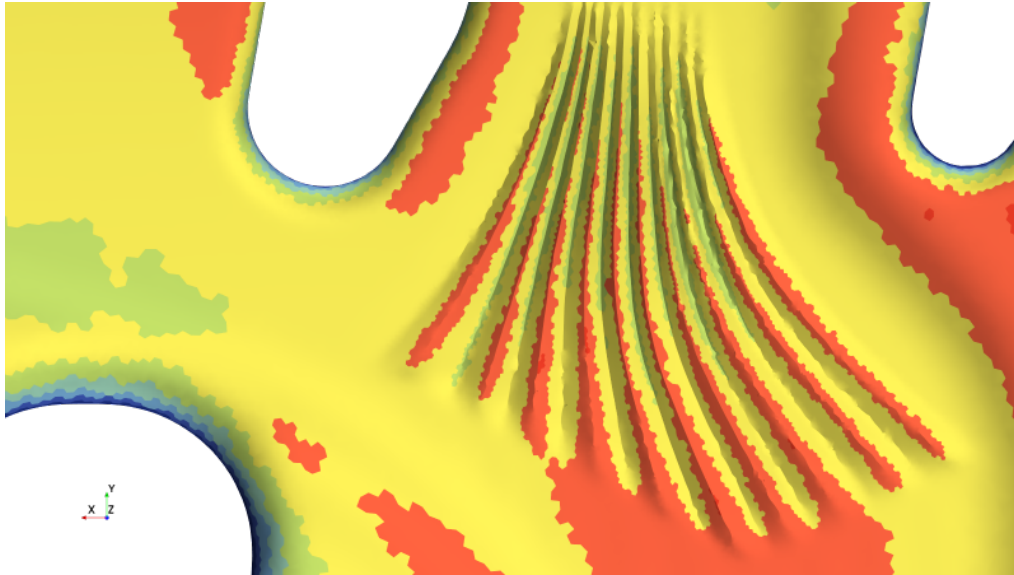


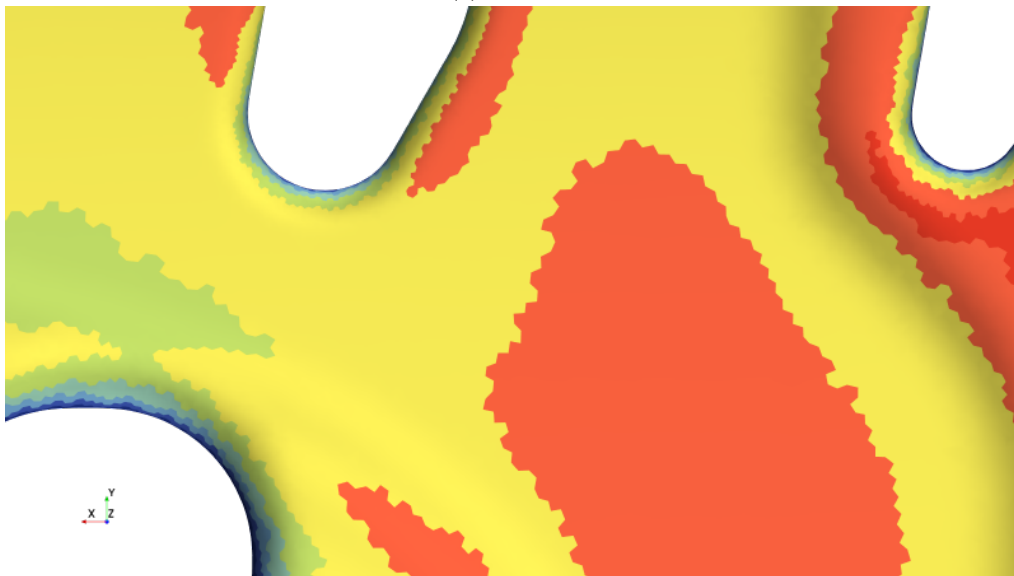
Figure A.68: *Wall boiling heat flux lower coolant jacket below IEM*

A.8 Surface modification

Temperature



(a) *modified*



(b) *reference*

Figure A.69: *Temperature in the upper coolant jacket around modified surface*

Heat flux

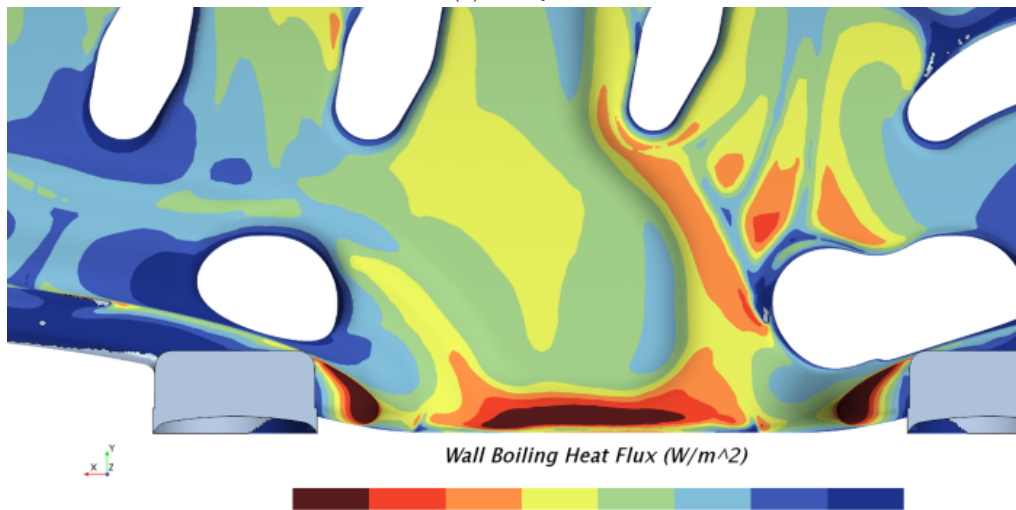
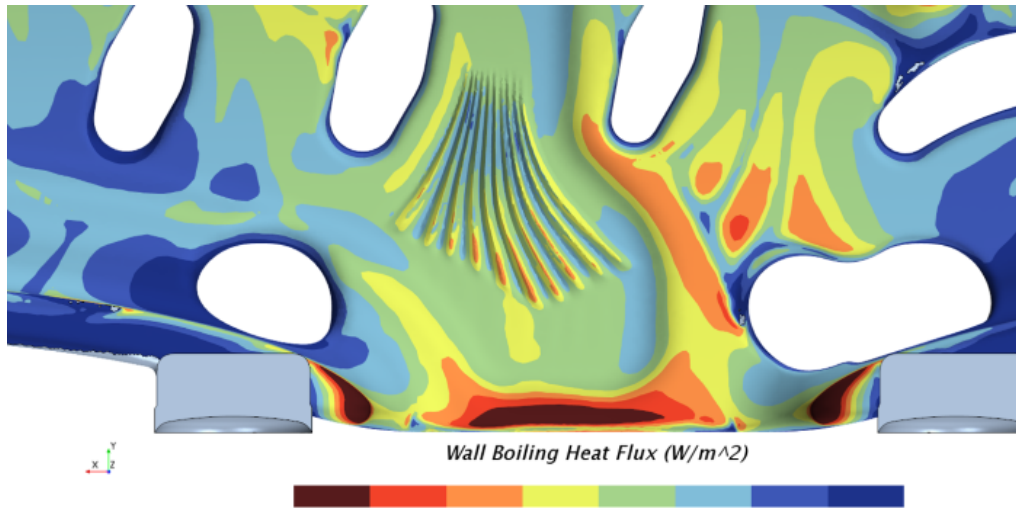


Figure A.70: Wall boiling heat flux in the upper coolant jacket around modified surface